Technical Report Documentation Page

1. Report No.	2. Government Accession No.	3. Recipient's Catalog No.
FHWA-PA-2007-007-030407-2		

4. Title and Subtitle	5. Report Date
District 3-0 Investigation of Fiber Wrap Technology for Bridge Repair & Rehabilitation – Phase II	March 1, 2007
	6. Performing Organization Code
7. Author(s)	**8. Performing Organization Report No.**
Julio F. Davalos, Karl E. Barth, Indrajit Ray, Chunfu Lin, William Sasher, and George Parish	
9. Performing Organization Name and Address	**10. Work Unit No. (TRAIS)**
West Virginia University P.O. Box 6103 Morgantown, WV 26506-6103	**11. Contract or Grant No.** 030407-2
12. Sponsoring Agency Name and Address	**13. Type of Report and Period Covered**
The Pennsylvania Department of Transportation Bureau of Planning and Research 400 North Street, 6th Floor East Harrisburg, PA 17120	Final Report: March 28, 2006 – March 5, 2007
	14. Sponsoring Agency Code

15. Supplementary Notes

16. Abstract

To demonstrate the technical and cost-effective application of externally bonded FRP for retrofit of a concrete T-beam bridge, the specific candidate bridge was selected from those defined as Class-1 structures in Phase I. An assessment and evaluation of in-situ materials and field-obtained samples was conducted. Structural analysis based on AASHTO specifications and finite element modeling was performed to examine the capacity of the selected bridge. The FE model was calibrated by using testing data of the bridge under truck loads. A design approach for the FRP strengthening was proposed and illustrated. Finally, advice on effective protocols to follow for successful implementation of the field work was given.

17. Key Words	18. Distribution Statement
Field assessment, evaluation, structural analysis, testing, FRP, design.	No restrictions. This document is available from the National Technical Information Service, Springfield, VA 22161

19. Security Classif. (of this report)	20. Security Classif. (of this page)	21. No. of Pages	22. Price
Unclassified	Unclassified	114	

DISTRICT 3-0 INVESTIGATION OF FIBER-WRAP TECHNOLOGY FOR BRIDGE REPAIR AND REHABILITATION (Phase II)

Final Report

Submitted to:

Pennsylvania Department of Transportation
Bureau of Planning and Research
400 North Street
6th Floor East
Harrisburg, PA 17120

Submitted by:

Dr. Julio F. Davalos, Benedum Distinguished Teaching Professor
Dr. Karl E. Barth, Associate Professor
Dr. Indrajit Ray, Research Assistant Professor
Dr. Chunfu Lin, Post-Doctoral Fellow
William Sasher, Graduate Research Assistant
George Parish, Graduate Research Assistant

Department of Civil and Environmental Engineering
West Virginia University
Morgantown, WV 26506-6103

March 1, 2007

ACKNOWLEDGMENTS

The authors would like to acknowledge the financial support received from the Bureau of Planning and Research, Pennsylvania Department of Transportation, and the invaluable suggestions from the officials and engineers of PennDOT, District 3-0. In addition, special thanks go to Mr. Jeffrey Levan, P.E., Project Technical Advisor, PennDOT, District 3-0, for his assistance in field evaluations, and testing of the selected bridge without whom this project could not have been successfully completed.

Table of Contents

DISTRICT 3-0 INVESTIGATION OF FIBER-WRAP TECHNOLOGY FOR BRIDGE REPAIR AND REHABILITATION (Phase II)

SUMMARY

In Phase I, both the technical and economical feasibility of externally bonded FRP for concrete bridge repair or retrofit was extensively evaluated. Through a comprehensive literature review and an effective survey of state DOTs, it was concluded that FRP technology showed favorable attributes and advantages over conventional repair methods. A criterion was developed for ranking the District 3 concrete T-beam bridges into three categories as candidates for possible repair with FRP: Level 1 having extensive damage and all work to be done by contract; Level 2 having moderate damage and the repair work to be implemented by a combination of contract and district forces; and finally Level 3 with minor damage and all repair work to be performed by district forces.

It was recommended in Phase I that the field implementation phase should follow sequentially bridge projects beginning with Level 1 and followed by Levels 2 to 3. This proposed approach will serve effectively to transfer knowledge to district personnel and permit them to participate in hands-on training. A cost analysis was performed for actual representative District 3 bridges for the 3 levels of proposed repair indicated above. In relation to conventional repair methods, the FRP technology was shown to be significantly more cost effective for Level 1, particularly in relation to total bridge replacement, and either less or equally costly for Levels 2 and 3, depending on the scenarios considered. Thus, it was concluded in Phase I that District 3 would significantly benefit from implementation of FRP technology for the repair of concrete T-beam bridges, with potential application to a large majority of the 300 District 3 bridges considered in this study. Moreover, the guidelines developed through a District 3 field demonstration project can serve PennDOT statewide for T-beam repair/retrofit and in general for future applications to various types of concrete bridges.

The objective of Phase II is to demonstrate the technical and cost-effective application of

externally bonded FRP for Level-1 retrofit of a concrete T-beam bridge. The goal is to develop guidelines for an effective implementation protocol and design standards to be used by PennDOT, and also to provide a forum for technology transfer by close involvement of District 3 personnel throughout all aspects of the demonstration project. The effort in Phase II includes selecting the candidate bridge, implementing field assessments and structural evaluations, proposing and illustrating a design approach for the FRP, and assisting with bid documents and requirements. This research will lead to future field implementation work and research support that will include assisting with QC procedures for materials and workmanship, implementing supporting small- and large-scale laboratory tests, performing structural and cost analyses of the completed work, and finally developing guidelines for PennDOT.

The Phase II project is organized into 8 tasks, namely Task A: Selection of Candidate Bridge, Task B: Field Assessment of Selected Bridge, Task C: Evaluation of In-situ Materials and Field Samples, Task D: Structural Analysis of Existing Bridge, Task E: Testing of Existing Bridge, Task F: Design of FRP Repair and Other Work, Task G: Assisting District 3 with Bid Documents and Requirements, and Task H: Reports and Presentations. This report includes the tasks listed above, as summarized next. Task A describes selection of a candidate bridge for repair. In collaboration with District 3, a suitable bridge was selected, from those classified for Level-1 repair in Phase I. The field assessment of the selected bridge is described in Task B, including material sampling and visual inspection. The methods for obtaining samples of deck concrete, beam concrete, and beam reinforcing steel are described. Task C describes both the in-situ and the laboratory testing of the bridge materials. The standard tests include an ultrasonic pulse velocity test on beam concrete, a rebound hammer test on beam concrete, compressive strength tests on deck concrete, a carbonation test on both beam and deck concrete, SEM-EDX analysis on beam and deck concrete, and tension tests of the beam reinforcing steel. Test methods, results, and commentary are provided. Task D outlines structural analysis of the existing bridge, including loading rating analysis based on BAR7 software and AASHTO specifications, and finite element analysis using the commercial software ABAQUS. The finite element model was implemented by simulating existing conditions and applying various loadings in order to determine current capacities of the bridge, and to identify critical load conditions for field testing. The results from finite element analysis were compared with those of field testing and analysis based on AASHTO specifications. Task E describes field testing of the existing bridge. The structural response of the bridge was evaluated by applying loaded trucks and recording displacements and frequency. The testing results were used to calibrate the finite element model to increase its accuracy. Task F outlines design of FRP for flexural and shear strengthening for members whose capacities are deficient in resisting the required demands based on the structural analysis in Task D. Task G provides advice on effective protocols to follow for successful implementation of the field work. Finally, a summary and conclusions is given.

Task A: Selection of Candidate Bridge

It was recommended in Phase I that the field implementation phase should begin with bridge projects rated at Level 1 and be followed by those rated at Levels 2 and 3. Seven candidate bridges for Level 1 repair with FRP were recommended by District 3 and are listed in Table 1. In close collaboration between District 3 personnel and the research team, the candidate bridge #49-4012-0250-1032, located near Sunbury, Northumberland County, PA, was selected. This is a 48 ft long single-span bridge with a total deck width of 26'-11". The superstructure consists of six reinforced concrete girders monolithically cast with an 8.5" deep deck, plus a 2.5" overlay placed over the deck. It can be assumed that the bridge is simply-supported by the abutments. As shown in Figure 1, this bridge has extensive overall damage and would require future replacement without extensive rehabilitation utilizing FRP or conventional repair methods.

.

Table 1: PennDOT District 3-0 Suggested Bridges for Repair (Best to Least)

Bridge Number	Class	Damage Rank	Status	Span (ft)	Year	ADT	ADTT	Note
59-0045-0310-2011	1	3	Extensive overall damage	1 (30)	38	10300	650	(a), (c)
59-0045-0430-1068	1	3	Extensive overall damage	1 (29)	37	10300	650	(a)
49-4012-0250-1032	1	3	Extensive to moderate overall damage	1 (48)	34	2200	100	(a), (b)
58-4024-0110-0000	1	3	Extensive overall damage	1 (46)	34	650	110	(a)
19-1014-0052-0422	1	3	Extensive overall damage	1 (29)	38	3300	100	(c)
41-0220-0131-1268	1	2	Extensive local damage	1 (45)	41	11000	1100	(c)
41-2005-0052-0000	1	3	Extensive overall damage	1 (39)	25	2400	210	(d)

Note:

(a) Bridge would require replacement without extensive superstructure rehabilitation using FRP or other conventional repairs
(b) If the spalling of the deck underside due to inadequate cover could be addressed, this would be the preferred choice
(c) Possible access issues for easy repair
(d) May encounter issues with getting in the stream (warm-water and over a trout stream)

Bridge: #49-4012-0250-1032
PennDOT Choice Number: 3
Our Choice Number: 1
Class #1
Span: 48 ft.
Damage Ranking: 3

This bridge has extensive overall damage. This bridge represents a repair-level 1 (Large Scale Repair) candidate.

*Note: This bridge is located 51 minutes South of PennDOT D-3 Headquarters.

* Note: If the spalling of the deck underside can be addressed, this is PennDOT D-3's top choice.

Figure 1: Underside views of the Selected Bridge for Level-1 Repair with FRP

Task B: Field Assessment of Selected Bridge

On May 24, 2006, a field-view was held at Bridge #49-4012-0250-1032 near Sunbury, Northumberland County, PA. Attending from WVU were: Dr. Julio Davalos, Dr. Karl Barth, Dr. Indrajit Ray, Dr. Chunfu Lin, George Parish, William Sasher, David Turner and Daniel Brayack; from PennDOT District 3: Jeffrey Levan and Todd Hardy; and from Fyfe Co. Zachary Smith. The purpose of this meeting was to discuss Phase II of the District 3-0 Investigation of Fiber-Wrap Technology for Bridge Repair and Rehabilitation project. The team from West Virginia University obtained material samples from both the beams and the deck, performed non-destructive evaluations of the concrete, and noted the current damage on the superstructure by means of visual inspection (Figure 2). The WVU team's work was observed by the PennDOT personnel listed above, and a flagging crew maintained traffic while the WVU team obtained core samples from the deck.

Figure 2: Underside of Bridge #49-4012-0250-1032

B.1 Core Sampling of Deck

Two core samples were obtained from the bridge deck using a commercial core-drill; one at midspan (22'- 6" from the South abutment) and one at the quarter point (11'- 3" from the South abutment). Both samples were taken at a location of 8'- 2" from the left edge of the bridge, which is between beams 2 and 3 (Figure 3). Each sample represented the entire depth of the deck (Figure 4 and Figure 5).

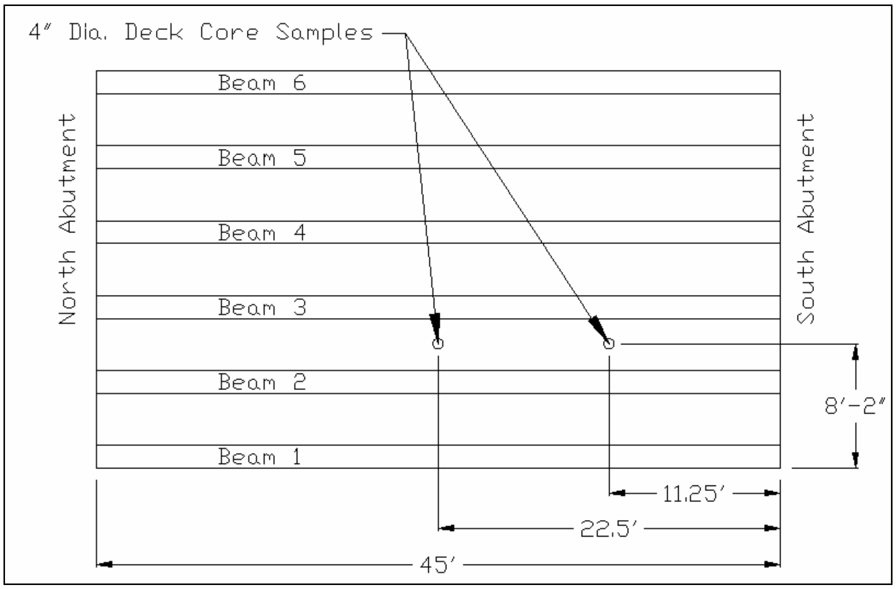

Figure 3: Location of Deck Core Samples

Figure 4: Core Drilling Deck

Figure 5: Deck Core Sample

B.2 Sampling of Beam Reinforcing Steel

A single sample of beam reinforcing steel was cut from the bottom row of reinforcement on the fascia outer side of beam 1. It can be seen in Figures 6 and 7 the sample bar that was taken and its relative location on the span. The steel sample was 8.5' long and this particular bar was chosen because it was completely exposed with no bond to the concrete. PennDOT design drawings show that the square reinforcing steel had a cross-section of 1.25"x1.25" at the time of construction.

Figure 6: Removing of Reinforcing Steel Sample from Beam 1

Figure 7: Cutting of Reinforcing Steel Sample from Beam 1

B.3 Visual Inspection

A visual inspection of the beams was performed by the WVU team. Fascia beams 1 and 6 showed the most damage with severe delamination and spalling along with several cracks. First interior beams 2 and 5 also showed significant areas of spalling, delamination, and localized cracking. Deterioration of beams 1 and 6 is primarily due to water leakage from inadequate downspouts and increased exposure to the elements. Interior beams 3 and 4 showed minimal damage with minor localized spalling or delamination. Figures 8-13 show example sections of each of the beams.

Figure 8: Beam 1 Spalling and Delamination of Cover

Figure 9: Beam 2 Spalling and Delamination of Cover

Figure 10: Localized Spalling on Beam 3

Figure 11: Localized Spalling on Beam 4

Figure 12: Spalling and Delamination of Cover on Beam 5

Figure 13: Extensive Damage on Beam 6

Task C: Evaluation of In-situ Materials and Field Samples

C.1 In-Situ Non-destructive Concrete Tests

Two non-destructive tests were performed on the concrete beams: an ultrasonic pulse velocity test, and a rebound hammer test.

C.1.1 Ultrasonic Pulse Velocity Test

In the ultrasonic test, pulse velocity was determined according to ASTM C 597 at ten different locations on the bridge girders. An ultrasonic pulse velocity V-Meter MK II, James Instruments, Inc., was used with an 82 kHz transducer. Four beams were included in this test: two determined to be in good condition by visual inspection (beams 3 and 4) and two determined to be in poor condition (beams 1 and 2). Transducers were placed on each side of the beam at locations of 4.5’, 5.0’, and 5.5’ from the South abutment. Transducers were placed on beams 2, 3, and 4 (approximately 4.5” from the bottom) spaced equally across the horizontal width of the web (see Figure 14). Because of the rough-textured coating on the fascia side of beam 1, a diagonal distance was measured from the inner face of the web to the bottom side of the beam (see Figure 15). However, the results for the diagonal readings were discarded due to the high concentration of steel reinforcement at this location. The test areas were prepared adequately and petroleum jelly was used as a coupling agent.

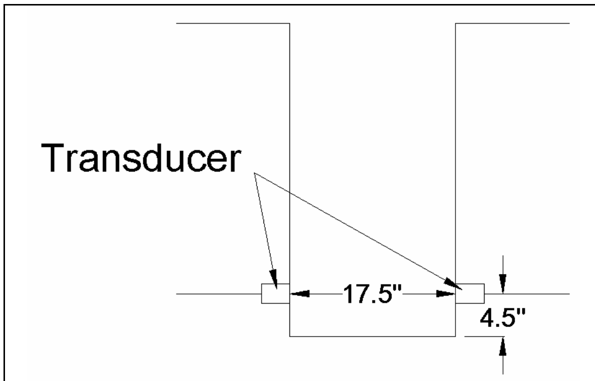

Figure 14: Location of Transducers for Ultrasonic Test on Beams 2, 3, and 4

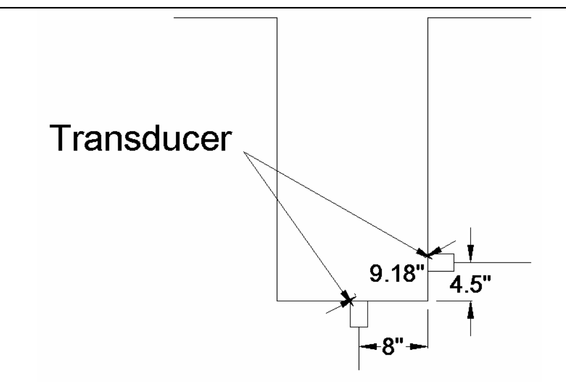

Figure 15: Location of Transducers for Ultrasonic Test on Beam 1. Fascia side is on left in this figure.

The pulse velocity was calculated by dividing the distance between transducers by the transit time. The results for beams 1 and 2 are taken from an average of 3 readings each, and the results for beams 3 and 4 are taken from an average of 6 readings each. The results show that the pulse velocity for beams 1 and 2 is 1900 m/s and that the pulse velocity for beams 3 and 4 is 4300 m/s. These readings indicate that, as predicted, the condition of beams 1 and 2 is inferior to that of beams 3 and 4. Typical values for pulse velocity of good concrete range from 3700 to 4200 m/s. Velocities greater than 4570 m/s indicate very good concrete and values less that 3050 m/s indicate poor concrete. From pulse velocity results (1900 m/s) it is evident that the quality of concrete in beams 1 and 2 is extremely poor and retrofitting will require major removal and replacement. The quality of concrete in beams 3 and 4, though they have experienced some deterioration, is within a typical range. These concretes (beams 3 and 4) can be used after filling the internal voids and cracks by epoxy injection grouting with some nominal removals. See Table A.2 in the Appendix for data obtained at the bridge site.

For comparison purposes, the effect of reinforcement need not be considered since each beam has the same percentage of reinforcement (as seen in the design plans). If the pulse velocity for individual beams is being analyzed, a corrected pulse velocity for plain concrete can be calculated as follows:

For Beam no. 1 and 2 (visually bad): Corrected pulse velocity = 0.85 x 1900 = 1615 m/s
For Beam no. 3 and 4 (visually good): Corrected pulse velocity = 0.85 x 4300 = 3655 m/s

The above numbers are based on four rebars in a row oriented perpendicular to the direction of propagation. Each bar was assumed to have a 1.25”x1.25” cross section.

C.1.2 Rebound Hammer Test

The rebound number was determined according to ASTM C 805 on six different locations on the beams of the bridge. Three locations were tested on two beams with high visible deterioration and corrosion (beams 1 and 2) and three locations were tested on two beams that were visually determined to be in relatively good condition (beams 3 and 4). The rebound number was measured on the web of the T-beams both horizontally and upwardly using Schmidt hammer Proceq SA, Model NR. The test area was prepared adequately, but no grinding was done. Eight readings were taken at each location and the average results were obtained. Any reading differing from the average by more than 7 was discarded. If two or more readings differed by more than 7, the entire data set was discarded.

On beams 1 and 2, the area tested was a 4"x 4" square on the right side of each beam centered approximately 5' from the South abutment and 4.5" from the bottom of the beam (see Figure 16).

On beams 3 and 4, the first area tested was the same as above. The second area tested was within a 4"x 4" square on the underside of and in the center of each beam (see Figure 17). See Table A.3 in the Appendix for data obtained at the bridge site.

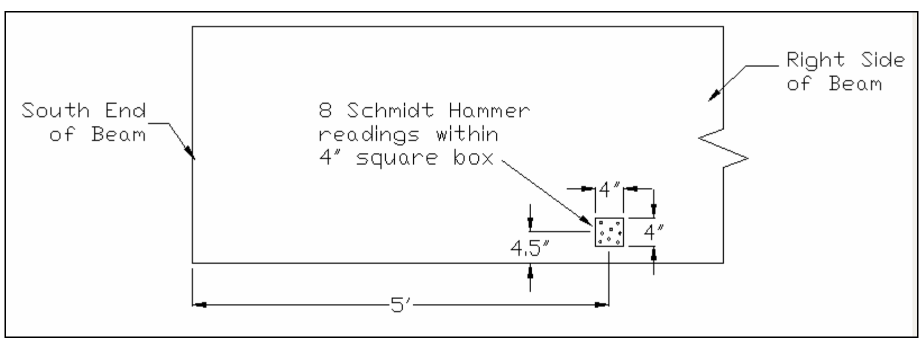

Figure 16: Location of Horizontal Rebound Hammer Tests

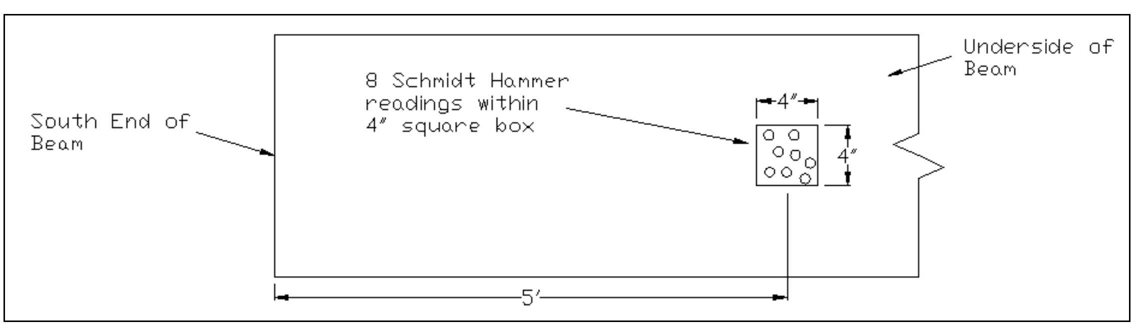

Figure 17: Location of Vertical Rebound Hammer Tests

The horizontal rebound number for the side of beams 1 and 2 was 40, and the horizontal rebound number for the side of beams 3 and 4 was 56. The undersides of beams 3 and 4 had a vertical (upward) rebound number of 51. These rebound hammer test results confirm the visual observation and pulse velocity results that beams 1 and 2 are in inferior condition compared to beams 3 and 4.

All values show a higher rebound number than is normally expected from this quality of concrete due to severe carbonation (which will be discussed later in this report). Though a calibration curve of rebound number and compressive strength can be provided, it should not be used to assess the compressive strength as the rebound numbers are high due to significant carbonation. However, the correlation of results between all beams is valid since all are carbonated to a similar degree and this comparison corroborates well with the results of the ultrasonic pulse velocity test results.

C.2 Laboratory Tests

Several tests were performed at WVU on material samples extracted from the bridge (Figures 18-21).

C.2.1 Core Sample Compression Test

One test cylinder was cut from each of the two core samples using a diamond saw. These cylinders were then tested in compression (ASTM C 42) using a Forney LT-700-2 testing machine. Cylinder 1 (taken from a location of 11'-3" from the South abutment) was found to have a compressive strength of 5005 psi and cylinder 2 (taken at midspan, 22'-6" from the South abutment) was found to have a compressive strength of 6560 psi. See Table A-1 in the Appendix for key values.

C.2.2 Concrete Carbonation Test

The fractured surfaces of the cylinders were tested for carbonation immediately after compression testing by using a Carbo Detect phenolphthalein indicator, James Instruments, Inc. (Figure 22). The reagent turned dark pink throughout the cross section of the cylinders indicating that the deck concrete was not carbonated.

Figure 18: Deck core sample #1 after being cut with diamond saw

Figure 19: Deck core sample #1 loaded in the compression testing machine

Figure 20: Deck core sample #1 immediately after compression failure

Figure 21: Deck core sample #2 immediately after compression failure

Figure 22: Freshly exposed concrete from deck core after compression test. No carbonation was detected in the deck concrete.

A similar carbonation test was conducted on the freshly exposed surfaces of two concrete beam samples as shown in Figures 23 and 24. The phenolphthalein solution on beam samples was found to be completely colorless to a depth of 1” to 1.5”, indicating thorough carbonation and lowering of pH below 9.0 near the beam cover zone. The phenolphthalein remains colorless until the pH drops to about 9; the passive layer breaks down at a pH of 10 or 11. This passive layer may be at a location of 0.2”– 0.4” deeper within the beam than the colorless layer indicates. Therefore, the depth of carbonation may be assumed to be approximately 1.2” to 1.9”.

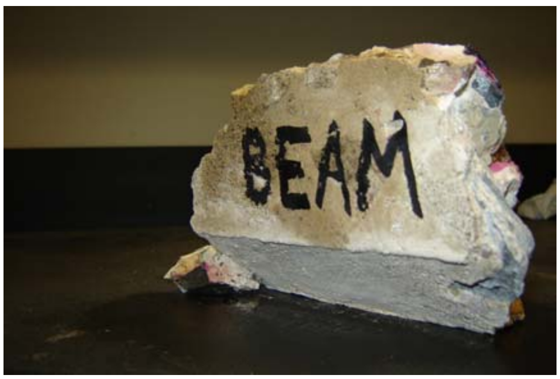

Figure 23: Portion of beam surface. Direct contact with carbon dioxide in the atmosphere has completely carbonated the surface concrete of the beams.

Figure 24: Portion of beam concrete. The beam surface is the left edge of this concrete. Carbonation was detected throughout a depth of 1” to 1½”

C.2.3 Scanning Electron Microscope (SEM) and Energy Dispersive X-Ray (EDX) Analyses

Figures 25, 26, and 27 are from the analysis of beam sample 1. SEM and EDX techniques were used to determine the morphology and qualitative compositions of hydrated pastes in concrete beam samples. The fractured concrete beam specimens were prepared by heating in an oven at 105°C for 24 hours, and then were vacuumed and gold coated. SEM and EDX analyses were performed using a Hitachi S 4700 model scanning electron microscope. Figures 25 and 26 show the formation of calcium carbonate (calcite), which is the result of the conversion of calcium hydroxide crystals to calcite and the decalcification of Calcium Silicate Hydrate (C-S-H) gel at a later stage. Typical calcium carbonate granular crystals and some dogtooth crystals can be seen in Figures 25 and 26. EDX confirmed the formation of calcite mostly at the expense of C-S-H gel (Figure 27). The phenolphthalein indicator test confirmed the carbonation of beam concrete, as previously described.

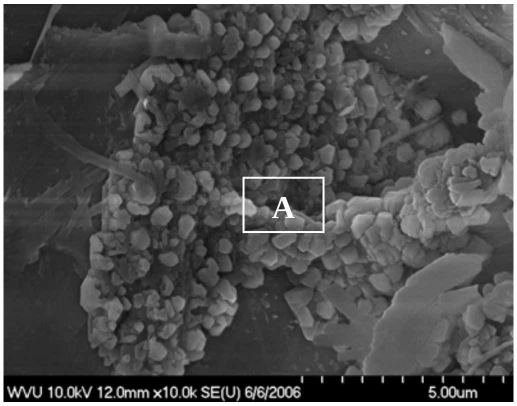

Figure 25: SEM Image from Beam Sample 1

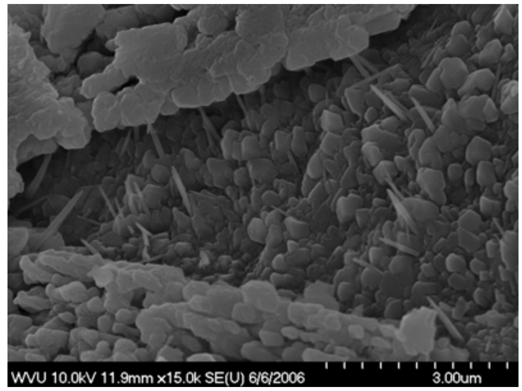

Figure 26: SEM Image of Beam Sample 1

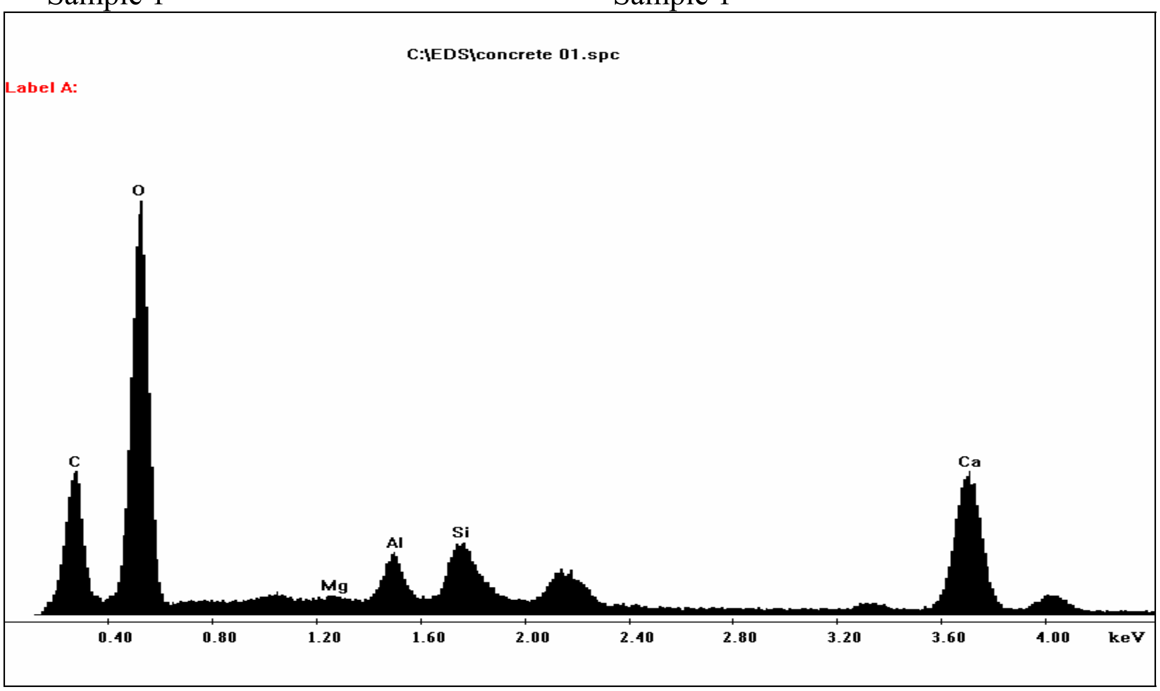

Figure 27: Beam Sample 1 - EDX Spectrum at Location A in Figure 26

Figures 28 and 29 are from the analysis of beam sample 2. Chloride based de-icing salt exposure for long periods of time might have reacted with aluminous phases and calcium hydroxide crystals in the cement paste to form platy crystals (Figure 28). It is also possible that chloroaluminate was formed. The EDX data in Figure 27 also confirms the formation of calcite, mostly at the expense of calcium hydroxide (C-S-H is less affected in this location). Traces of sodium are detected in the EDX due to the effect of sodium chloride de-icing salts (Figure 29).

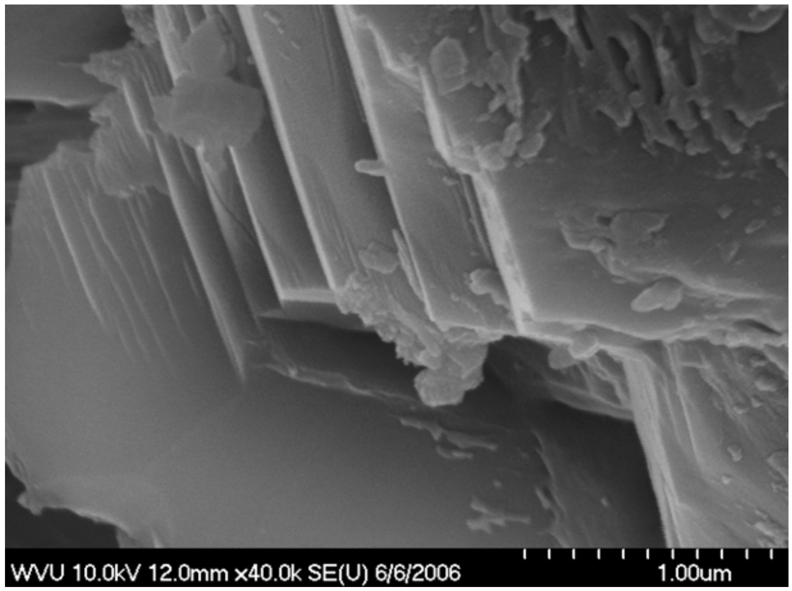

Figure 28: SEM of beam sample 2

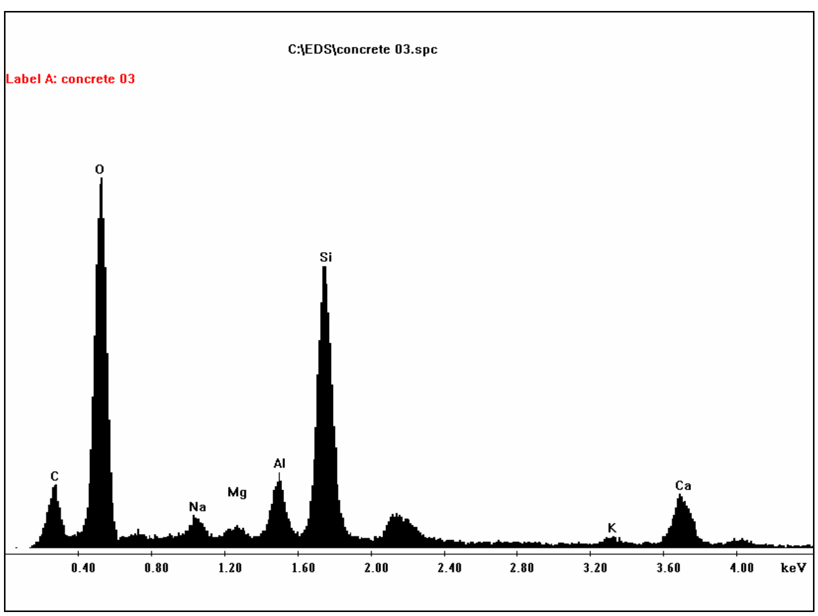

Figure 29: EDX spectrum at center of Figure 28

Figures 30 and 31 are from the analysis of beam sample 3. The solubility of calcium hydroxide increases when exposed to saline solutions. Figure 30 indicates the substantial leaching of calcium hydroxide due to the presence of chloride solutions in the concrete. Stacked prismatic crystals with some needle shaped morphology can also be seen in Figure 30, which indicates the formation of calcite. The EDX data shown in Figure 31 strongly confirms what is observed in the SEM photo.

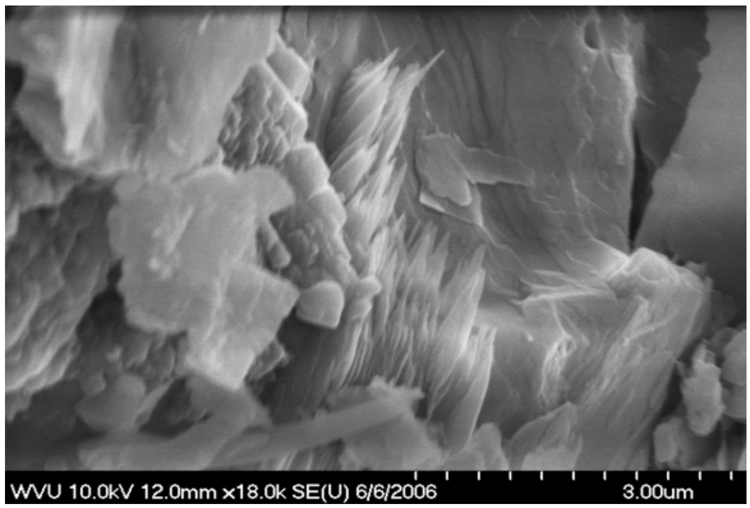

Figure 30: SEM of beam sample 3

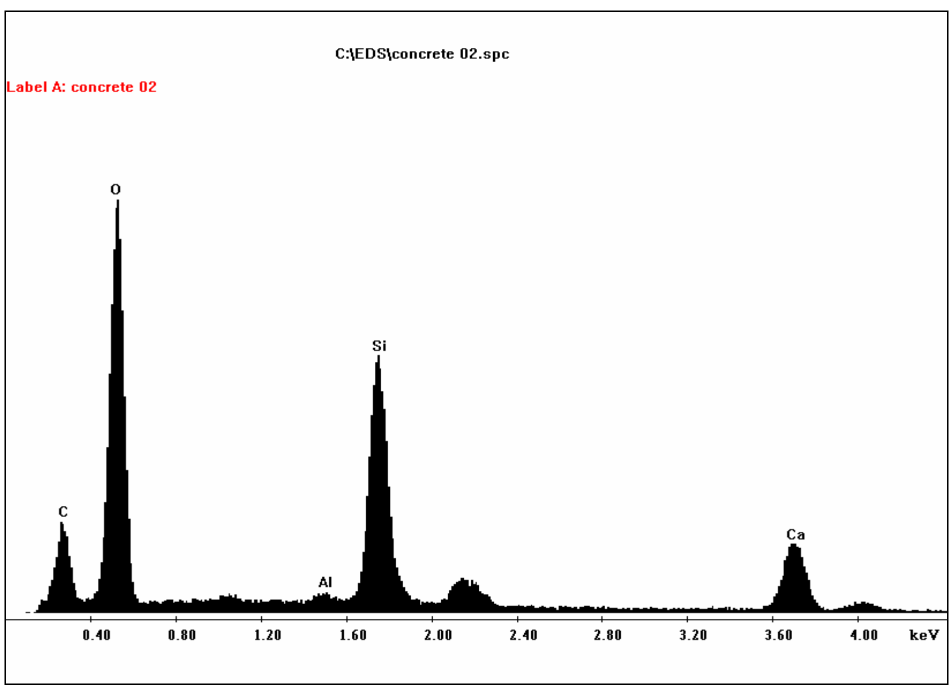

Figure 31: EDX spectrum at center of Figure 30

C.2.4 Chemical Analysis of Concrete Powder Samples

Powder samples were made from beam 1 and each of the two deck cores using a mortar and pestle and a 45-micron sieve. Acid soluble chloride content and cement content analysis was performed using the soluble silica method.

C.2.4.1 Cement Content by Soluble Silica

The cement content analysis was performed according to ASTM C 1084. Three powder samples were taken from each of the 3 specimens: beam, deck core 1, and deck core 2. The average results from each set of three samples are reported below:

(a) Soluble silica for beam = 2.16 % by mass of concrete powder
(b) Soluble silica for deck core 1 = 3.01 % by mass of concrete powder
(c) Soluble silica for deck core 2 = 2.76 % by mass of concrete powder

Soluble silica is directly related to the quantity of portland cement in hardened concrete. Since the silica content of the original portland cement is unknown, the percentage of cement in the concrete is calculated by dividing the percent silica (above values) by 21% and multiplying by 100 (ASTM C 1084). Although the values are approximate, they are still very useful for comparison.

(a) Cement percentage for beam = 10.3%
(b) Cement percentage for deck core 1= 14.33%
(c) Cement percentage for deck core 2= 13.14%

Assuming the dry density of concrete is 145 lb/ ft^3 (a value that also agrees well with measured bulk density), the cement content for one cubic yd of concrete may be estimated in each case as:

(a) Estimated cement content in beam = 10.3 x 145 x 27/100 = 403 lb/yd^3
(b) Estimated cement content in deck core 1= 14.33 x 145 x 27/100 = 561 lb/yd^3
(c) Estimated cement content in deck core 2= 13.14 x 145 x 27/100 = 515 lb/yd^3

A comparison of data shows that the beam sample has very low cement content compared to that of deck core 1 and deck core 2 (28% lower than core 1 and 21% lower than core 2). The values from core 1 and core 2 differed by only 9%. These results indicate that, over time, much leaching of C-S-H gel and calcium hydroxide has occurred within the beam. The SEM-EDX and phenolphthalein tests indicate that carbonation and severe chloride attack may have caused this leaching. In some cases, the carbonation and chloride attack may have converted C-S-H gel and calcium hydroxide to weak reaction by products, mainly calcite along with some chloroaluminates. The ultrasonic pulse velocity test confirmed the presence of cracks and voids across the beam. The deck slab was in a relatively better condition, although there was some evidence of chloride attack. This low cement content increases the risk of corrosion as will be discussed further.

C.2.4.2 Acid soluble chloride

The acid soluble chloride test was performed according to ASTM C 1152. The results are as follows:

(a) Soluble chloride for beam = 0.164% by mass of concrete powder
(b) Soluble chloride for deck core 1 = 0.199% by mass of concrete powder
(c) Soluble chloride for core 2 = 0.025% by mass of concrete powder

ACI 318 provides a maximum water soluble chloride ion limit for concrete in percent by mass of cement to protect against corrosion. For a structure in service containing regular reinforced (not epoxy- or zinc-coated) concrete exposed to chloride (such as the PennDOT bridge), the limit is 0.15% water soluble chloride ions by mass of cement. Another chloride threshold is 0.2 to 0.4% acid soluble chlorides by mass of cement or 1 lb/yd^3 of chloride in concrete in order to limit corrosion. Using the soluble chloride values determined by ASTM C 1152 and by using the cement content values as estimated by ASTM C 1084, the quantities of acid soluble chloride in the beam specimen, core 1, and core 2 are calculated as 1.6 %, 1.4%, and 0.19%, respectively. From these results, it may be concluded that the concrete in the beam and core 1 have no protection against corrosion since the chloride threshold limits are grossly exceeded.

As displayed previously, visual observation shows severe spalling and delamination at the bottom faces of the beams. Measuring ultrasonic pulse velocity horizontally across the width of the beam can detect delamination and loss of structural integrity. SEM-EDX analysis confirmed the formation of reaction by products due to severe carbonation and chloride attack, a sign that the concrete strength was negatively affected. The phenolphthalein test also indicated carbonation of the beam concrete by the reduction of its pH. The high chloride content in the beam and deck core 1 sample strongly shows the potential for continued corrosion.

The comparison of data shows that the core 2 sample contained the least amount of chloride, whereas both the beam and deck core 1 samples had similarly high chloride contents. The primary source of this chloride is de-icing salts, although it is unknown if a chloride-based accelerator was used during the bridge's construction. It should be mentioned that not all the chlorides detected by this method are available for corrosion initiation. However, the large quantities of chloride salt crystals and their reaction products (chloroaluminate) in deck core 1 and the beam indicate that their concrete is more porous than that of deck core 2. The confirmation of a higher porosity can also be seen in the results of the compression test since deck core 1 had a 25% lower compressive strength than deck core 2.

C.2.5 Steel Tension Test

Six threaded-end test specimens were fabricated from the extracted piece of rebar. The specimens had a length of 5". Tension tests were performed according to ASTM Standard Test Methods for Tension Testing of Metallic Materials (ASTM E 8-04) as shown in Figure 32. The samples were loaded in a Baldwin Tate-Emery Testing Machine.

Dimensions of ASTM Standard Type 1 Threaded Specimen (inches)

D: Diameter = 0.500 ± 0.010

R: Radius of Fillet = ⅜

A: Length of Reduced Section = 2¼

L: Over-all Length = 5

B: Length of End Section = 1⅜

C: Diameter of End Section = ¾

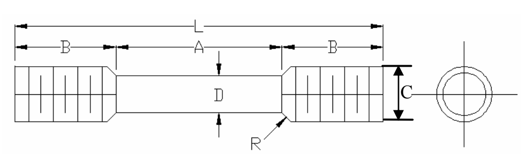

Figure 32: Test Specimen with Dimensions

An MTS Extensometer was used along with a data acquisition system to record load vs. strain throughout the test. This data was used to define the stress vs. strain curve in Figure 33. The average yield stress of the six samples was 37 ksi and the average ultimate stress of the samples was 64 ksi.

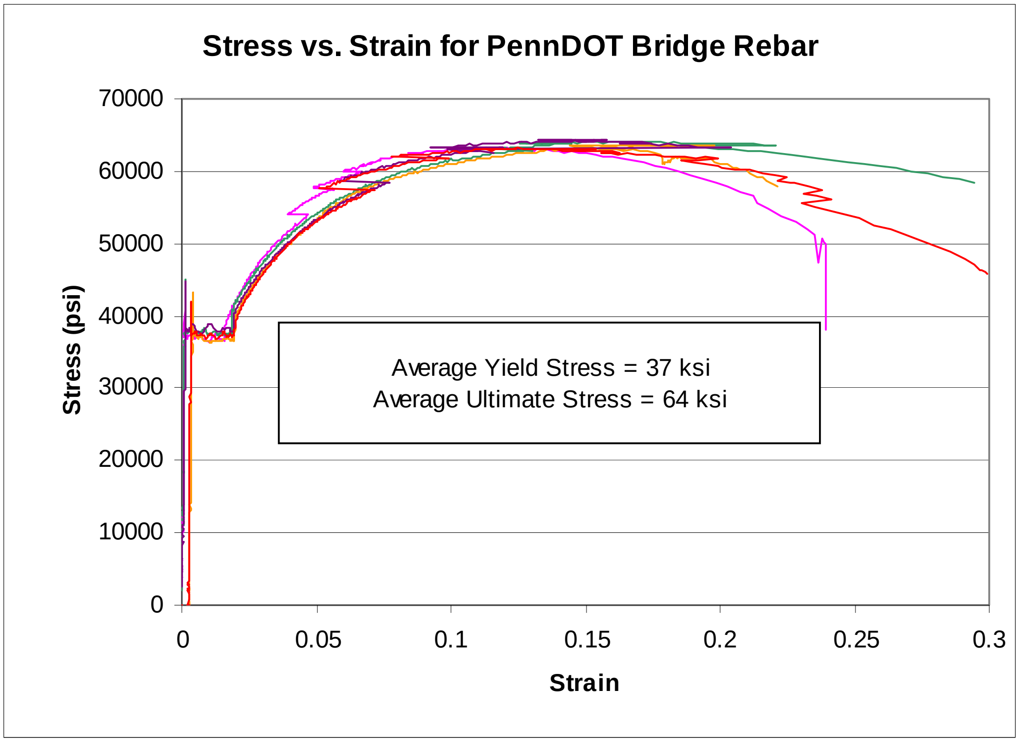

Figure 33: Steel Tension Test Results

Task D: Structural Analysis of Existing Bridge

In this section, the selected bridge is analyzed for existing conditions to examine the capacity of the bridge. Load rating analysis was first performed based on AASHTO Standard Specifications. A Finite Element model was then built, using the commercial program ABAQUS 6.5.

D.1 Load Rating Analysis of Existing Bridge

D.1.1 BAR7 Analysis

The first step in the analysis of the bridge was to identify any limitations of the current analysis procedures and see if there were possible changes to the procedures that would allow a better load rating estimate, while still acceptable within AASHTO specifications. Using Microsoft EXCEL, a program was designed to match the data provided from PennDOT in the BAR7 load rating analysis. Formulating this EXCEL program revealed some limitations of the BAR7 program. The BAR7 program only analyzes one girder at a time. Separate analysis and input data would have to be entered in order to check interior or exterior girders. The data input for PennDOT calculations analyzed an interior girder with a 20% reduction in original flexural reinforcement steel area. Allowances had to be made for the actual loss of flexural reinforcement steel, including the bar that was cut and removed out of Girder 1 for sampling needs.

In the shear calculations, the inclined bars were taken as being present through the entire length of the bridge, as shown Figure 34, but they only go out to about one-third length of the bridge span from the abutment to the centerline. Also, the vertical stirrups input data did not allow for the excessive loss of steel section due to corrosion (see Figures 35 and 36). In some cases, the vertical stirrups were corroded completely through the cross section. The input data also used AASHTO recommended values for steel yield strength and concrete compressive strength. The core samples taken from the deck of the bridge showed concrete compressive strength twice as high as the recommended AASHTO value. The yield strength of the flexural reinforcing steel bar taken from the field sample of Girder 1 was also higher than the AASHTO suggested value.

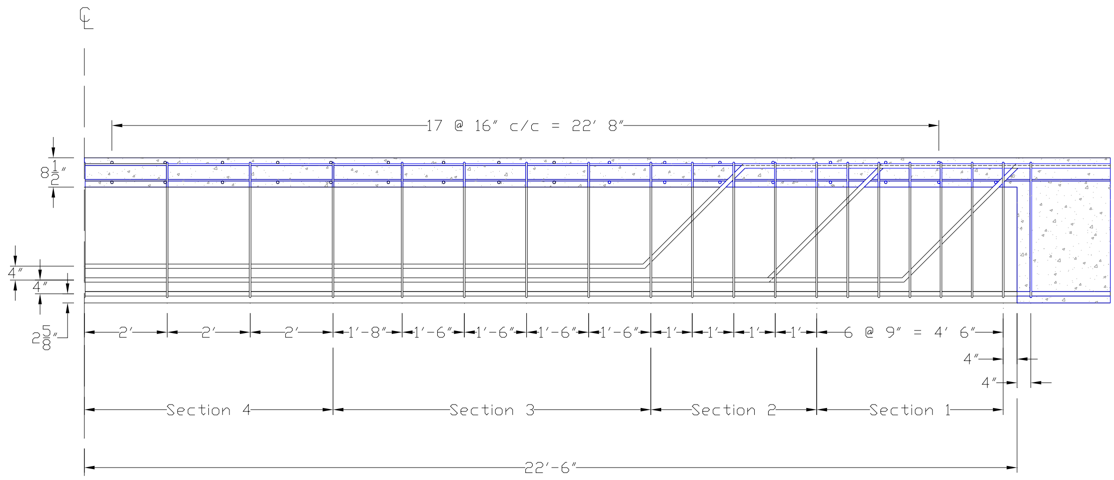

Figure 34: **Shear Reinforcement Diagram**

Figure 35: Visual Inspection of Rebar Deterioration

Figure 36: Flexural Reinforcement Deterioration

D.1.2 AASHTO Analysis

All of the discrepancies and limitations noted in the previous section led to the design of a new program using Microsoft EXCEL. This program allowed the user the ability to include the analysis of all the girders at the same time. It also allowed the user to change certain input values to tailor the program to the specific conditions observed at the bridge site. The program user could specify the percentage of steel section loss in flexural and shear reinforcement as an overall loss, by individual girder, or by girder and section separately. In addition, the user could specify the percentage of parapet load distribution to interior girders. Input values of concrete compressive strength, and steel yield strength were examined using both experimental and AASHTO recommended values under different combinations of steel loss and parapet distributions. The shear calculations were performed to allow the user to include extreme losses of concrete and steel sections. The user could specify whether or not to include the concrete cover on the inside and outside faces of the web. The output could be presented in a simple table format as seen in Table 2. The output would tell the user the controlling girder and section if applicable. Also, the differences between the new results and PennDOT's BAR7 program analysis could easily be seen, in order to determine how the changes were affecting the load rating of the bridge.

Table 2: Sample EXCEL AASHTO Analysis Output

Bridge Load Rating					Controlling Girder	Controlling Section	PennDOT Output	Difference	% Difference
Moment	Inventory Rating Factor	RF_{IRM}		1.03	1 and/or 6	-	0.77	0.26	34.14
	Operating Rating Factor	RF_{ORM}		1.72	1 and/or 6	-	1.28	0.44	34.70
	Inventory Rating Capacity	IR_M	(kips)	37.18	1 and/or 6	-	27.72	9.46	34.14
	Operating Rating Capacity	OR_M	(kips)	62.07	1 and/or 6	-	46.08	15.99	34.70
Shear	Inventory Rating Factor	RF_{IRV}		1.01	2 and/or 5	Section 3	1.05	0.04	3.79
	Operating Rating Factor	RF_{ORV}		1.69	2 and/or 5	Section 3	1.75	0.06	3.64
	Inventory Rating Capacity	IR_V	(kips)	36.37	2 and/or 5	Section 3	37.8	1.43	3.79
	Operating Rating Capacity	OR_V	(kips)	60.71	2 and/or 5	Section 3	63	2.29	3.64

D.1.3 Results of Analysis

After examining the differences in the BAR7 analysis and best and worst case scenarios using AASHTO analysis, it can be seen from Table 3 that the bridge inventory and operating rating factors of Girder 3 and Girder 4 for moment are satisfactory. However, the flexural capacities of Girders 1, 2, 5, and 6 are not adequate and additional reinforcement is needed. Also, the shear calculations showed that additional shear reinforcement is required for all interior girders within Section 3, as defined in Figure 34.

Table 3: Girder Analysis

Bridge Load Rating Summary	Moment					Shear					
	Inv. RF	Diff. from BAR7	Oper. RF	Diff. from BAR7	Cont. Girder	Inv. RF	Diff. from BAR7	Oper. RF	Diff. from BAR7	Cont. Girder	Cont. Sect.
	RF_{IRM}	(%)	RF_{ORM}	(%)		RF_{IRV}	(%)	RF_{ORV}	(%)		
PennDOT BAR7 #'s	0.77	0.00	1.28	0.00	Interior	1.05	0.00	1.75	0.00	Interior	4
Check PennDOT #'s by AASHTO Method	0.78	1.24	1.30	1.66	2 or 5	1.07	1.46	1.78	1.62	2 or 5	1
Exp. Values w/ Min.Vertical Steel Estimate	1.03	34.14	1.72	34.70	1 or 6	0.78	**-25.48**	1.31	**-25.36**	2 or 5	3
Exp. Values w/ Full Concrete Cover on Web	1.03	34.14	1.72	34.70	1 or 6	1.01	**-3.79**	1.69	**-3.64**	2 or 5	3
Worst Estimation Using Exp. Values	0.66	-14.29	1.11	-13.28	1 or 6	0.8	**-23.81**	1.34	**-23.43**	2 or 5	3
Best Estimation Using Exp. Values	1.04	35.06	1.74	35.94	2 or 5	1.02	**-2.86**	1.7	**-2.86**	2 or 5	3
Finite Element Analysis	2.68	248.05	4.47	249.22	Interior	2.53	140.95	4.22	141.14	Interior	3

A slab analysis was done to check whether extra reinforcement would be needed in the slab. Though it is not customary to check shear in the slab, both shear and moment values were checked analyzing the slab as simply supported between the webs of the girders according to AASHTO specifications. The only variables changed between the AASHTO and experimental values were the compressive strength of the concrete and the yield strength of the steel. Since the deterioration of the steel could not be easily investigated, the minimum amount required to be able to maintain an inventory rating of 1.00 was investigated. Using AASHTO values, the minimum percentages of steel required from the original steel are 88% for flexural reinforcement and 66.5% for shear reinforcement. For the experimental values, the minimum required steel areas were 78.5% for flexural reinforcement and 47.5% for shear reinforcement.

Table 4: Slab Analysis

Load Rating Factors		AASHTO Values	AASHTO Values- Min % Tension Steel	Experimental Values	Experimental Values-Min % Tension Steel
Moment Inventory Rating Factor	IR_M^+	1.13	1.00	1.28	1.00
Moment Operating Rating Factor	OR_M^+	1.89	1.66	2.13	1.67
Shear Inventory Rating Factor	IR_V^+	1.46	1.00	1.81	1.00
Shear Operating Rating Factor	OR_V^+	2.43	1.67	3.02	1.67

D.2 Finite Element Analysis of Existing Bridge

The information for the FE analysis was obtained from a combination of available design documents provided by PennDOT District 3 and field information obtained from previous tasks. The model was developed in order to: (1) determine current capacities of the bridge, (2) identify critical load conditions for field testing of the structure, and (3) compare predictions with field responses when actual test truck-loads are used. Subsequently, this model was calibrated using the field test results and modified to increase its accuracy. The calibrated model will permit its confident use in designing the FRP reinforcement.

D.2.1 FE Modeling and Results

The 8-node linear brick element C3D8R, with reduced integration and hourglass control, was chosen to model the concrete. C3D8R was used for the three-dimensional modeling of concrete with or without reinforcing bars. Three-dimensional linear truss element T3D2 was chosen to model flexural and shear reinforcement in girders, deck, parapets, and curbs. T3D2 was embedded into solid element C3D8R (truss-in-solid) to provide a realistic representation for the reinforcement and the displacements of the reinforcing bar coinciding with those of the concrete (perfect bond between the reinforcing bar and the concrete was assumed). This refined approach to 3D geometric-replica analytical modeling is now practical and enables explicitly simulating every material point of the bridge for an accurate representation of the geometry, the actual behavior mechanisms and existing deterioration or damage. The 2.5" overlay was also modeled using C3D8R elements. The surface-based "TIE" constraint was used to couple the non-composite overlay with the composite deck. To simplify the modeling, the cross-section of the parapets was assumed to be rectangular with the same height as of the actual structure. The details of the reinforcing system in the model are shown in Figure 37, and Figure 38 shows the meshed finite element model.

Several assumptions were made in modeling. The bridge was assumed to have consistent material properties in all locations. Their elements represented linear-elastic and isotropic material since the applied load was relatively low with respect to the ultimate load condition. The modulus of elasticity of the concrete was based on the measured compressive strength of the cores obtained from the slab according to the standard equation ACI 318-02, Section 8.5.1: $E_c = 57000\sqrt{f_c^{'}}$. The cross-sectional area of rebar was reduced by 20 percent based on the measured dimension of the rebar sample. In order to account for the presence of the cracks, delamination, and spalling in the girders and curbs, the modulus of elasticity was reduced to near zero for blocks of elements representing these damaged areas, as shown in Figure 39. The depth and width of these blocks were chosen based on the data collected during the field inspection. The concrete Poisson's ratio was set to 0.15. Different element sizes were used to optimize the model and decrease the computation time. The size chosen for the longitudinal and transverse cross sections allowed for easier and more accurate location of the steel rebar and reduced the number of the elements in the "secondary" parts of the model, such as the parapets and the diaphragm beams. Based on the test results of the rebar sample, the modulus of elasticity and the Poisson's ratio for the steel reinforcement were assumed to be 29000 ksi and 0.3, respectively. Since one sample reinforcing steel was cut from the bottom row of reinforcement in beam 1, this section of steel was removed from the model. The structure was modeled using 73,961 elements and 95,754 nodes.

Since the super structure is sitting on and connected to the abutments by 18 anchors at one end and 18 dowels at the other end through the stiff diaphragm beams, pin-pin boundary conditions were then chosen to accurately represent the actual restrains at the boundaries. The bridge was vertically, longitudinally, and transversely restrained at 18 nodes corresponding, respectively, to anchor and dowel positions at each end. Besides the dead load, two lanes were loaded with an HS20 AASHTO truck loading on the top of the overlay. The load was positioned at center span and also at near the support, which were determined to be the critical positions for bending and shear respectively. The wheel loads were assumed as uniformly distributed over an area of 20x10 in^2, as per AASHTO specifications. The uniform loads were discretized as concentrated forces at the nodes corresponding to the truck wheel foot print, and each force was determined by dividing the total distributed load by the number of nodes. The wheel loads are listed in

Table 5. The wheel spacing is shown in Figure 40. As an example, the position of the tandem truck loads used for testing the bridge (see Figure 40) is shown in Figure 41.

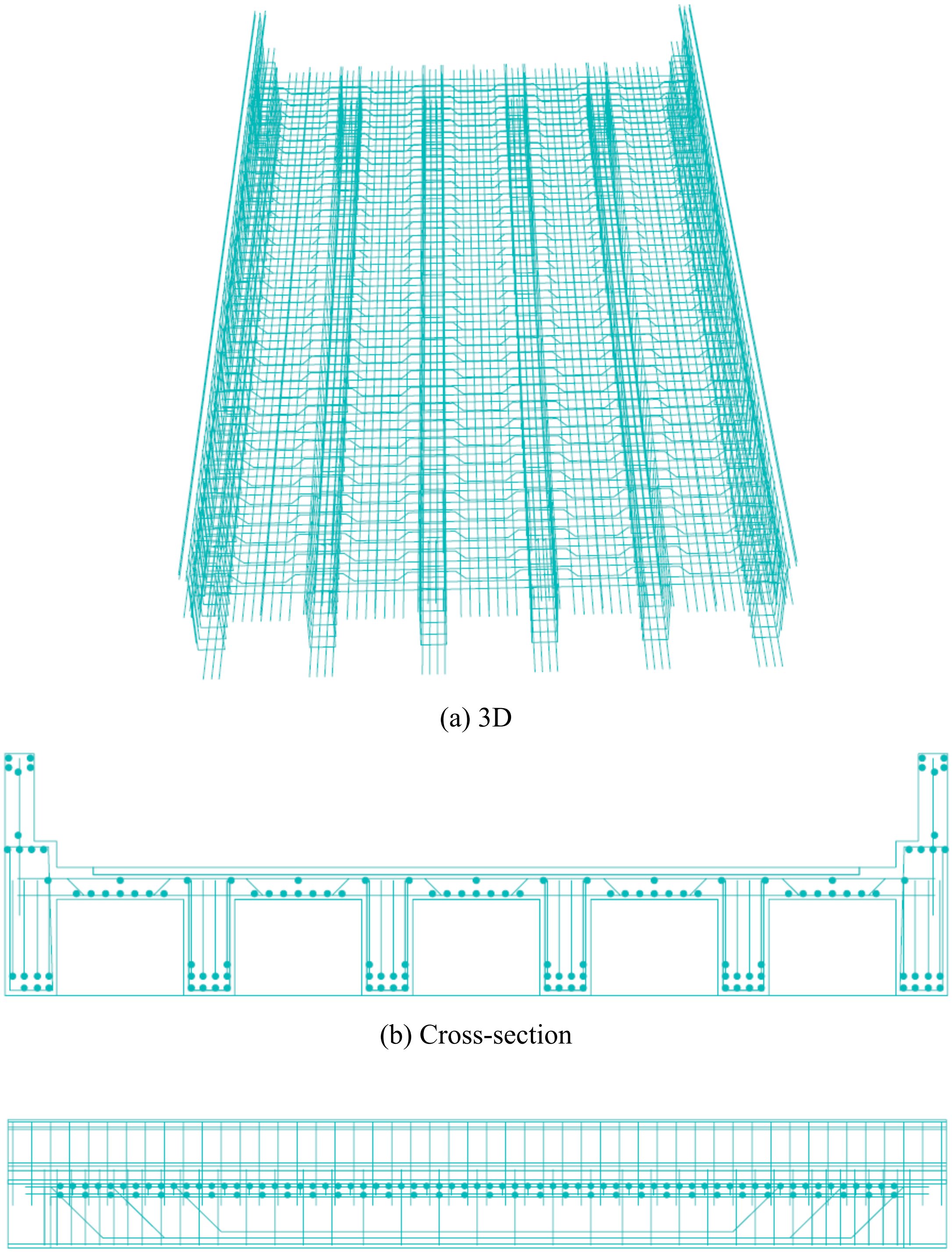

(a) 3D

(b) Cross-section

(c) Side View

Figure 37: Rebar System of the Model

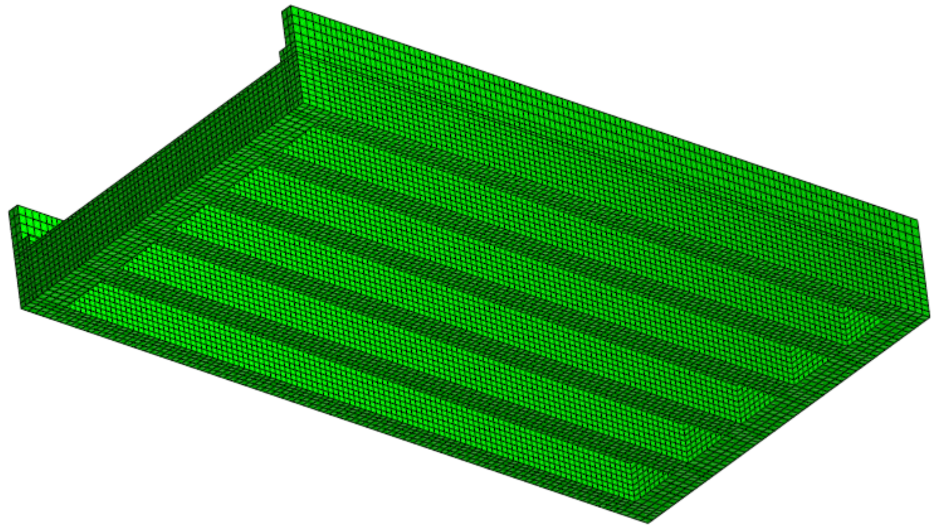

Figure 38: Meshed FE Model

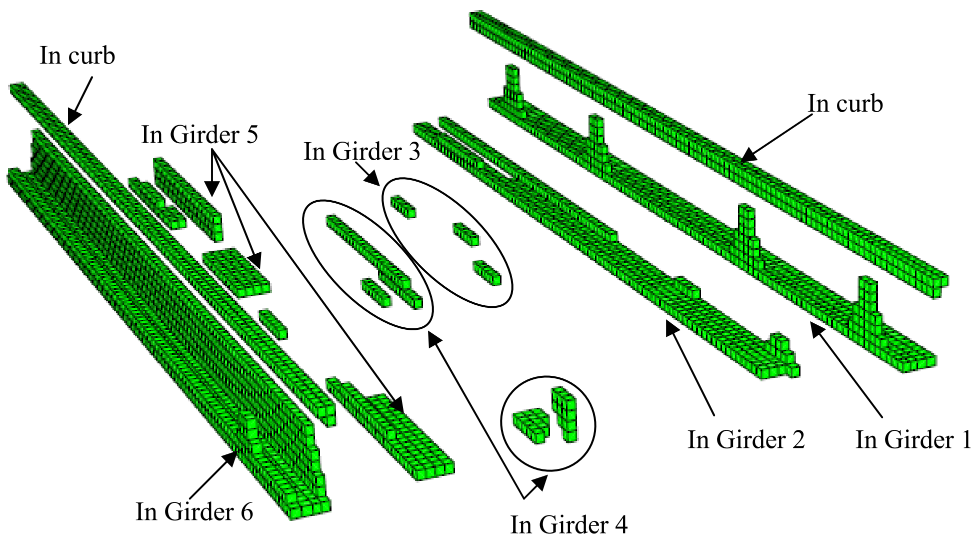

Figure 39: Blocks of Concrete Elements Corresponding to Damage Sections

Table 5: Wheel Loading (lbs) for AASHTO and Tandem Trucks

	AASHTO Truck- HS20			PennDOT Tandem Truck		
	Left	Right	Total	Left	Right	Total
Front	4000	4000	8000	7075	7300	14375
Rear 1	16000	16000	32000	8950	9475	18425
Rear 2	16000	16000	32000	9225	9150	18400
Total			**72000**			**51200**

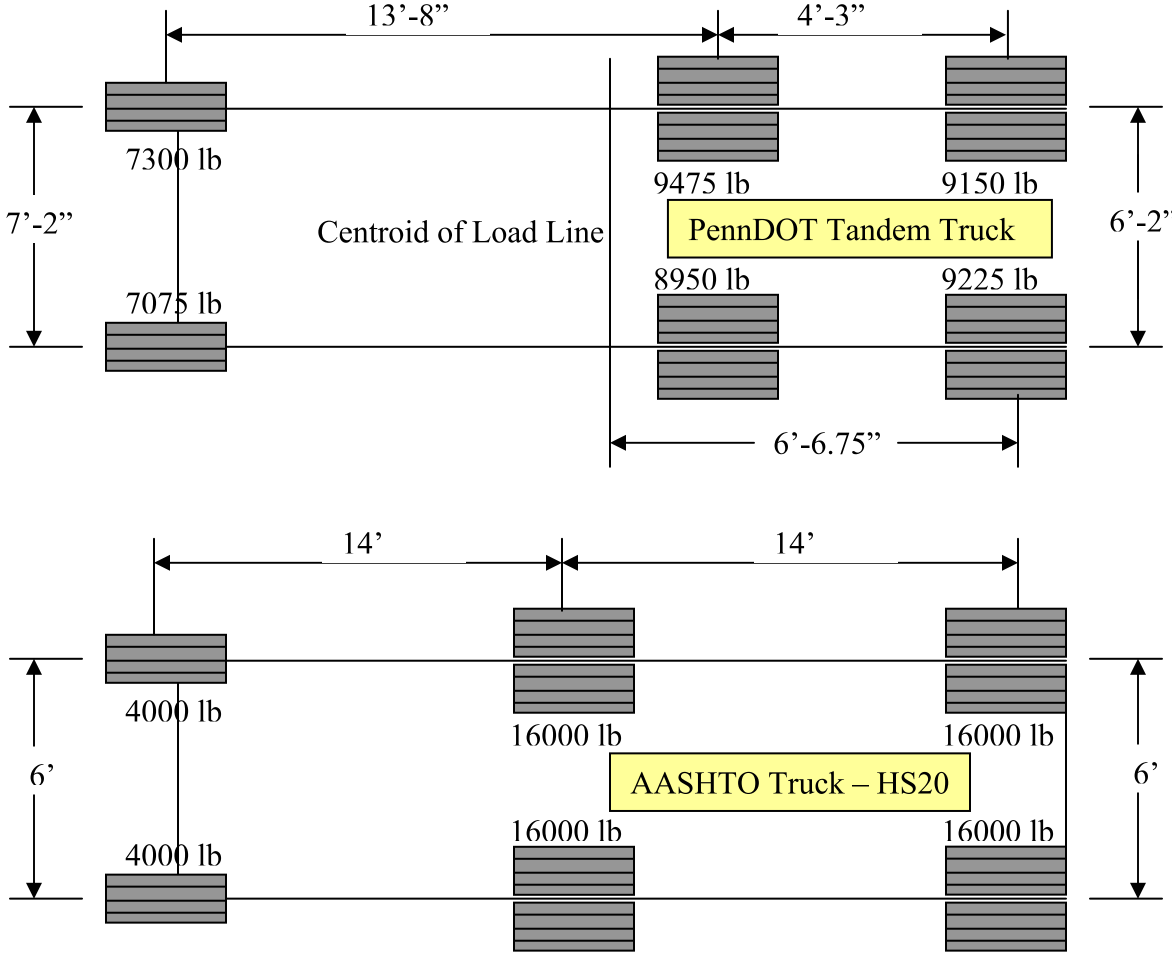

Figure 40: Wheel Spacing

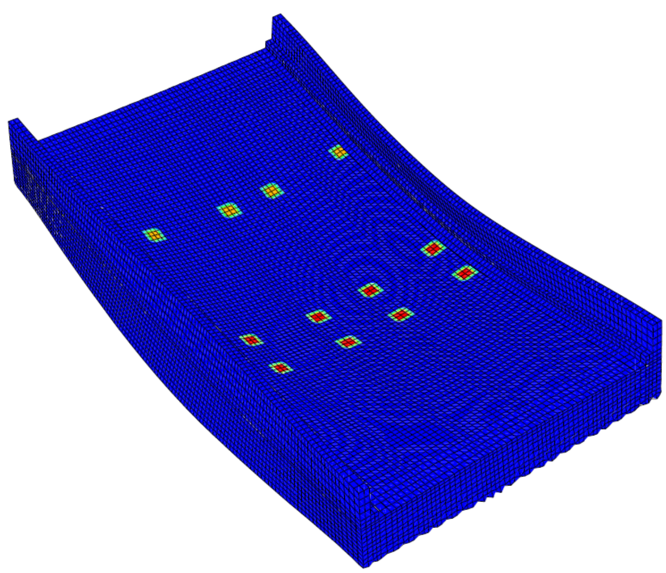

Figure 41: Tandem Truck Load Position

The loading conditions were based on AASHTO specifications. Four load cases were considered in the analysis, as shown in Figure 42. The most critical load condition was determined as Case 3 (Case 1 is almost the same as Case 3). Figure 43 shows a vertical deformation contour plot, and Figure 44 shows two in-plane stress view-cuts.

Figure 45 reports the analytical mid-span displacements under live load relative to Case 1, when the center of gravity of the PennDOT tandem truck is at the mid-span. Figure 46 plots the longitudinal distribution of the displacement in each girder under live load. The testing results are also shown in Figure 45 for comparison, with the FE model under predicting the response by about 11.4%. There are two main reasons for the FE model to be stiffer than the actual structure. One reason is that the overlay was assumed fully composite with the deck, which may not accurately represent the actual condition. The overlay effect on the transverse displacements was studied and the results are shown in Figure 47. We found that removing the overlay from the model will increase the transverse displacements of interior girders by 7% and decrease the transverse displacements of exterior girders by 3%. The other reason is that the concrete material properties, which were obtained from the core samples of the deck, were assumed to be consistent in all locations, but there is uncertainty on the material properties of the girders. However, from field observation and testing of the concrete in the girders, especially in the exterior girders that experienced extensive deterioration, the concrete properties of the girders is inferior to that of the deck.

The boundary conditions have the most significant impact on the response. The friction of anchors and dowels between the stiff diaphragm beams of the superstructure and the abutments create a very effective restraint, preventing any slippage. Lateral soil pressure and pavement thrust further slightly contribute to the restraint. Considering these effects, pin-pin boundary conditions were used in the FE model. When these effects are ignored and the pin-pin boundary conditions are changed to pin-roller, the transverse displacement at mid-span will increase by about 63% as shown in Figure 48. The stiff diaphragm beams also have significant effects on the response. Excluding the diaphragm beams will increase the vertical displacement of girders at mid-span by 20%.

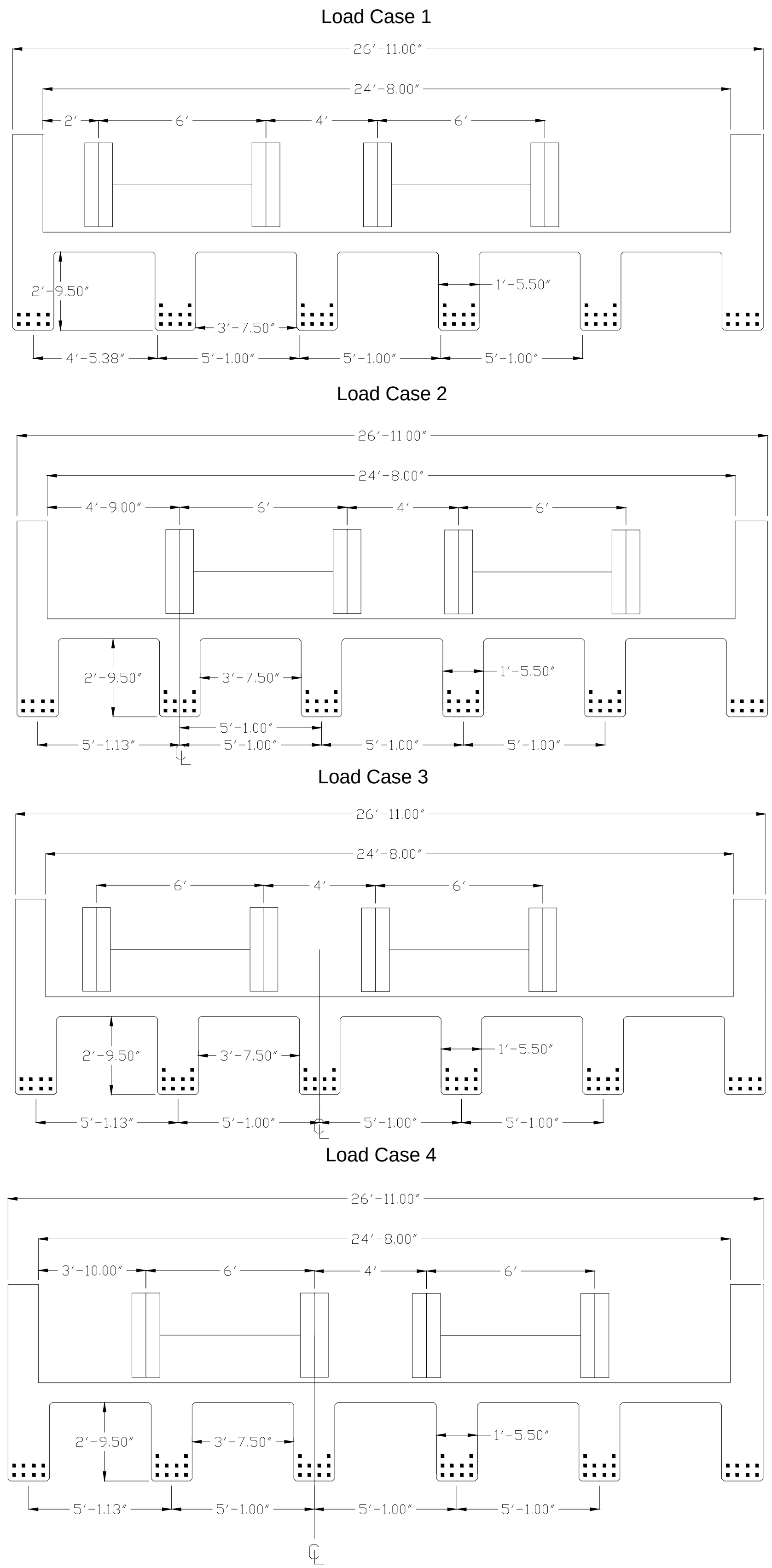

Figure 42: Loading Cases

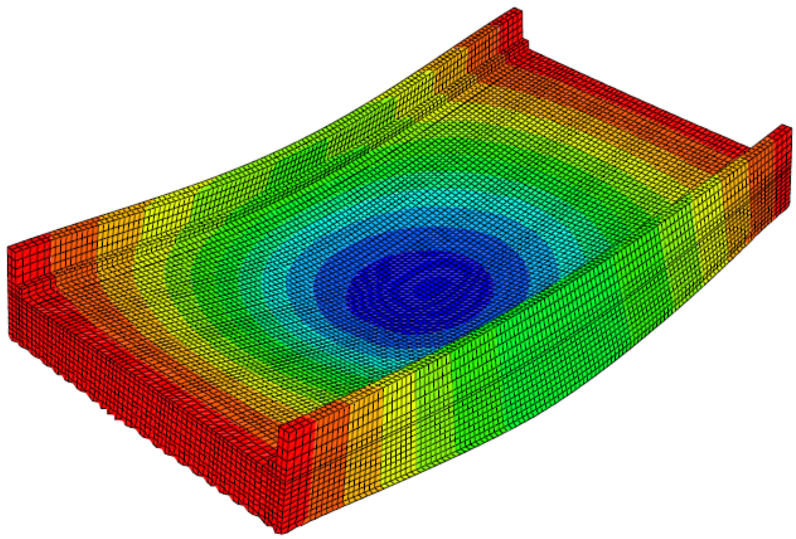

Figure 43: Vertical Deformation Contour Plot

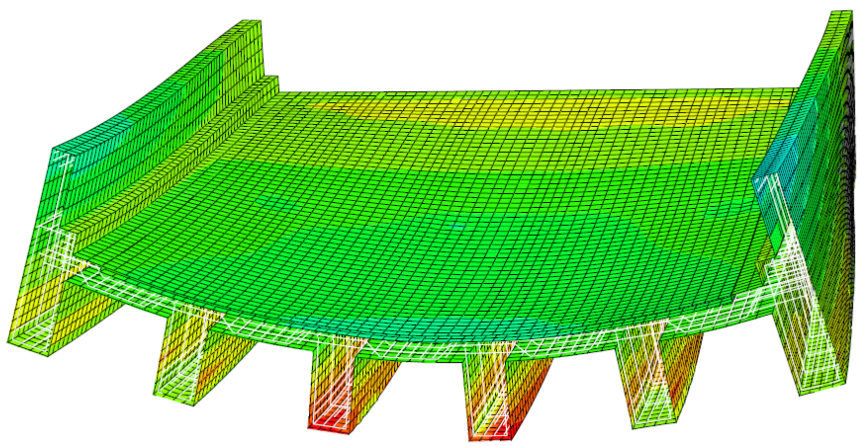

(a) Unfilled Style

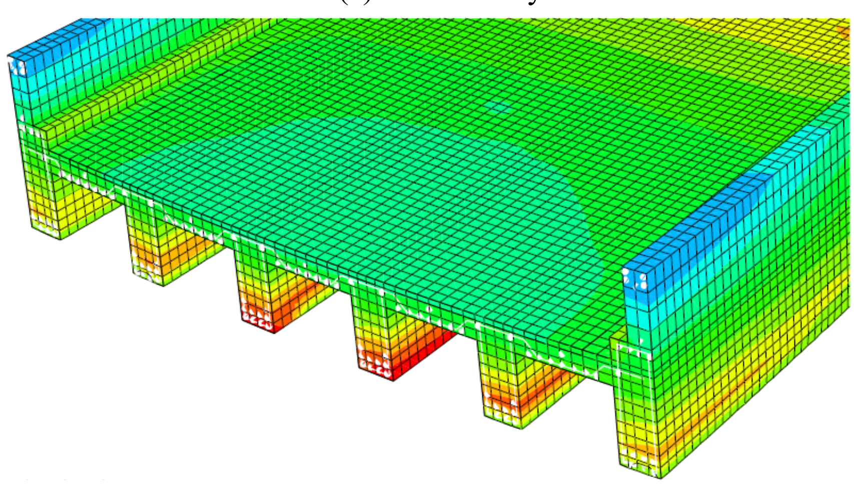

(b) Filled Style

Figure 44: In-plane Stress View Cut

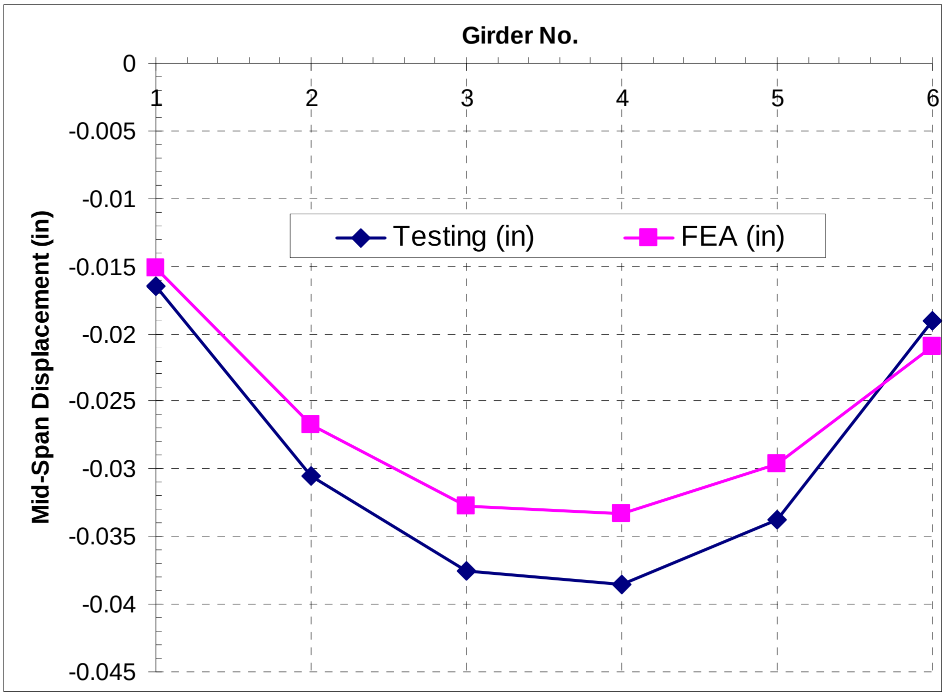

Figure 45: FEA Results for Mid-span Displacement,
Case 1 and Center of Gravity of PennDOT Tandem Truck at Mid-span

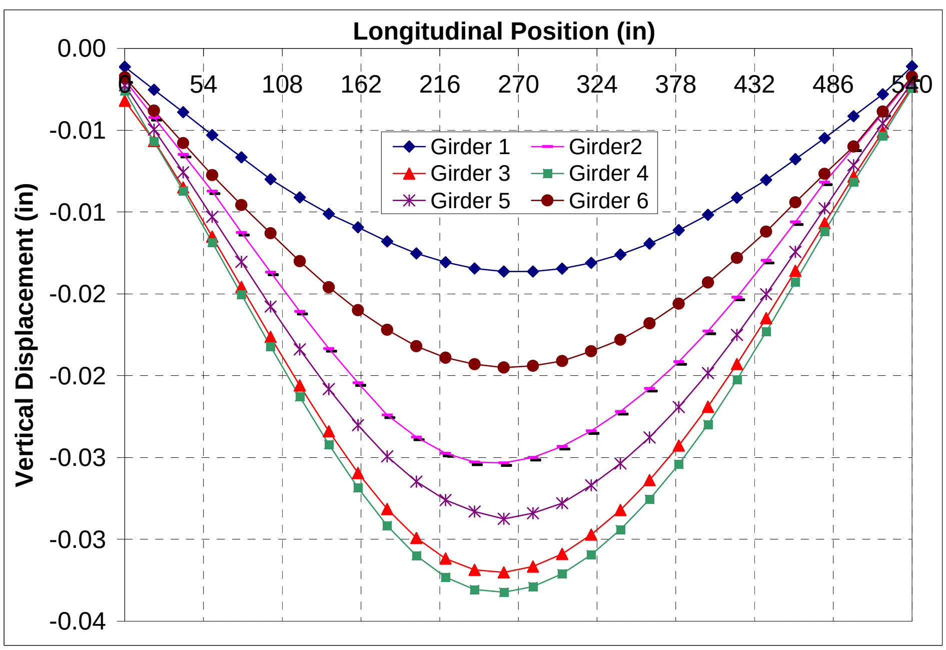

Figure 46: FEA Results for Longitudinal Distribution of Displacement in Girders
Case 1, PennDOT Tandem Truck, Center of Gravity at Mid-span, Live Load.

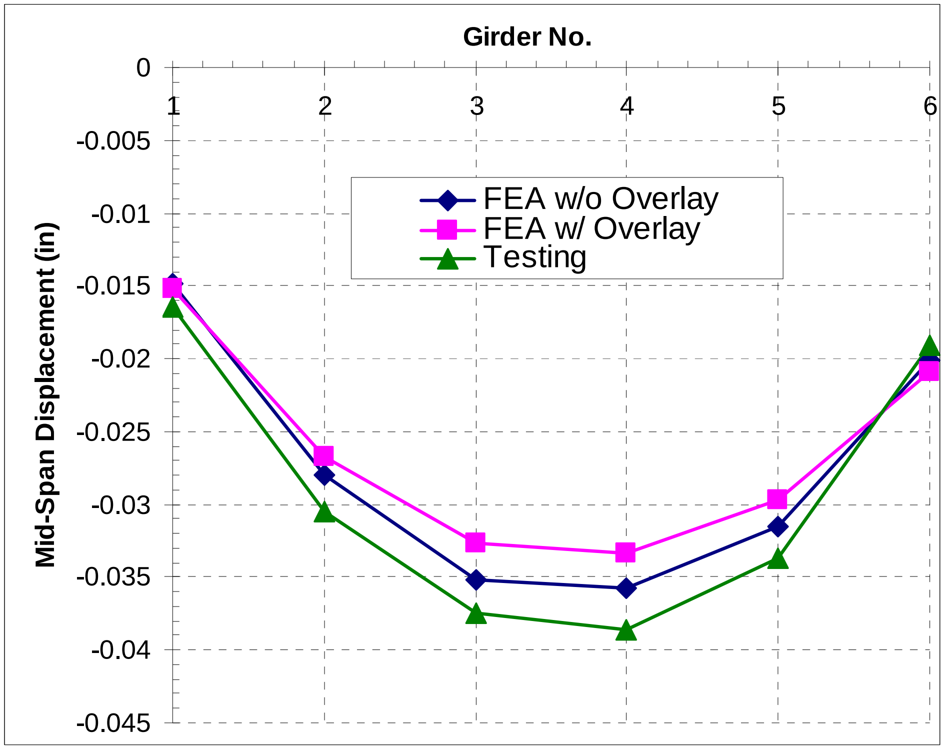

Figure 47: Overlay Effect on Transverse Displacements

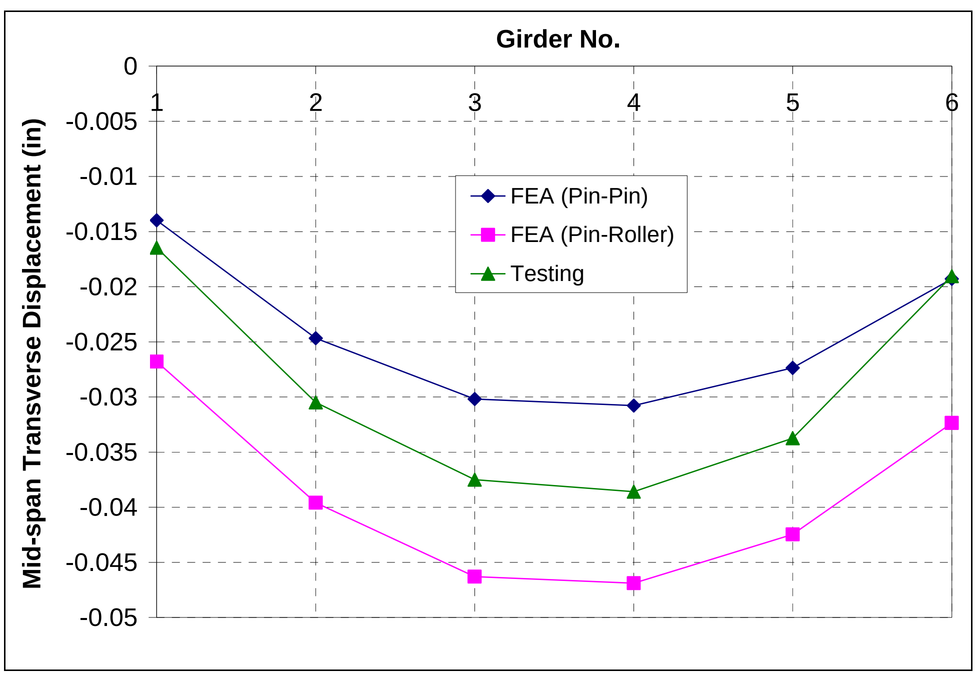

Figure 48: Vertical Displacement of Girders for Different Boundary Conditions under PennDOT Tandem Truck, Case 1 and Center of Gravity at Mid-span

D.2.2 Moment and Shear Force Computation

The output from the 3D solid and truss elements used for FE modeling provides the stress profile, which is used to compute the girder and the slab moments. The effective slab width was calculated based on AASHTO specifications. The deck slab is considered to be a one-way slab system due to its large aspect ratio (panel length divided by the panel width).

The most critical position for girder bending was determined to be at the middle of the girder for load Case 3, when the center of gravity of the truck was at mid-span. Load Case 1 was determined to be the most critical position for girder shearing when the rear wheels were at near the support.

To obtain the maximum bending moments of the slab, the left wheels of one truck were set at the mid-span of the bay. To obtain the maximum shearing of the slab, the left wheels of one truck were positioned near Girder 2 edge. Both one-lane and two-lane load cases were analyzed. The two-lane load case was more critical for moments, while the one-lane load case was more critical for slab shearing.

The maximum tension and compression stresses occurred at the top and bottom faces of the sections. The neutral axis was determined from the stress profile. The moment of inertia was then calculated based on the transformed cross-section, which was used for moment calculation. The shear stresses were integrated to compute the resulting shear force of the section. The maximum moments and shear forces under dead load and live load for slab are given in Table 6. The maximum moments and shear forces under dead load and live load for girders are given in Table 7.

Table 6: Ultimate Moments and Shear Forces per Unit Slab Strip

	HS20 Truck	Dead Load	Factored Load
Positive Moment (k-ft/ft)	1.71 (2 trucks)	1.34	6.58
Negative Moment (k-ft/ft)	1.97 (2 trucks)	1.39	7.36
Shear Force (kips/ft)	4.46 (1 truck)	7.39	22.19

Table 7: Maximum Moments and Shear Forces for Girders at the Critical Cross-Sections

			HS20 Truck	Dead Load	Factored Load
Moment (k-ft)	Interior Girder		134.8	213.3	657.6
	Exterior Girder		52.9	105.1	286.0
Shear Force (kips)	Interior Girder	Region 1	19.05	28.20	90.42
		Region 2	9.86	26.40	62.15
		Region 3	10.58	19.55	55.25
		Region 4	6.84	10.50	32.95
	Exterior Girder	Region 1	6.73	21.42	46.85
		Region 2	3.34	17.24	31.83
		Region 3	4.07	12.79	28.12
		Region 4	2.64	6.40	15.76

D.2.3 Load Rating Factor Based on FE Model

Load rating calculations provide a basis for determining the safe load carrying capacity of a bridge. Inventory and operating ratings are required using the Load Factor Method specified in AASHTO. The bridge should be rated at two load levels, the maximum load level called the Operating Rating and a lower load level called the Inventory Rating. The Operating Rating is the maximum permissible load that should be allowed on the bridge. Exceeding this level could damage the bridge. The Inventory Rating is the load level the bridge can carry on a daily basis without damaging the bridge.

For comparison, the rating factors are computed using the ultimate capacities calculated from the above described FE model. The Rating Factor *RF* is determined by

$$RF = \frac{C - A_1 D}{A_2 L(1+I)}$$

where *C* is the capacity of the member from cross-section analysis, *D* is the dead load effect on the member, *L* is the live load effect on the member, *I* is the impact factor to be used with the live load effect, A_1 is the factor for dead loads, and A_2 is the factor for live loads. A_1 is taken as 1.3 and A_2 is taken as 2.17 for Inventory Rating or 1.3 for Operating Rating.

Load ratings are calculated for AASHTO truck HS20. The maximum shear and maximum moment were listed in Table 6 and Table 7. An impact factor is also taken into account for load rating. This value for the bridge studied is 30%. Table 8 gives the results of the Rating Factor for the girder. Table 9 summarizes the Rating Factor for the slab. For comparison, the Rating Factor based on AASHTO specifications is also listed in Table 8 and Table 9.

Table 8 indicates that the current flexural load capacity rating and shearing load capacity rating of the girder are at least as much as 2.69 times and 2.15 times higher, respectively, than its current load rating based on AASHTO specifications. Both moment and shear rating factors suggest that no rehabilitation is needed for this particular bridge. Note that the calibrated FE model simulates all of the deterioration that was identified during field assessment, including reduced cross-section of rebar and spalling and delamination of concrete. The corresponding load rating values are still much higher than the load rating based on AASHTO specifications, although the latter do not incorporate any deterioration.

Similar results were obtained by Catbas et al. (2003). They conducted extensive field investigations and experiments leading to field calibrated FE models of a RC T-beam bridge and concluded that the current flexural load capacity rating of a T-beam bridge in PennDOT's inventory is expected to be at least as much as twice higher than its current load rating based on AASHTO recommendations. They conducted extensive parametric analytical studies with 3D FE models as well as with idealized simple beam models, and concluded that even after ignoring all of the secondary elements such as the diaphragm beams and mechanisms such as the actually restrained boundary conditions that enhance load distribution, and by complying with all of the capacity and demand calculation requirements of AASHTO, it is still possible to increase the load rating of RC T-beam bridges in PA by 10% ~ 55% depending on the geometry of the bridge.

Table 8: Rating Factors for the Girders

			Rating Factor Based on FEA		Rating Factor Based on AASHTO		Ratio of Rating Factor (FEM/AASHTO)	
			OR	IR	OR	IR	OR	IR
Moment	Interior Girder		4.16	2.49	1.54	**0.92**	2.69	2.69
	Exterior Girder		8.13	4.87	1.11	**0.66**	7.35	7.35
Shear	Interior Girder	Region 1	3.64	2.18	1.69	1.02	2.15	2.15
		Region 2	6.64	3.98	1.99	1.19	3.33	3.33
		Region 3	3.00	1.80	1.01	**0.60**	2.97	2.97
		Region 4	5.39	3.23	1.90	1.14	2.84	2.84
	Exterior Girder	Region 1	9.25	5.54	4.04	2.42	2.29	2.29
		Region 2	18.35	10.99	4.77	2.85	3.85	3.85
		Region 3	8.63	5.17	2.92	1.75	2.95	2.95
		Region 4	13.60	8.15	4.76	2.85	2.85	2.85

Table 9: Rating Factors for the Slab

	Rating Factor Based on FEA		Rating Factor Based on AASHTO		Ratio of Rating Factor (FEM/AASHTO)	
	OR	IR	OR	OR	IR	OR
Moment	10.5	6.22	1.89	1.13	5.56	5.50
Shear	1.93	1.14	2.43	1.46	0.79	0.78

This discrepancy is because of the conservatively imprecise nature of the lateral live-load distribution factors that have been recommended in the AASHTO specifications (see Table 10). In the current load capacity rating practice based on AASHTO specifications, an individual beam is taken out as a free-body, idealized as simply-supported, while the continuity of the bridge in the transverse direction is indirectly accounted by means of axle-load distribution factors. This approach is known to underestimate the plate contributions. It is clear that the differences in modeling assumptions between 3D FE bridge models and 2D AASHTO simplified beam models will lead us to different load capacity ratings for the same structure. As discussed earlier, support conditions and secondary structural elements have great effects on the response of the bridge. The diaphragm beams provide effective rotational restraints and thereby increase bending stiffness at the boundaries, which in turn reduce the critical flexural demand at the mid-span. Similarly, parapets help distribute the flexural stresses from the mid-span towards the edges by creating very stiff girders at the edges. The AASHTO method incorporates idealized pin-roller boundary conditions, excessively increasing the flexural demand at the mid-span. However, this does not reflect the actual design and measured behavior of the bridge. Lateral and longitudinal movement is restrained with dowels at both ends. In addition, the lateral diaphragm beams restrain the movement of the superstructure. Therefore, the boundary conditions can not be visualized as pin-roller boundary conditions.

Table 10: Live Load Moment Distribution Factors (LDF)

	LDF based on FE Model	LDF based on AASHTO Specification	LDF based on Series Solution [Davalos et al. 2006]
Interior Girder	0.240	0.423	0.396
Exterior Girder	0.148	0.423	0.380

D.2.4 Dynamic Response Analysis

A dynamic analysis was also performed in order to determine the natural frequency of the bridge. This information will provide verification that the FE model and the actual bridge are yielding the same results and responding to loading in similar fashions. The natural frequencies of the bridge were determined to be 17.55, 22.67, 26.81, 32.21, and 43.86 Hertz for Mode 1, Mode 2, Mode 3, Mode 4, and Mode 5, respectively. The Mode 1 natural frequency from field testing is 14.66 Hertz, which is about 16% lower than the predicted value. Figure 49 shows the first five mode shapes.

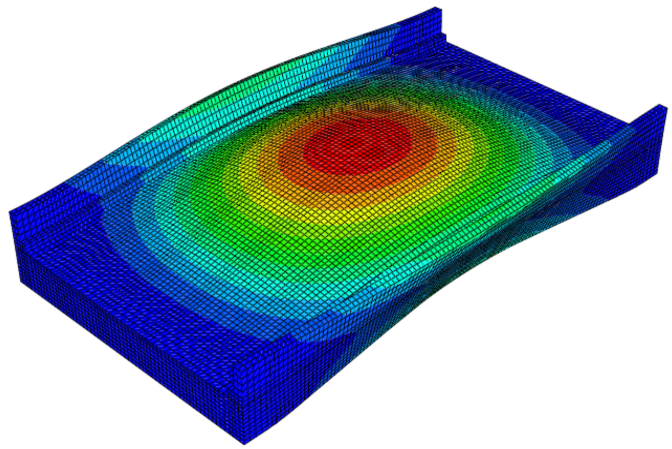

Mode 1 - 17.55 Hz

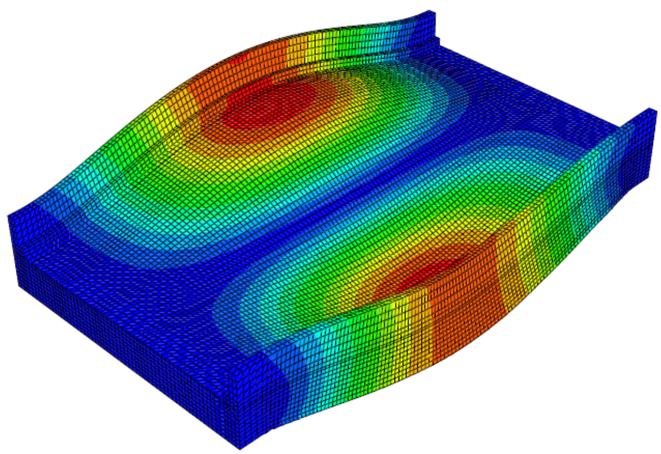

Mode 2 - 22.67 Hz

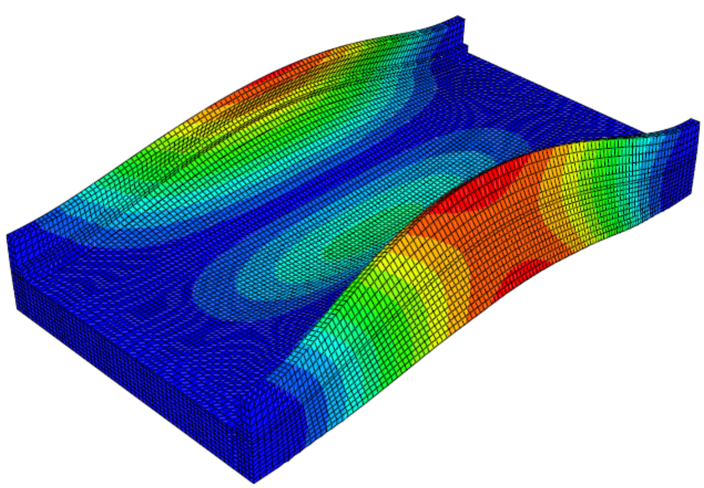

Mode 3 - 26.81 Hz

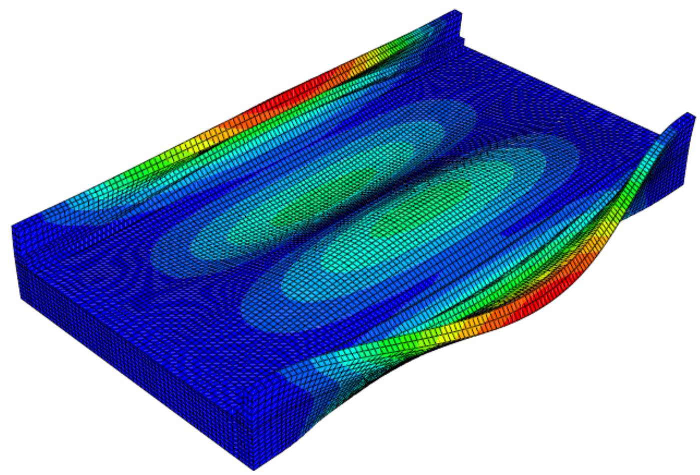

Mode 4 – 32.21 Hz

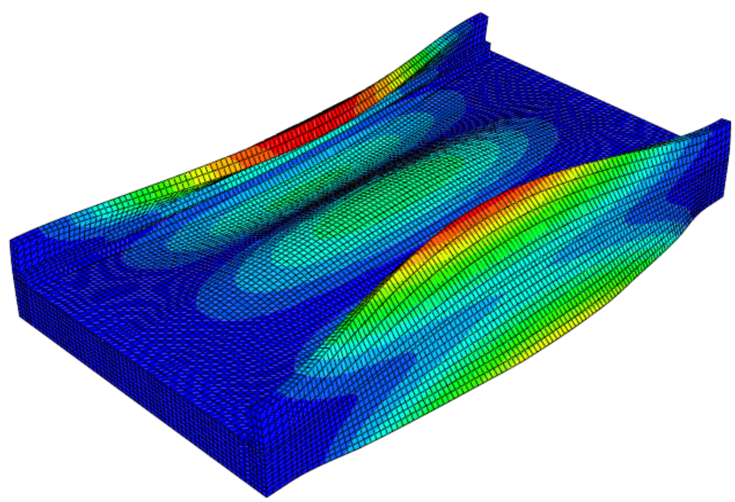

Mode 5 – 43.86 Hz

Figure 49: Mode Shapes and Frequencies

Task E – Testing of Existing Bridge

The objective of testing the existing bridge was to acquire data that would be useful in correlating results from the finite element analysis, and for calibrating and improving the accuracy of the FE model, so that an accurate analysis of the bridge could be performed with allowances for unknown variables. The age and deterioration of the bridge left many questions as to how much structural integrity was still left in the bridge and could still be counted on for future use. The qualitative inspection of the bridge showed many deterioration areas that would suggest further deterioration that were not visible. Observable loss of steel reinforcement and concrete section made the bridge look worse than it actually was when the load testing results were examined.

E.1 Setup

The initial testing plan was to record bridge strains, displacements, and accelerations at the midpoint of the bridge span under each girder to correlate the data with FEA results. See Figure 50 for positioning.

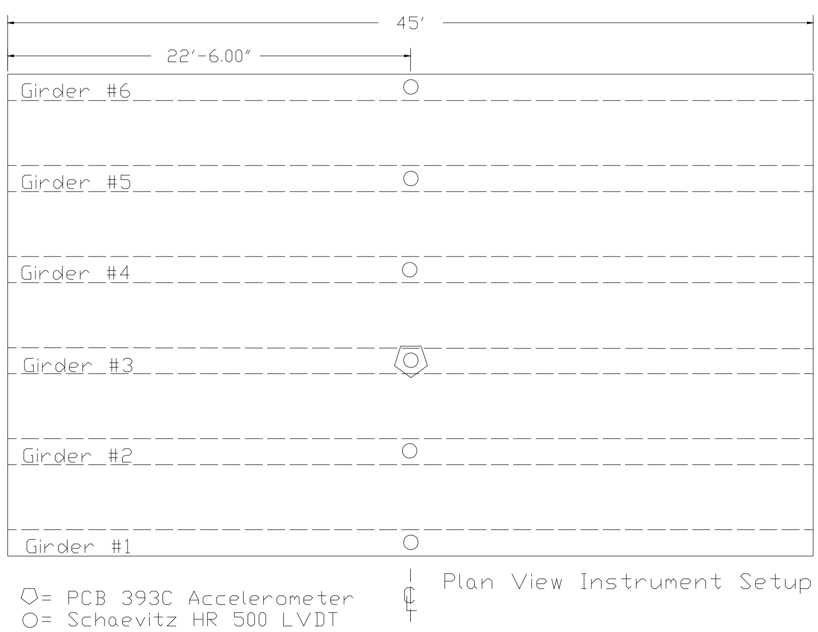

Figure 50: Plan View Instrumentation Placement

Strain Gages

The strain gages were to be placed at the quarter, half, and three-quarters height of the girder web, measured from the bottom of the T-beam to the bottom of the deck on all six girders (see Figure 51). The goal of this positioning was to find the neutral axis of each girder under loading. The strain gages to be used were Vishay Model N2A-06-40CBY-350, 4-inch general-purpose strain gages. The concrete surface required preparation due to the excessive amount of voids on the surface. Surface preparation required filling with a 100% solid adhesive. The adhesive used to attempt filling the surface voids was Vishay M-Bond AE-10. The epoxy required six hours time to cure at a temperature minimum of 75˚F (see Figure 52). Due to weather conditions, we were unable to place the strain gages. After three days curing time at temperatures no higher than 45˚F in the shade, the epoxy was still tacky and the strain gages to the concrete could not be attached.

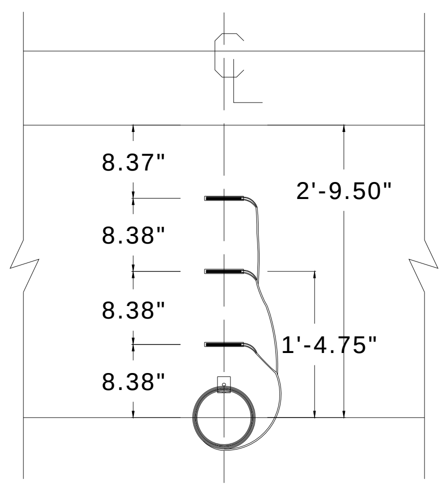

Figure 51: Strain Gage Positioning on Web

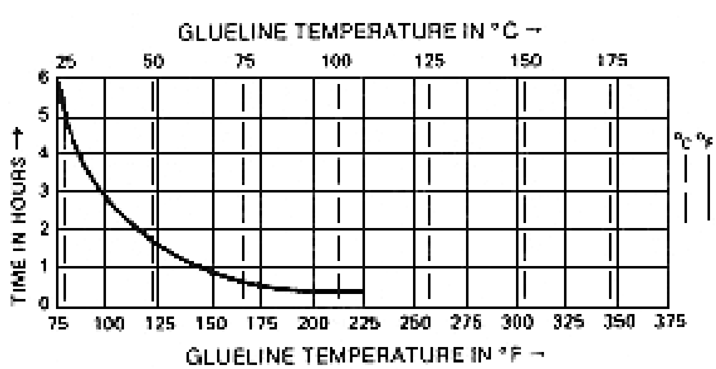

Figure 52: Epoxy Cure Time

LVDT's

Six Shaevitz HR500 LVDTs were placed at the bottom-inside face of each girder (see Figure 53). The LVDTs had a range of ±0.5 inches with a sensitivity of 0.001 inches. The LVDTs were placed into PVC tubing that was attached to U-Channel fence posts (see Figures 54 and 55). The PVC tubing helped limit magnetic interference that might have been caused by the U-channel posts. The posts were set into the stream under the bridge and tied back with 2x4 wood planks (see Figure 55). The posts were attached together with inclined and horizontal bracing to limit as much side-sway movement and provide as accurate of data as possible. The displacement data was taken at ten scans per second during the static load tests.

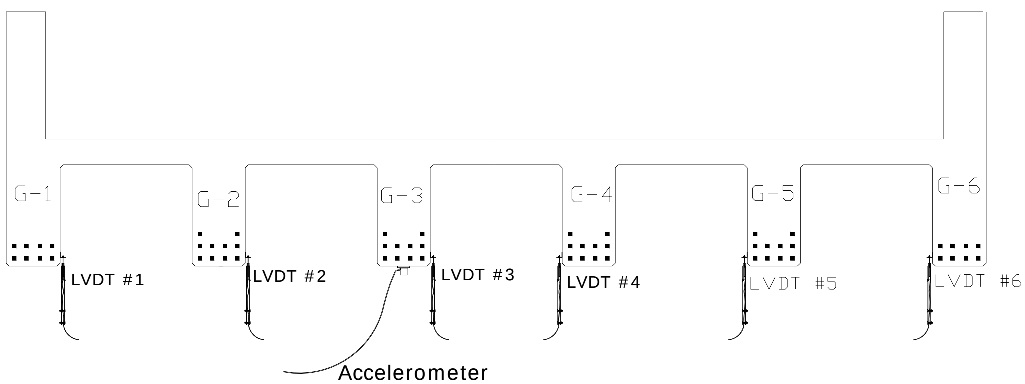

Figure 53: Cross-Section View Instrumentation Setup

Figure 54: LVDT Setup

Figure 55: LVDT Bracing

Accelerometer

A PCB Model 393C accelerometer was used to measure the vibration response of the bridge due to dynamic loading. The accelerometer was placed under the interior Girder 3 due to excessive deterioration of the exterior and adjacent interior girders on the bottom of the T-beams (see Figure 56). The data was collected using a Vishay System 6000 data acquisition system. The system allowed data collection at a rate of up to 10,000 scans per second. The acceleration data was taken at 10,000 scans per second.

Figure 56: PCB 393C Accelerometer Mounted

E.2 Trucks

PennDOT provided 2 fully loaded tandem dump trucks for the load test. PennDOT personnel weighed the truck's individual wheel loads using scales. The loads were then used to calculate the centroid of truck loading to define where to line up the trucks on the bridge during testing for maximum load effects. The truck dimensions differed slightly from expected dimensions (See Figure 40 in Section D.2). The trucks tires were wider than expected which limited the truck placement on the bridge. Some of the load tests were initially planned with two trucks side-by-side on the bridge. However, the width of the trucks made it impossible to place both trucks on the bridge for some of the load cases.

E.3 Static Load Cases

The initial load cases were designed to place the maximum load into particular girders (see Figure 42 in Section D.2). Load case #1 was designed to maximize the load effects in the exterior girder by placing the trucks as close as possible to the exterior girder as AASHTO standards would allow. Load case #2 was designed to place a full wheel line load over girder #2. The same reasoning was behind load case #4 in placing a wheel line directly over girder #3. Load case #3 was designed to place the maximum loading into girder #3 but could not be used because the dimensions of the bridge and trucks did not allow both trucks on the bridge in that configuration. Figure 57 shows the actual load cases used except for the modified load cases shown in Figure 58. The goal of the modified load cases was to have an extreme loading event that could be modeled in FE. The trucks were placed back to back as close as possible over the centerline and straddling girder #3 in modified load case 1 and straddling girder #4 in modified load case #2. There are no AASHTO specifications for the modified load cases.

The trucks were moved onto the bridge one at a time and the centroid of the trucks were lined up at the quarter, mid, and three-quarter points of the bridge. While continuous data was taken from the initial time the trucks were moved onto the bridge, 30 to 40 seconds were allowed at each placement to let the bridge dampen itself so that there would be no impact loads recorded in the results.

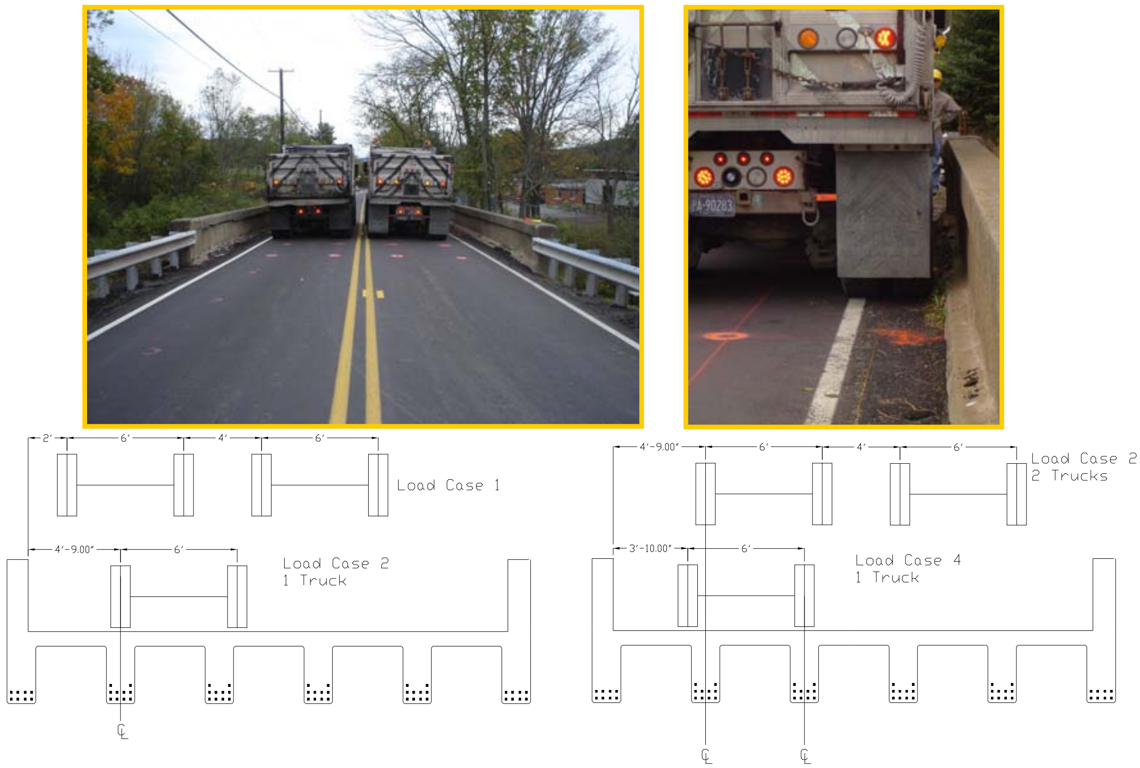

Figure 57: Actual Load Cases

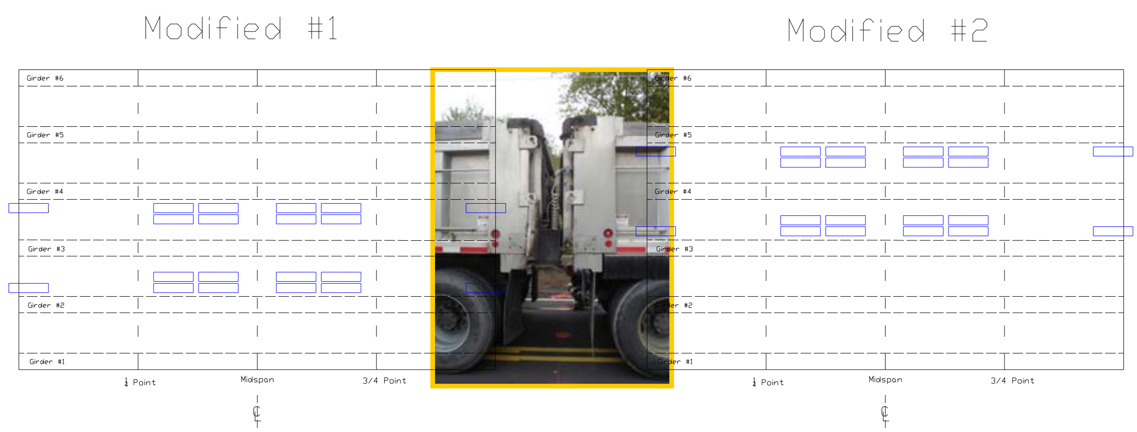

Figure 58: Modified Load Cases

E.4 Dynamic Load Cases

Six load cases were tested for the dynamic testing of the bridge. For the first three cases, a 2x4 wood plank was placed at the start of the bridge in order to excite the trucks suspension system and excite the bridge under forced vibration. The data was recorded at 10,000 scans per second, the limit of the data acquisition system. The trucks rolled across the bridge at about 30 mph. For the last three load cases, the 2x4 wood plank was removed and the truck simply jammed on the brakes around the middle of the bridge. The truck speeds for these tests ranged from 30 mph up to 50 mph hour. The damping curve was much clearer in all of the braking tests when compared to the tests using the wood plank.

E.5 Testing Results

The load testing deflection results are shown below in Figures 59-62 for load cases #1, #2- 1 truck, #2- 2 trucks, and #4. The three lines on each figure represent the deflection under each girder when the truck is positioned at quarter, mid, and three-quarter points along the span of the bridge. The transverse load placement is also shown in each figure. The modified load case results are shown in Figure 63. Since the load cases had the same longitudinal placement, and were balanced over Girder 3 and Girder 4, the results have been shown to corroborate evidence of similar deterioration throughout the bridge. That is that Girder 1 doesn't have an excessive amount more deterioration than Girder 6. The same is seen with Girder 2 and Girder 5, and Girder 3 and Girder 4. The figure is shown with the truck loading over Girder 3. The results for the truck being centered over Girder 4 were flipped so that the data could easily be compared.

A sample natural frequency curve is shown in Figure 64. The data was analyzed through a Fast Fourier Transform (FFT) analysis available in the Strain Smart software. The values from these charts correlate well with FE results as seen in Figure 65. The field tests showed a first mode frequency of 14.66 Hz and a second mode of 21.96 Hz. This gives about 16% difference from the predicted value for the first mode and 3% difference from the predicted value for the second mode.

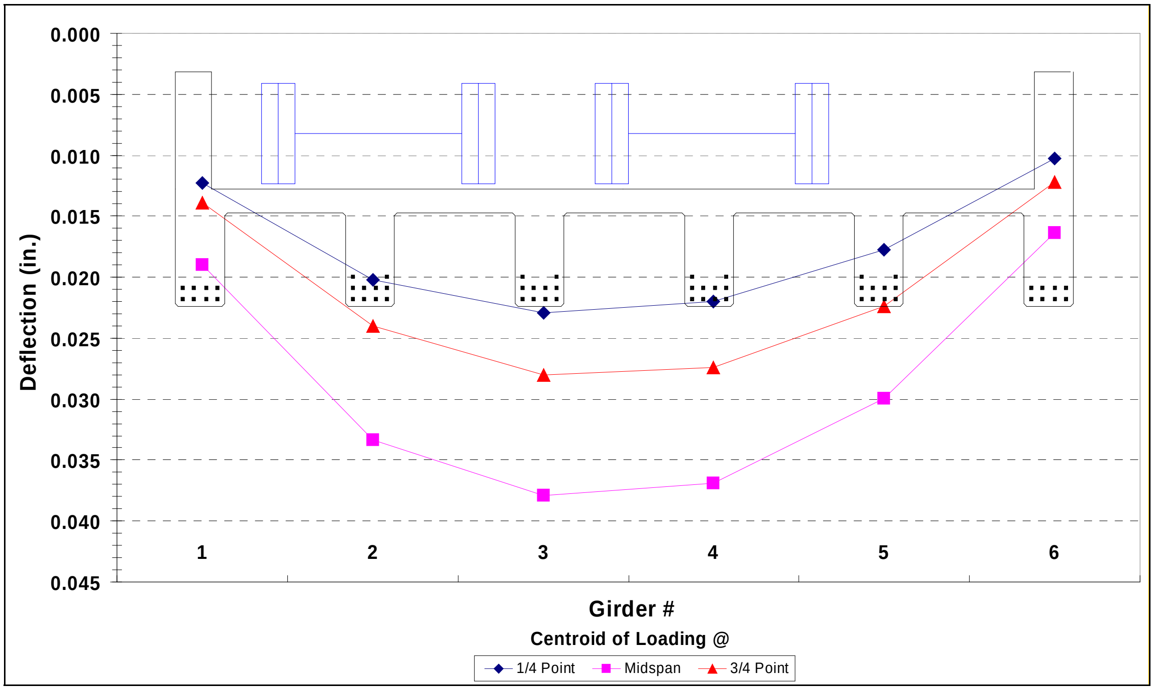

Figure 59: Load Case #1 – 2 Trucks

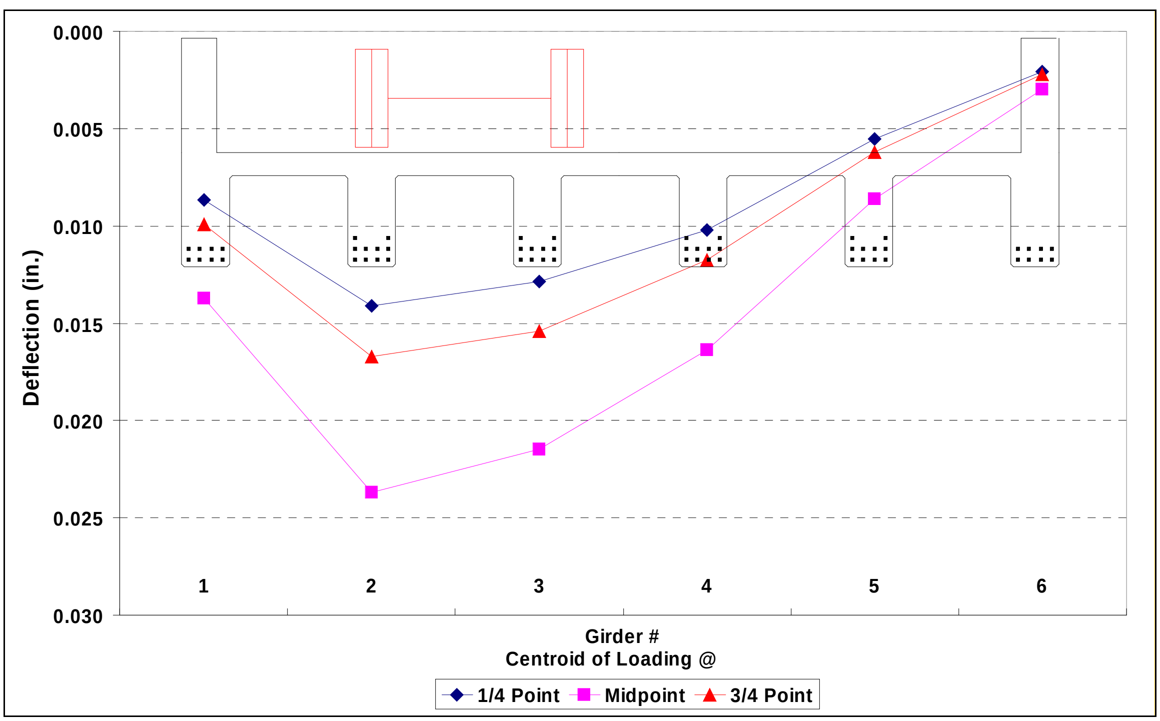

Figure 60: Load Case #2- 1 Truck

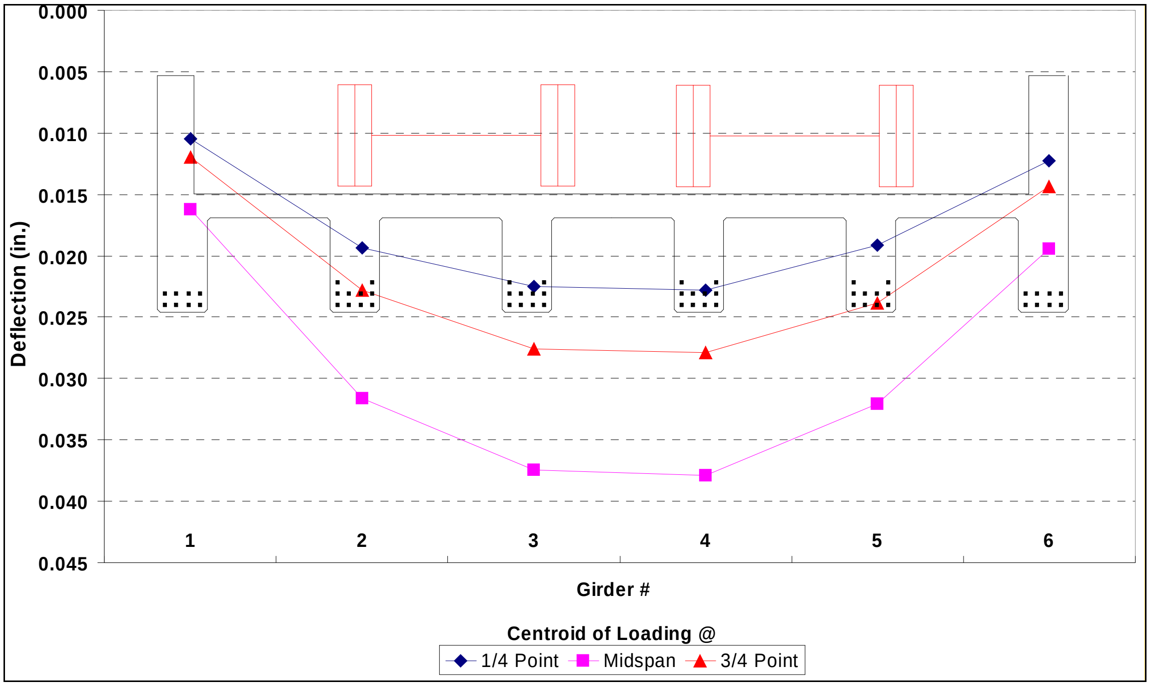

Figure 61: Load Case #2- 2 Trucks

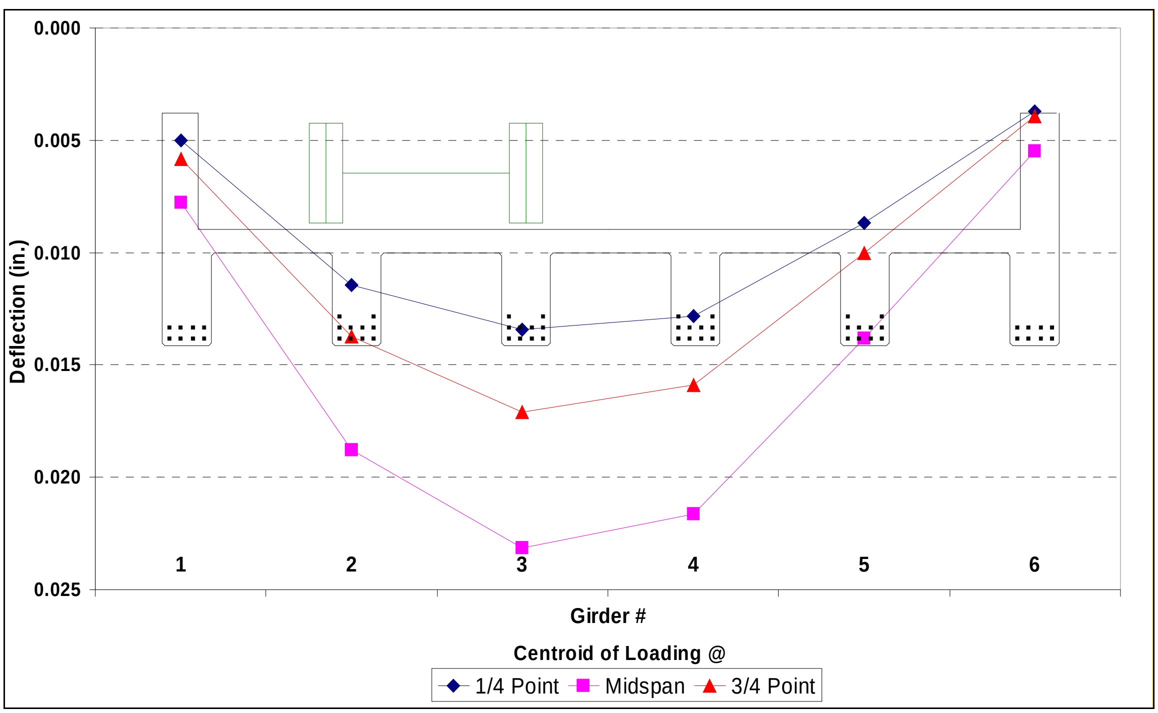

Figure 62: Load Case #4- 1 Truck

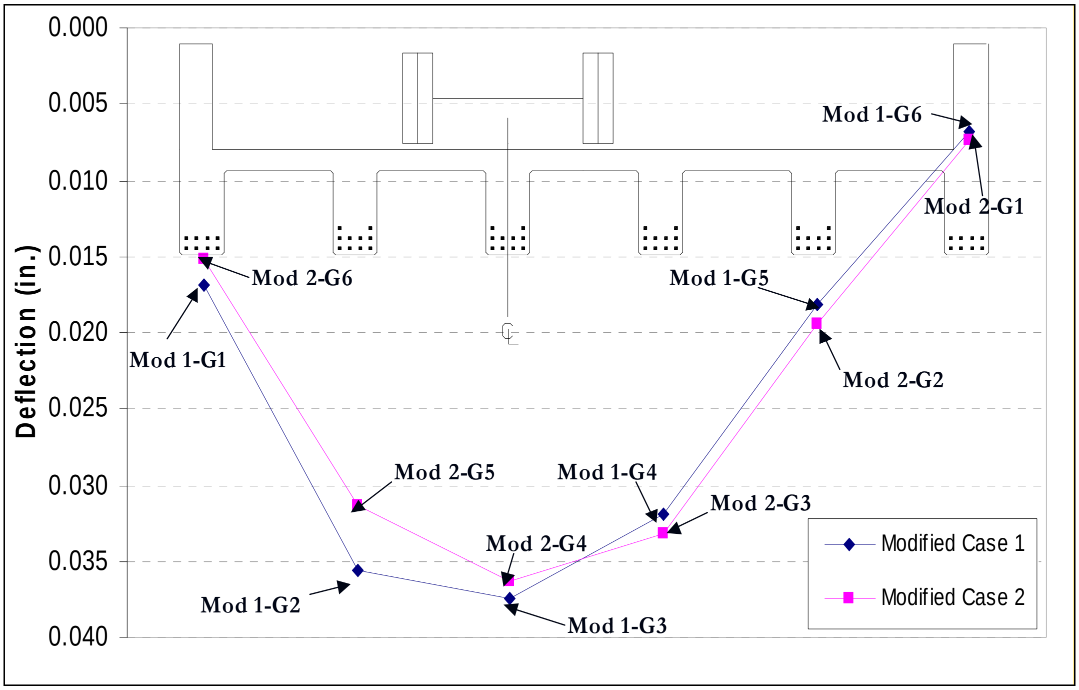

Figure 63: Even Deterioration Response

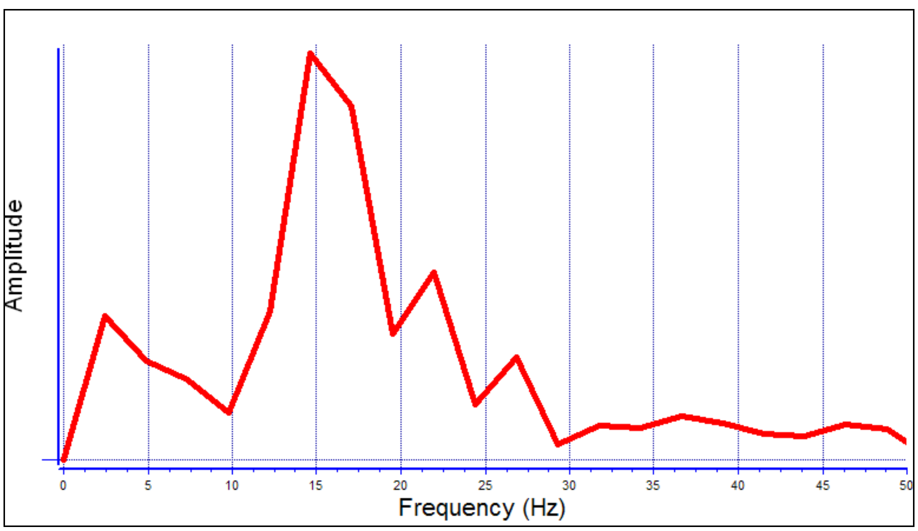

Figure 64: Natural Frequency Chart

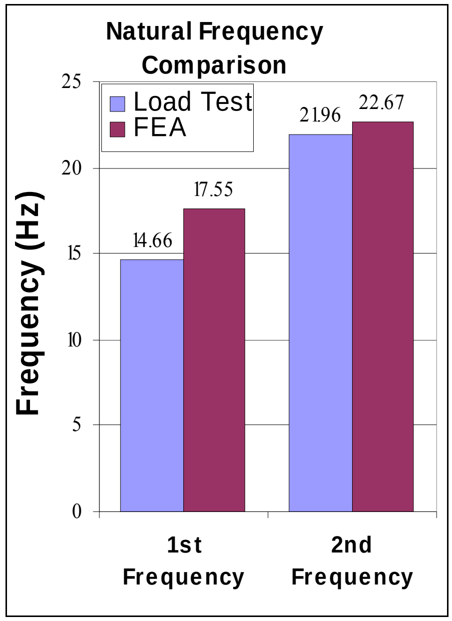

Figure 65: Natural Frequency Comparison

Task F – Design of FRP Repair and Other Work

F.1 Assumptions

Strengthening design is carried out according to the guidelines of ACI 440.2R-02, AASHTO, and ACI 318-99. To be conservative and conform to AASHTO specifications, we use the analysis results based on AASHTO specifications (Section D.1) as the basis (required capacities) for the design. The properties of concrete, steel, and FRP laminates used in the design are summarized in Table 11. The reported carbon FRP laminates properties are guaranteed values by the supplier.

Table 11: Material Properties

Concrete $f_c^{'}$ (psi)	Steel f_y (ksi)	FRP System Type	FRP System Properties			
			Tensile Strength f_{fu}^{*} (ksi)	Modulus of Elasticity E_f (ksi)	Thickness t_f (in)	Ultimate Strain ε_{fu}^{*}
5005 [(a)] 2212 [(b)]	37	Wet-layup	127	10,500	0.04	0.012

[(a)] From testing of concrete cores. Used for slab and interior girders.
[(b)] Estimation from the measured pulse velocities of girders. A linear relationship between compressive strength and pulse velocity was assumed (Malhotra and Carino 2004). Used for exterior girders.

Material properties of the composite reinforcement reported by manufactures, such as the ultimate tensile strength, typically do not consider long-term exposure to environmental conditions, and should be considered as initial properties. Composite properties to be used in all design equations are given as follows (ACI 440.2R-02):

$$\begin{aligned} f_{fu} &= C_E f_{fu}^{*} \\ \varepsilon_{fu} &= C_E \varepsilon_{fu}^{*} \end{aligned} \tag{1}$$

where f_{fu} and ε_{fu} are the FRP design tensile strength and ultimate strain considering the environmental reduction factor (C_E), and f_{fu}^{*} and ε_{fu}^{*} represent the FRP guaranteed tensile strength and ultimate strain as reported by the manufacturer (see Table 10). C_E is 0.85 for carbon/epoxy and exterior exposure (bridges) condition. The FRP design modulus of elasticity is the average value as reported by the manufacturer, which is not affected by environmental conditions. The modulus is the same as the initial value reported by the manufacturer.

$$E_f = \frac{f_{fu}}{\varepsilon_{fu}} \tag{2}$$

The following basic assumptions are made for a section strengthened with an externally applied FRP system. The strength design of members is based on satisfying conditions of equilibrium of internal stresses and compatibility.

- Design calculations are based on the actual dimensions, internal reinforcing steel arrangement, and material properties of the existing member being strengthened.
- The strains in the reinforcement and concrete are directly proportional to the distance from the neutral axis.
- The maximum usable compressive strain in the concrete is 0.003.
- The tensile strength of the concrete is neglected.
- There is no relative slip between external FRP reinforcement and the concrete.
- The shear deformation within the adhesive layer is neglected.
- The FRP reinforcement has a linear elastic stress-strain relationship to failure

F.2 Girder Design

F.2.1 Geometrical Properties

Girder geometrical properties are reported in Table 12, and Table 13. Figure 66 summarizes internal flexural and shear reinforcement at different cross-sections where there is a change in the lay-out of the reinforcement.

The expression for the flange width, *b*, is given by the following equations, according to AASHTO for interior and exterior girders, respectively:

$$b^{Int} = \min\left(\frac{L}{4}, 12h_f + b_w, S\right) \tag{3a}$$

$$b^{Ext} = b_w + \min\left(\frac{L}{12}, 6h_f, \frac{S - b_w}{2}\right) \tag{3b}$$

where L is the girder length, h_f is the slab thickness, b_w is the web width, and S represents the center-to-center girder spacing.

Table 12: Geometrical Properties of Girders

Girder Type	Overall Height h (in)	Web Width b_w (in)	Flange Width b (in)	Slab Thickness h_f (in)
Interior	41.5	17.5	61	8.5
Exterior	41.5	17.75	39.44	8.5

Table 13: Internal Steel Reinforcement

Girder Type	Section (Fig. 1)	Tensile Steel Area A_s (in^2)	Effective Depth d (in)	Stirrup Area A_{vs} (in^2)	Bent Bar Area A_{vb} (in^2)	Stirrup Spacing S_s (in)	Bent Bar Spacing S_b (in)
Int.	1	5.06 [(a)] 7.59 [(b)]	38.88 [(a)] 37.54 [(b)]	0.35	2.53	9	Single
	2	7.59 [(b)] 10.13 [(c)]	37.54 [(b)] 36.88 [(c)]	0.35	2.53	12	Single
	3	12.66 [(d)]	35.68 [(d)]	0.35	0	18	-
	4	12.66 [(d)]	35.68 [(d)]	0.35	0	24	-
Ext.	1	5.06 [(a)] 7.59 [(b)]	38.88 [(a)] 37.54 [(b)]	0.35	2.53	9	Single
	2	7.59 [(b)] 10.13 [(c)]	37.54 [(b)] 36.88 [(c)]	0.35	2.53	12	Single
	3	10.13 [(c)]	36.88 [(c)]	0.35	0	18	-
	4	10.13 [(c)]	36.88 [(c)]	0.35	0	24	-

[(a)] Region including "*a*" bar only; [(b)] Region including "*a*" bar and "*b*" bar; [(c)] Region including "*a*" bar, "*b*" bar, and "*c*" bar; [(d)] Region including "*a*" bar, "*b*" bar, "*c*" bar, and "c_1" bar. All areas are 80% of original values based on measured dimensions.

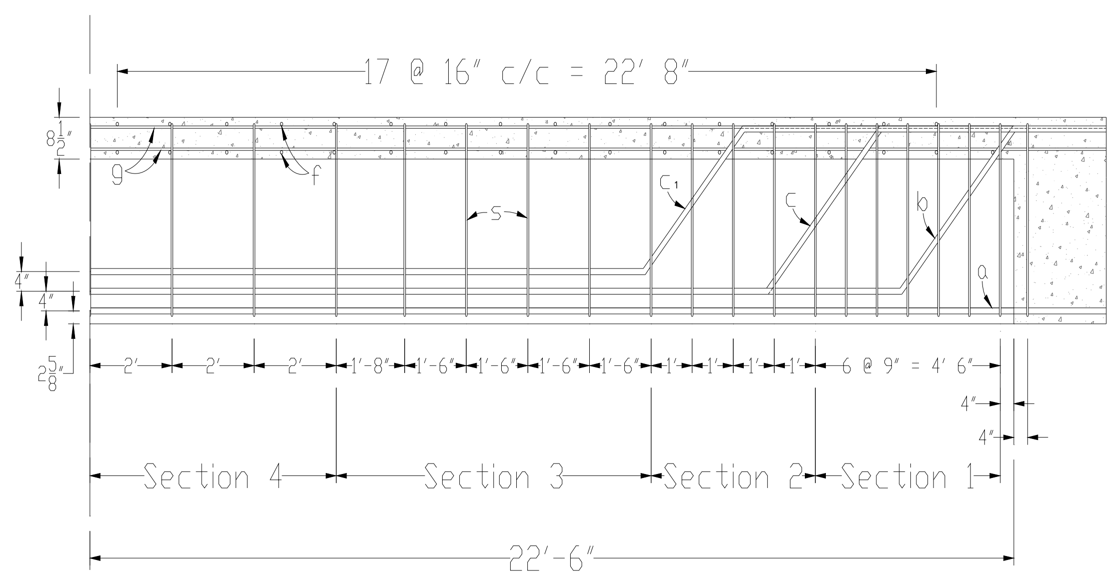

(a) Interior Girder – Side-view

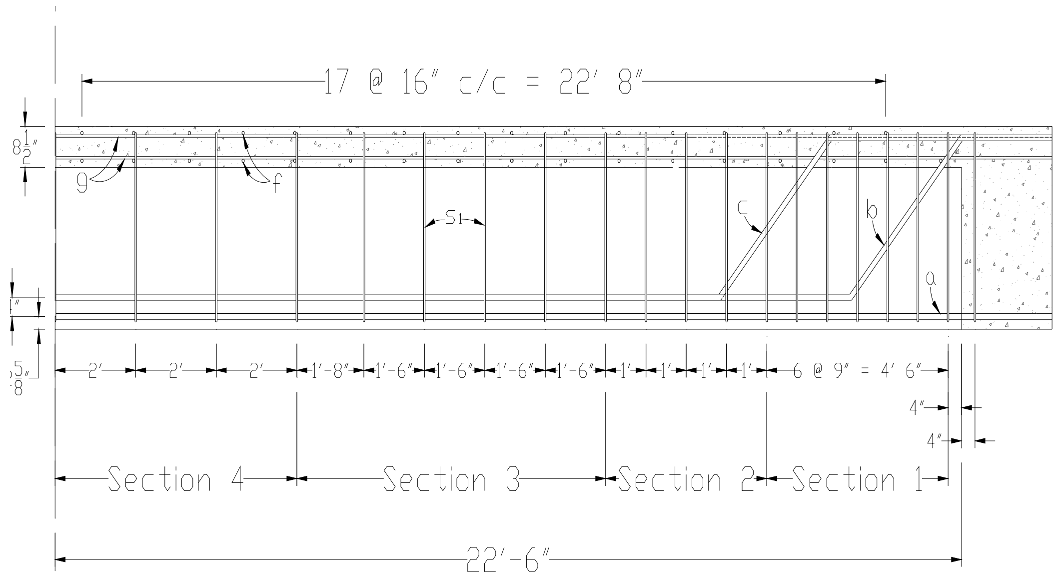

(b) Exterior Girder – Side-view

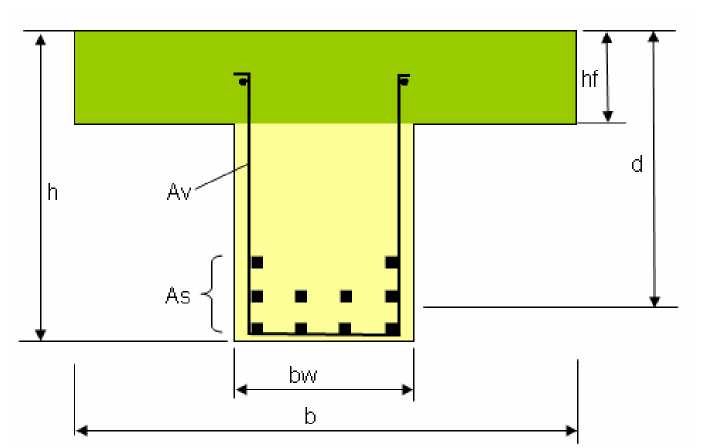

(c) Interior Girder – Cross-section

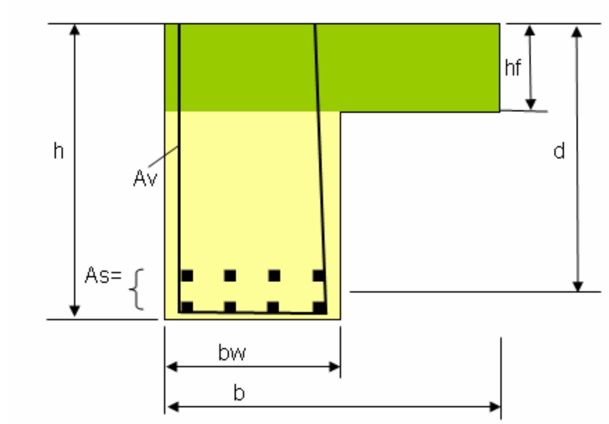

(d) Exterior Girder – Cross-section

Figure 66: Girder Dimensions and Internal Reinforcement

F.2.2 Positive Moment Strengthening

Table 14 summarizes the achieved flexural capacity at mid-span for interior and exterior girders. A detailed design protocol is shown in Appendix B.

When FRP laminates are used, the bond dependent coefficient, κ_m, defined by Eq. (9-2) of ACI 440.2R-02, accounts for cover delamination or FRP debonding that could occur if the force in the FRP cannot be sustained by the substrate. When adding FRP, the failure mode is usually governed by FRP rupture because of its limited ultimate strain at failure as compared to that of steel. This also represents an optimal use of an expensive material. Only when the amount of applied FRP becomes larger, the failure mode changes from tension controlled (FRP rupture) to compression controlled (concrete crushing). The amount of FRP listed in Table 14 is the minimum value required to resist the ultimate capacities, and ensure the tension controlled failure mode with FRP rupture. The maximum amount of FRP that is allowed in design can be determined by checking balanced failure mode (concrete crushing, steel yielding, and FRP rupture) as shown in Appendix B. Beyond this value the failure mode will change from tension controlled to compression controlled. Figure 67 shows a sketch of the layout of FRP flexural reinforcement.

Table 14: Girder Flexural Capacity at Mid-span

Girder Type	Description	Failure Mode [(a)]	κ_m	ϕM_n (k-ft)	M_u (k-ft)
Interior Girder 2, 5	No FRP	CC	-	1221.3	1270.7
	1 layer 15” wide, 40’7” long	TC	0.9	1366.6	
Exterior Girder 1	No FRP	CC	-	845.1 [(b)]	1021.8
	2 layers 15” wide, 42’7” long	TC	0.9	1109.9	
Exterior Girder 6	No FRP	CC	-	965.1	1021.8
	1 layer 15” wide, 42’7” long	TC	0.9	1096.4	

[(a)] CC=Concrete Crushing; TC=Tension Control
[(b)] Calculated existing design capacity which accounts for the rebar cut for sample (one rebar on the bottom row was removed)

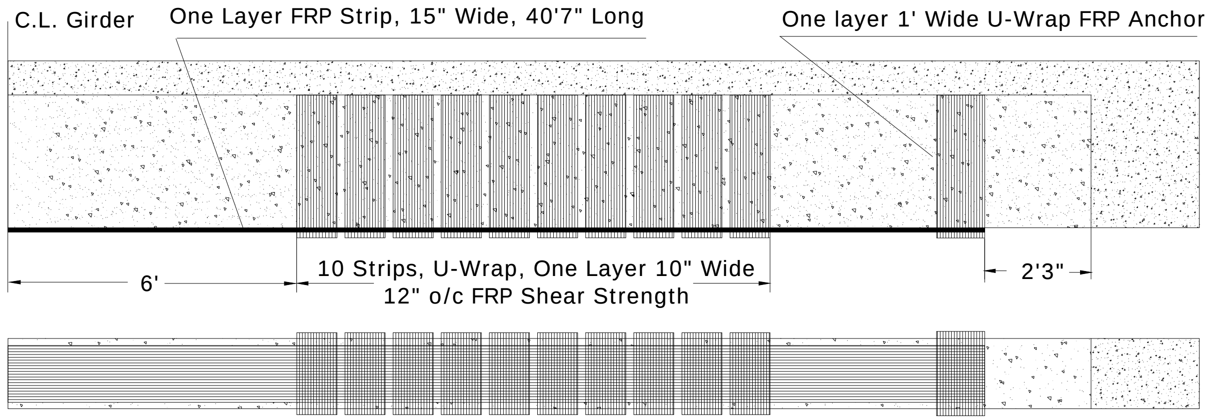

(a) Interior Girder 2 and 5

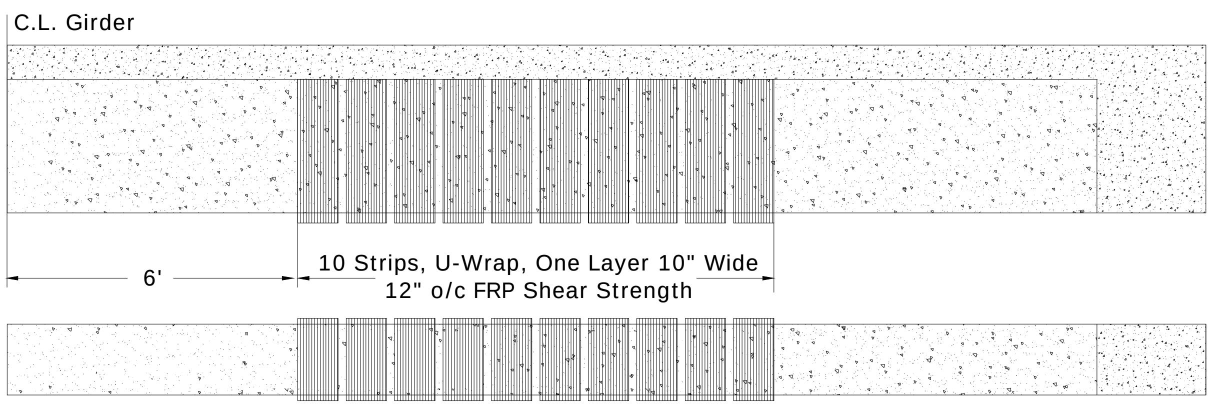

(b) Interior Girder 3 and 4

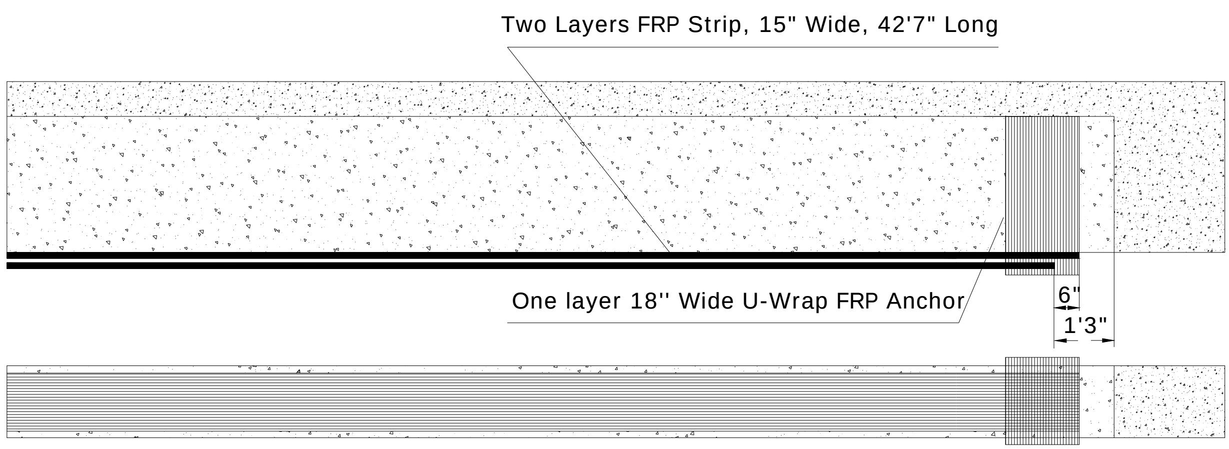

(c) Exterior Girder 1

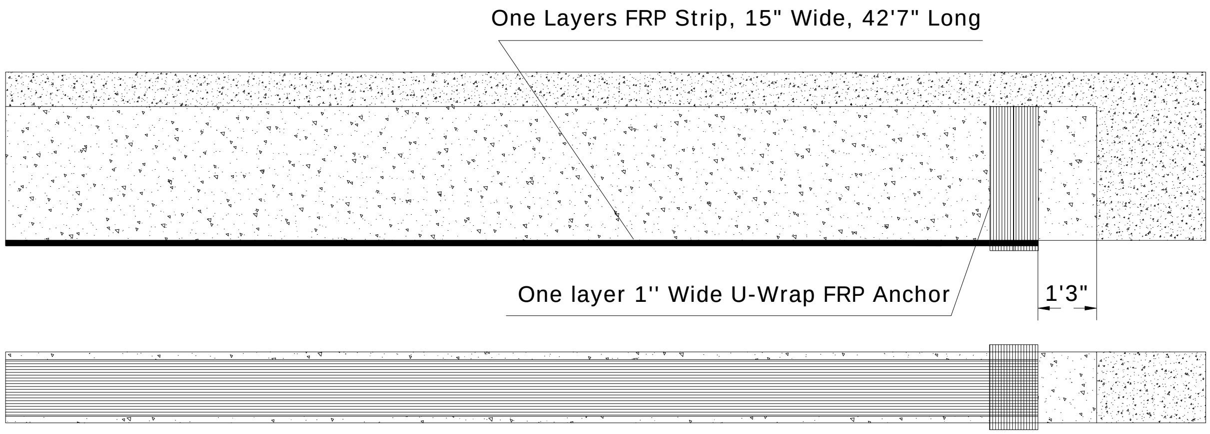

(d) Exterior Girder 6

Figure 67: FRP Strengthening

F.2.3 Shear Strengthening

The concrete contribution to the shear capacity was calculated as:

$$V_c = 2\sqrt{f_c^{'}} b_w d \tag{4}$$

The stirrup contribution to the shear capacity can be expressed as follows:

$$V_{ss} = \frac{A_{vs} f_y d}{s_s} \tag{5}$$

The bent bars contribution to the shear capacity is

$$V_{sb} = \frac{A_{vb} f_y}{\sin\alpha} \tag{6}$$

The FRP contribution to the shear capacity is expressed as follows (ACI 440.2R-02):

$$V_f = \frac{A_{fv} f_{fe} (\sin\alpha + \cos\alpha) d_f}{s_f} \tag{7}$$

where A_{fv} is the FRP laminate area, f_{fe} is the effective tensile strength allowable to the FRP reinforcement, d_f is the depth of the FRP reinforcement, and s_f is the FRP spacing.

Table 15 summarizes the achieved shear capacity in Region 3 for interior girders. A detailed design protocol is shown in Appendix C. Figure 67 shows a sketch of the layout of FRP shear reinforcement.

Table 15: Girder Shear Capacity at Region 3

Girder Type	Description	κ_v	ϕV_n (kip)	V_u (kip)
Interior Girder 2, 3, 4, and 5	No FRP	-	79.0	106.8
	1 layer 10" wide @ 12" o/c U-wrap	0.32	113.7	

F.3 Slab Design

The existing shear and flexural capacities of the slab are adequate. No FRP strengthening is needed.

Task G – Assisting District 3 with Bid Documents and Requirements

To assist District 3 personnel to plan and draft the bid package for implementation of the FRP retrofit and to develop formal documents and engineering drawings for bidding purposes, information is presented in this section as advice for District 3 to follow protocols for effective technology implementation and work completion.

G.1 Information Resources

Concrete and steel repairs; surface preparations and installation of FRP system; acceptance of testing requirements and inspections; and provisions for authorizing rework and repairs are to be done following the relevant sections of existing guidelines, standards and published documents, and acceptance of work by District engineers. The latest editions of the following publications are recommended to be used. If necessary additional information from other sources may be used:

- ACI 546 R: Concrete Repairing Guides
- ACI 440.2R: Guide for the Design and Construction of Externally Bonded FRP Systems for Strengthening of Concrete Structures
- ACI 503R: Use of epoxy compounds with Concrete
- ACI 503.4-92: Standard Specification for Repairing Concrete with Epoxy Mortars
- ACI 503.5R: Guide for the Use of Polymer Adhesives in Concrete
- ACI 503.6R: Guide for the Application of Epoxy and Latex Adhesives for Bonding Freshly Mixed and Hardened Concrete
- ICRI guidelines No. 03730: Guide for Surface Preparation for the Repair of Deteriorated Concrete Resulting from Reinforcing Steel Corrosions
- ICRI guidelines No. 03732: Selecting and Specifying Concrete Surface Preparation for Sealers, Coatings, and Polymer Overlays
- ICRI guidelines No. 03733: Guide for Selecting and Specifying Materials for Repairs of Concrete Surfaces
- ASTM D 4541: Test Method for Pull-Off Strength of Coatings Using Portable Adhesion Tester
- ASTM D3039: Test Method for Tensile Properties of Polymer Matrix Composite Materials

- NCHRP Report 514: Bonded Repair and Retrofit of Concrete Structures Using FRP Composites, Recommended Construction Specification and Process Control Manual
- The data sheet of the proprietary concrete repairing systems and FRP composites by the manufacturer
- Any other relevant information

The concrete and steel repairing, surface preparation and installation of FRP is suggested to be performed by following the recommendations given below. At every stage of work the approval of the engineer of record is needed. During executions, the contractors or applicators may suggest some necessary changes to this proposed plan depending on the in-situ findings.

G.2 Deteriorated or Damaged Concrete removal and cleaning of reinforcement

For girders 1 and 6 the deteriorated concrete is to be removed up to 1 in. (25.4 mm) inside the reinforcement from both bottom and side to expose sound concrete. For girders 2 and 5, the deteriorated concrete is to be removed up to the reinforcement level to expose sound concrete. For girders 3 and 4, the deterioration is much less so the concrete removal may consist of thinner layers, but should expose the sound concrete. In general the concrete removal is recommended to be continued until the fractured or broken concrete surface shows fractured aggregates rather than whole aggregates coming out loosely. Suitable methods per ACI 546R, ICRI guidelines No. 03730 and NCHRP report 514 and to the satisfaction of engineers are to be followed.

Blast cleaning including sandblasting, shot blasting and water jetting or equivalent methods can be followed per ACI 546R, ICRI guidelines 03730 and to the satisfaction of engineers. The use of impact tools or heavy jackhammer should be avoided which may cause micro-fractures. The cleaning with water jet has to continue until no chloride salt deposits and efflorescence are visible. Exposed reinforcing bars should be cleaned thoroughly from rust, corrosion products, loose concrete or mortar, oil and other contaminants by suitable methods. Visual inspection and sounding can be made on concrete to ensure a good exposed surface. The rebar should not have any loose rust or products.

Similar techniques and procedures for concrete removal are to be followed for deteriorated and damaged curbs, parapet and decks. The objective is to remove the defective concrete and rust products and expose the sound concrete and steel surface.

G.3 Surface preparation

Suitable surface preparation per ACI 546R, ICRI guidelines 03730, and 03732 are recommended to be done. There are several methods of surface preparation before applying concrete repairing materials. One of the common ways is to keep the surface profile rough during concrete removal and blast cleaning procedure. The same method should be followed for girders, curbs, parapets and decks under retrofitting.

G.4 Reinforcement repair

All defective reinforcements need to be repaired according to ICRI No. 03730. If it is necessary to cut the rebar, it is to be replaced by splicing or lapping (According to ACI 318) with new rebar of equivalent cross section at that location under the supervision of engineers and to their satisfaction. The engineering decision will be taken depending on the condition of the exposed reinforcements. The cleaned and exposed or new rebars (if any) may be coated with proprietary products made of latex-cement slurry or epoxy. As the decisions of coatings are dependent on the condition of the rebars exposed, these will be determined in-situ in consultation with engineers. The same method should be followed for girders, curbs, parapets and decks under retrofitting. (Note: For longitudinal flexural rebars, 20% of original steel can be lost for all girders as in the design this number was assumed. If more steel needs to be removed, it must be replaced with splicing. For stirrups, for exterior girders (1 and 6) 40% of original steel can be lost, and for interior girders (2 through 5) 20% of original steel can be lost at maximum.)

G.5 Restoration of concrete cross sections

Firstly low viscous or standard proprietary injection epoxy should be used to seal the cracks according to ACI 224.1R and/or manufacturer's manual. The exact procedures and extent of crack injections will be decided depending on the cracks and voids revealed after removal of concrete and cleaning. The minimum crack width at the point of introduction can be taken as 1/12 in. (2 mm). Any crack approximately equal to or larger than 1/12 in. (2 mm) should be filled up by low-viscous injection epoxy. The locations of the crack will only be known after removal of defective concretes by light jack hammer and water jetting or other standard procedure of concrete removal.

The removed concrete is to be restored to original dimension using proprietary products based on guidelines stated in ACI 546R and in manufacturers specification and/or manual. The concrete repair system consists of corrosion inhibitors, bonding agents, and polymer mortar/concrete or conventional mortar/concrete per ACI 546R and supplier's manual. Before restoring the concrete surface, commercial corrosion inhibitors (one or two layers) should be applied. After application, the bonding agents can be used. The proprietary repair materials are to be applied much before it cures or sets. The exact material and methodology for application will be decided depending on the in-situ condition. The bond strength between the repair material and the original concrete surface shall be at least 200 psi (1.4 MPa) according to ASTM D4541. The repair materials are to be properly cured before installing FRP according to the guidelines of the product data sheets. The girders will be restored to original shape with polymer modified mortar systems by trowel methods.

G.6 Surface preparation of repaired concrete surface

The repair and restored surfaces should be approved by the engineer before surface preparation. Surface preparation methods as prescribed in ACI 440.2R, NCHRP report 514, and recommendations by manufacturer of FRP as per the project requirements should be followed typically a light sandblast, grinding or other equivalent methods. The surface roughness and humidity of the surface have significant effect on the bond between repaired surface and FRP. The objective of the surface preparation should be such that FRP installed can function as bond-critical wrapping. The surface preparations are to be approved by the engineer before installing the FRP.

G.7 Installation of FRP system

This activity will be accomplished following ACI 440.2R, NCHRP report 514, and guidelines by the manufacturer of FRP. A final contract documents is needed for specific procedure for a particular type of FRP system. A proprietary carbon fiber reinforcing fabric and epoxy system will be used. This may be a custom weave unidirectional carbon fabric with aramid cross fibers or an equivalent product and two-component epoxy. A suitable primer is to be applied in one or two coats prior to application of fabric to penetrate the open pores. This should be installed by trained and certified applicators and in compliance with the manufacturer's quality control manual.

Based on the design, girders 1, 2, 5, and 6 will be repaired for flexure (Fig. 68) using longitudinal strips at bottom and anchorage wraps. Girders 2, 3, 4, and 5 will be repaired for shear with U-wraps (Fig. 67). The zones of U-wrap are displayed in Fig. 68.

If necessary the field samples of FRP system need to be tested in accordance with ASTM D-3039. Environmental conditions for installation should be examined before and during installation of FRP to comply with the requirements in the contract documents and manufacturer's recommendations. All necessary equipment for application is to be provided by the contractors. The equipment details will depend on the FRP systems to be used. Necessary guidelines from NCHRP report 514, ACI 440.2R, and manufacturer's recommendation need to be followed for multiple-ply installation (in case it is used), overlapping, alignment, anchoring, curing, protective coating and finishing.

For the inspection of materials, QA/QC of the project, daily inspection; inspection of debonding, cure of resin, adhesion, and cured thickness, the NCHRP report 514, ACI 440.2R and relevant information are to be followed. After 24 hours (at least) of initial cure of the resin and before applying the protective coating and finishing, a pull-off test according to ASTM D4541 will be conducted to evaluate the bond strength between the FRP system and concrete. The locations of the test and sampling frequency need to be specified in the contract document. For acceptance, the failure should occur at a tensile stress of 200 psi (1.4 MPa) or higher and within the substrate concrete. The acceptance criteria for bond test should be mentioned in the contract document. If necessary, the tensile test of coupon witness samples will be carried out in accordance with ASTM D3039 with acceptable limits to be shown in the contract. If the test does not conform to the requirements laid out in the contract, necessary repair of the defective work is to be done following the guidelines as stated in NCHRP 514, and ACI 440.2R.

G.8 Management Protocol

Management of the project is an important component for successful implementation of the technology. The entities involved will include: (1) PennDOT District 3 engineers, who will have responsibility for supervising and approving the work at each stage; (2) The contract, who will carry out the work according to contract documents, plans, specifications, and other official documentation; and (3) The WVU research team, serving in an advisory capacity and as consultants to PennDOT-District 3.

Summary and Conclusions

Based on the research study conducted the following can be summarized and concluded:

(1) A Level-1 bridge (extensive damage) was selected to demonstrate the technical and cost-effective application of externally bonded FRP for a successfully repaired RC T-beam bridge strengthened to original capacity.

(2) Visual inspection, in-situ non-destructive concrete tests (ultrasonic pulse velocity and rebound hammer tests), and laboratory tests (chloride ions, SEM-EDX, and phenolphthalein tests) showed that the quality of concrete in the exterior and first interior girders is extremely poor due to severe delaminations, high chloride ions, carbonation and corrosions. Prior to retrofitting, the deteriorated concrete surface will require major removal and replacement. The quality of concrete in the interior girders is within a typical range and can be used after filling the internal voids and cracks by injection grouting. Minor void filling and localized spalling patching are needed for the deck slab.

(3) The actual load capacity of the bridge is higher than the results given by BAR7 analysis. This is mostly due to the higher concrete compressive strength and steel yield strength tested from concrete core and steel samples taken from the bridge and to limitations of the line girder analysis utilized by BAR7.

(4) A 3D finite element model was built using available as-built drawings and field information. The effects of secondary structures and boundary conditions on the response of the bridge were investigated. The model was calibrated using the data collected in the field test. The calibrated finite element model can be utilized in further studies involving the FRP reinforcement.

(5) The field-calibrated FE model showed that the idealized simple-beam models with pin-roller boundary conditions do not reflect the actual design and measured behavior of

the bridge due to the imprecise nature of the lateral live-load distribution factors recommended in the AASHTO specifications.

(6) Secondary elements such as diaphragm beams and parapets and actual restrains at the boundaries, which are neglected in the idealized simple-beam models are the main reasons of the differences between rating factors calculated by the calibrated FE model and AASHTO.

(7) The FRP repair for girder shear and flexure was designed following existing guidelines (ACI 440.2R-02). In order to be conservative, many of the mechanisms that provide actually higher load capacity rating of the bridge were ignored, and the analysis results based on AASHTO specifications were used as the basis (required capacities) for the design.

(8) AASHTO analysis results showed that the flexural capacities of the exterior girders 1 and 6 and the first interior girders 2 and 5, as well as shear capacities of all interior girders in Region 3 are not adequate for PennDOT live loads. FRP strengthening is needed for these girders. Properties for wet-layup carbon FRP laminates were chosen for the design of FRP repair. The capacities of the strengthened girders meet both AASHTO and PennDOT requirements.

(9) Protocols, including concrete removal and restoration, reinforcement cleaning and repair, surface preparation, FRP system installation, and management protocol are being provided for District 3 personnel to plan and draft the bid package for implementation of the FRP retrofit contract.

(10) Although specific to PennDOT District 3, a general prescription for the possible adoption of FRP repair as a viable and cost-effective method for rehabilitation of deficient concrete bridges statewide was presented.

References:

ABAQUS (2005). ABAQUS/Standard User's Manual, Version 6.5, Hibbitt, Karlsson, and Sorensen, Inc., Pawtucket, RI.

AASHTO (2002). Standard Specifications for Highway Bridges, 17th Edition, Published by the American Association of State Highway and Transportation Officials, Washington D.C.

AASHTO (2004). LRFD Bridge Design Specifications, Second Edition, Published by the American Association of State Highway and Transportation Officials, Washington D.C.

ACI 224.1R-93 (Reapproved 1998). Causes, Evaluation, and Repair of Cracks in Concrete Structures.

ACI 440.2R-02 (2002). Guide for the Design and Construction of Externally Bonded FRP Systems for Strengthening Concrete Structures. American Concrete Institute.

ACI 318-99 (1999), Building Code Requirements for Structural Concrete and Commentary (318R-99), American Concrete Institute, Farmington Hills, MI.

ACI 546R-04 (2004). Concrete Repair Guide, American Concrete Institute.

ACI 503R (1993). Use of Epoxy Compounds with Concrete, American Concrete Institute.

ACI 503.4-92 (1992): Standard Specification for Repairing Concrete with Epoxy Mortars, American Concrete Institute.

ACI 503.5R (1992). Guide for the Selection of Polymer Adhesives with Concrete, American Concrete Institute.

ACI 503.6R (1997). Guide for the Application of Epoxy and Latex Adhesives for Bonding Freshly Mixed and Hardened Concretes, American Concrete Institute.

ASTM C 597. Standard Test Method for Pulse Velocity Through Concrete. ASTM International.

ASTM C 805. Standard Test Method for Rebound Number of Hardened Concrete. ASTM International.

ASTM C 42. Standard Test Method for Obtaining and Testing Drilled Cores and Sawed Beams of Concrete. ASTM International.

ASTM C 1084. Standard Test Method for Portland-Cement Content of Hardened Hydraulic-Cement Concrete. ASTM International.

ASTM C 1152. Standard Test Method for Acid-Soluble Chloride in Mortar and Concrete. ASTM International.

ASTM E 8-04 (2004). ASTM Standard Test Method for Tension Testing of Metallic Materials. ASTM International.

ASTM D 4541 (2002). Test Method for Pull-Off Strength of Coatings Using Portable Adhesion Tester.

ASTM D3039 (2000). Test Method for Tensile Properties of Polymer Matrix Composite Materials.

F.N. Catbas, S.K. Ciloglu, O. Hasancebi, J.S. Popovics, A.E. Aktan (2003), Re-Qualification of Aged Reinforced Concrete T-Beam Bridges in Pennsylvania, Final Report, submitted to Pennsylvania Department of Transportation, Bridge Quality Assurance Division and Federal Highway Administration, submitted by Drexel Intelligent Infrastructure Institute, Drexel University.

J.F. Davalos, B. Zou, and K.E. Barth (2006), An Approximate Series Solution for Orthotropic Stiffened Plate and Application on Load Distribution Factor, paper in preparation.

ICRI Guideline No. 03730 (2003). Guide for Surface Preparation for the Repair of Deteriorated Concrete Resulting from Reinforcing Steel Corrosion.

ICRI Guideline No. 03732 (2003). Selecting and Specifying Concrete Surface Preparation forSealers, Coatings, and Polymer Overlays.

ICRI guidelines No. 03733 (2003). Guide for Selecting and Specifying Materials for Repairs of Concrete Surfaces.

V.M. Malhotra and N.J. Carino (2004), Handbook on Nondestructive Testing of Concrete, 2nd Edition, CRC Press, New York.

Mirmiran A, Shahawy M, Nanni A and Karbhari V (2004). NCHRP Report 514: Bonded Repair and Retrofit of Concrete Structures Using FRP Composites-Recommended Construction Specifications and Process Control Manual, Transportation Research Board, Washington, D.C.

Appendices

Appendix A – Testing Results

Table A.1: Results from Compression Test

Deck Core #1	
Diameter	4.125”
Length	4.5”
Weight	5.2 lbs
Ultimate Load	75,000 lbs
Clear Cover	0.25”
Diameter of Rebar	0.75”
Concrete Density	149.4 lb/ft^3
Length/Diameter Ratio	1.09
ASTM C 42 Strength Correction Factor	0.892
Compressive Strength	5005 psi

Deck Core #2	
Diameter	4.125”
Length	4.25”
Weight	5.0 lbs
Ultimate Load	100,000 lbs
Clear Cover	0.25”
Diameter of Rebar	0.75”
Concrete Density	152.0 lb/ft^3
Length/Diameter Ratio	1.03
ASTM C 42 Strength Correction Factor	0.877
Compressive Strength	6560 psi

Table A.2: Values Obtained from Ultrasonic Pulse Velocity Test

Distance from South Abutment	4’-6”	5’	5’-6”
Visually Bad Concrete Surface			
Beam 1	---	58.2	53.6
Beam 2	166.4	320	216
Visually Good Concrete Surface			
Beam 3	99.2	97.7	115.4
Beam 4	103.5	105.2	98.3

Table A.3: Values Obtained from Rebound Hammer Test

	Horizontal Readings from Right Side of Beam	Vertical Readings from Underside of Beam
Visually Bad Concrete Surface		
Beam 1*	39, 43, 44, 52, 51, 52, 50, 48	---
Beam 2	52, 32, 56, 58, 56, 56, 50, 48	43, 48, 46, 43, 45, 47, 46
Visually Good Concrete Surface		
Beam 3	---	58, 58, 54, 55, 56, 53, 48, 56
Beam 4	56, 51, 55, 50, 48, 46, 52, 48	64, 54, 59, 56, 60, 57, 58, 58

*Diagonal measurement

Table A-4: Specimen Measurements from Steel Tension Test of Rebar

This table shows the 3 diameter measurements from each of the 6 specimens. Diameters (D1, D2, and D3) were taken at 3 locations along the length of the specimen and averaged (D). This average D was used to calculate an average cross sectional area (A). This is the area that was used to calculate the stress values from raw load data. Also shown on this table is the start time and date of the tension tests recorded by the data acquisition system.

Scan Session: "no1"				
Start Time: 6/23/2006 5:10:57 PM				
D1	D2	D3	Avg D	A
0.4965	0.4970	0.4995	0.4977	0.1945

Scan Session: "no2"				
Start Time: 6/23/2006 5:26:31 PM				
D1	D2	D3	Avg D	A
0.5045	0.5015	0.5005	0.5022	0.1981

Scan Session: "no3"				
Start Time: 6/23/2006 5:46:18 PM				
D1	D2	D3	Avg D	A
0.4925	0.5015	0.5000	0.4980	0.1948

Scan Session: "no4"				
Start Time: 6/23/2006 5:58:49 PM				
D1	D2	D3	Avg D	A
0.5005	0.5010	0.5040	0.5018	0.1978

Scan Session: "no5"				
Start Time: 6/23/2006 6:12:51 PM				
D1	D2	D3	Avg D	A
0.4975	0.4985	0.4995	0.4985	0.1952

Scan Session: "no6"				
Start Time: 6/23/2006 6:22:35 PM				
D1	D2	D3	Avg D	A
0.5060	0.5030	0.5015	0.5035	0.1991

Appendix B – Design of FRP Flexural Strengthening for Girders

1. Interior Girders 2 and 5

The T-beam shown in Figure B.1 is required to resist a dead load, live load, and factored moments of $M_{DL} = 508.5$, $M_{LL} = 280.8$, and $M_u = 1270.7$ kips-ft, respectively (based on AASHTO HS20 truck load).

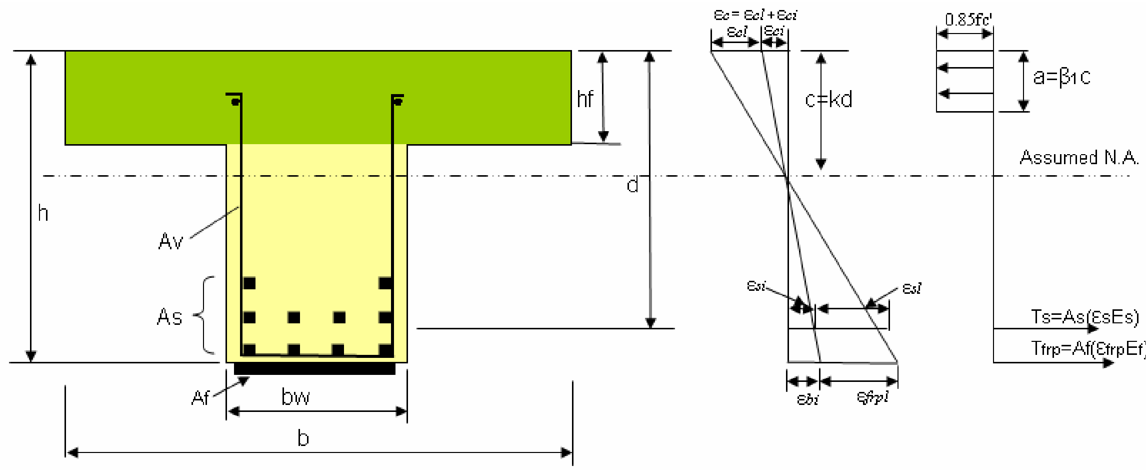

(a) (b) (c)

Figure B.1: Stress and Strain Distribution in FRP Reinforced concrete T-beam (Interior) under Ultimate Load.

- **Beam and Rebar Properties**

  Concrete compressive strength: fc' = 5005 psi (lower value of test results on deck core samples)

  Effective depth of T-beam, d = 35.7 in (centroid of the rebar group)

  Steel yield stress, fy = 37,000 psi

  Elastic modulus of steel, Es = 29,000,000 psi

  Effective width of T-beam, b = 61 in

  Rebar area, As = 12.7 in2

  Web width of T-beam, bw = 17.5 in

  T-beam depth, h = 41.5 in

  Elastic modulus of concrete, Ec = 4,032,523 psi

  Flange thickness, hf = 8.5 in

- **Calculate Existing Flexural Capacity of T-Beam without Composites**

Step1: Determining the depth of the equivalent rectangular stress block *a*

$0.85 f_c^{'} ab = A_s f_y$ (C = T) (Assume *a* is within the flange)

$$a = \frac{A_s f_y}{0.85 f_c^{'} b} = 1.80 \text{ in}$$

$$\beta_1 = 0.85 - 0.05 \frac{f_c^{'} - 4000}{1000} = 0.80$$

$c = a / \beta_1 = \boxed{2.26}$ in (N.A. depth from the top surface of beam)

$k = c / d = 0.0632$

Is *a* in the flange? Yes, assumption is correct.

Step2: Calculating the existing moment capacity

$M_n = A_s f_y (d - a/2) = 16283429.7$ lb-in = 1,357.0 k-ft

$\Rightarrow \phi M_n = \boxed{\mathbf{1221.3}}$ k-ft < $M_u = 1{,}270.7$ k-ft

$(\phi M_n)_{w/oFRP} = 1{,}221.3$ k-ft > $(1.2 M_{DL} + 0.85 M_{LL})_{new} = 848.9$ k-ft

The existing moment capacity without FRP wrap is greater than the unstrengthened moment limit. The level of strengthening is acceptable because the criterion of the strength limit is satisfied.

The properties of the existing reinforcing steel:

$$\rho_s = \frac{A_s}{bd} = 0.00582$$

$$n_s = \frac{E_s}{E_c} = 7.19$$

$$\rho_s n_s = 0.0418$$

$$\rho_{\min} = 3 \frac{\sqrt{f_c^{'}}}{f_y} = 0.00574$$

$\rho_{provided} > \rho_{\min}$ (0.00582 > 0.00574)

The strain in steel:

$$\varepsilon_s = 0.003\left(\frac{d-c}{c}\right) = 0.0444 > 0.005$$

$$\varepsilon_y = \varepsilon_{sy} = \frac{f_y}{E_s} = 0.00128$$

The beam is ductile with a steel strain exceeding the yield value of 0.00128 and the minimum limit of tension-controlled failure mode strain value of 0.005. A nominal strength reduction factor $\phi = 0.9$ will be used.

- **Flexural Strengthening with Composites**

Step3: Material Properties of FRP and Preliminary Calculations

Use carbon FRP wet-layup laminate.

Environmental Durability Factor, $C_E = 0.85$

Ultimate tensile strength, $f_{fu} = C_E f_{fu}^* = 0.85(127000) = 107{,}950$ psi

Elastic modulus, $E_f = 10{,}500{,}000$ psi

Ultimate strain, $\varepsilon_{fu} = C_E \varepsilon_{fu}^* = 0.85(0.012) = 0.0102$

Nominal thickness of laminate, $t_f = 0.04$ in

Number of FRP laminate layer, n = 1

Width of FRP strip, $w_f = 15$ in

Area of FRP strip, $A_f = n*t_f*w_f = 0.6\ in^2$

$$\rho_f = \frac{A_f}{bd} = 0.000276$$

$$n_f = \frac{E_f}{E_c} = 2.60$$

$$\rho_f n_f = 0.000718$$

Step4: Determine the Existing State of Strain on the Soffit

The existing state of strain is calculated assuming the beam is cracked and the only loads acting on the beam at the time of the FRP installation are dead loads.

First try rectangular beam analysis:

$$k = \sqrt{(\rho_s n_s)^2 + 2(\rho_s n_s)} - (\rho_s n_s) = 0.250$$

$c = kd = 8.93$ in, which is larger than the flange thickness, h_f. Therefore *T-beam analysis is needed* (see Figure B.2)

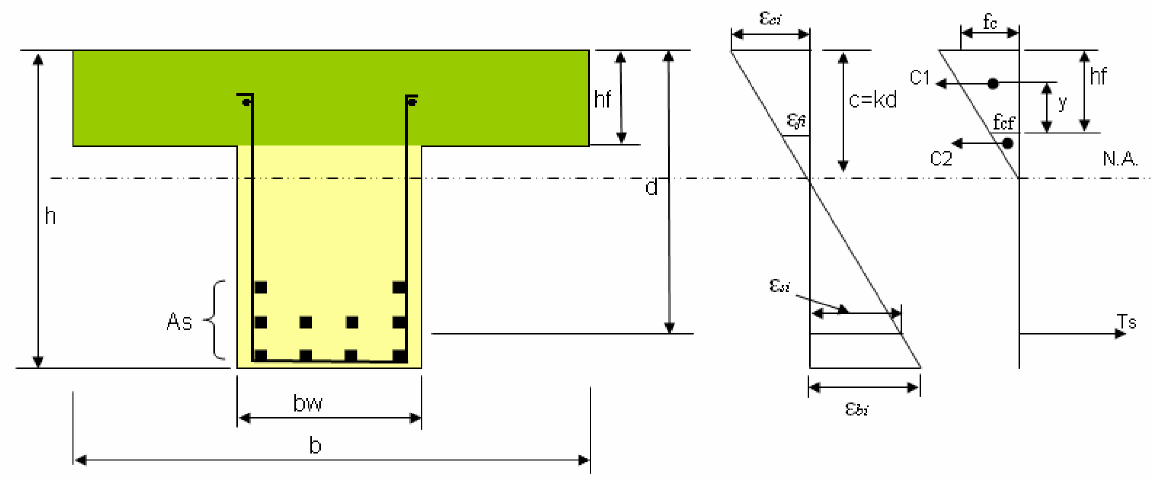

Figure B.2: Stress and Strain Distribution in Steel Reinforced concrete T-beam (Interior) under Dead Load

Considering the force equilibrium in a cracked T-beam, and referring similar triangles and Hooke's Law, we obtain the depth of neutral axis under dead load,

$$c = \frac{-(h_f b - h_f b_w + A_s n_s) + \sqrt{(h_f b - h_f b_w + A_s n_s)^2 + b_w(h_f^2 b + 2A_s n_s d - b_w h_f^2)}}{b_w} = \boxed{8.94} \text{ in}$$

The moment of inertia of cracked cross-section is

$$I_{cr} = \frac{1}{12} b h_f^3 + b h_f (c - h_f / 2)^2 + \frac{1}{3} b_w (c - h_f)^3 + n_s A_s (d - c)^2 = 79{,}583.2 \text{ in}^4$$

Therefore, the initial strain level is

$$\varepsilon_{bi} = \frac{M_{DL}(h - c)}{I_{cr} E_c} = \boxed{0.000619}$$

Step5: Determine the Bond-dependent Coefficient of the FRP System

The dimensionless bond-dependent coefficient for flexure, κ_m, is calculated using the following equation:

$$\kappa_m = \begin{cases} \dfrac{1}{60\varepsilon_{fu}}\left(1 - \dfrac{nE_f t_f}{2{,}000{,}000}\right) \le 0.90 & (nE_f t_f \le 1{,}000{,}000) \\ \dfrac{1}{60\varepsilon_{fu}}\left(\dfrac{500{,}000}{nE_f t_f}\right) \le 0.90 & (nE_f t_f > 1{,}000{,}000) \end{cases}$$

$nE_f t_f = 420{,}000 < 1{,}000{,}000$

Therefore,

$\kappa_m = 1.29 > 0.9 \Rightarrow$ Thus, choose $\kappa_m = \boxed{0.9}$

Step6: Determine the Depth of the Neutral Axis for a Balanced Failure and the Amount of FRP Reinforcement Needed for a Balanced Failure

Compare the calculated amount of FRP reinforcement for a balanced failure and compare it with the amount of FRP provided to determine the possible failure mode for the FRP strengthened beam.

Hypothetical balanced failure mode is assumed to occur when strain in extreme tension and compression fibers have reached their limit values simultaneously.

Strain in concrete: $\varepsilon_c = \varepsilon_{cu} = 0.003$

Strain in steel: $\varepsilon_s = \varepsilon_y$ (this is a consequence of strain in extreme FRP tension fiber reaching its ultimate value)

Strain in FRP: $\varepsilon_{frp} = \varepsilon_{frpu}$

These strain conditions at balanced failure can be expressed as follows from similar triangles principle:

$$\frac{c_b}{h} = \frac{\varepsilon_{cu}}{\varepsilon_{cu} + \varepsilon_{bi} + \varepsilon_{frpu}} \quad \text{or} \quad a_b = \beta_1 h\left(\frac{\varepsilon_{cu}}{\varepsilon_{cu} + \varepsilon_{bi} + \varepsilon_{frpu}}\right)$$

where $\varepsilon_b =_{bi} + \varepsilon_{frpu}$ and $\varepsilon_{bi} = \left(\dfrac{\varepsilon_{ci} + \varepsilon_{si}}{d}\right)h - \varepsilon_{ci} = \dfrac{M_{DL}(h - kd)}{I_{cr}E_c}$

$\varepsilon_{bi} = 0.000619$ (from Step 4)

$a_b = 7.21$ in

Force equilibrium:

$$0.85 f_c^{'} a_b b = A_s f_y + A_{frp} E_{frp} \varepsilon_{frpu}$$

Therefore,

$$A_{frp,b} = \frac{0.85 f_c^{'} b a_b - A_s f_y}{E_{frp} \varepsilon_{frpu}} = 13.1 > 0.6 \text{ (provided)}$$

The area of FRP needed for a balanced failure is 13.1 in^2, which is much larger than the provided area of 0.6 in^2. Hence, the failure mode is tension-controlled failure with FRP rupture*.

* The maximum strain level that can be achieved in the FRP reinforcement will be governed by the strain level developed in the FRP at the point at which the FRP debonds from the substrate.

Step7: Determine the Depth of the Neutral Axis and Design Strength

Assuming the failure mode to be tension-controlled with FRP rupture, and verify if the conditions for tension-controlled failure mode with FRP rupture are satisfied, i.e., $\varepsilon_s \geq 0.005$ and the FRP is at the point of incipient rupture,

$$\varepsilon_{frp} = \kappa_m \varepsilon_{frpu}$$

$$a = \frac{A_s f_y + A_{frp}(E_{frp} \kappa_m \varepsilon_{frpu})}{0.85 f_c^{'} b} = \boxed{2.03} \text{ in}$$

$$c = a / \beta_1 = 2.53 \text{ in}$$

$$\varepsilon_c = \left(\frac{\kappa_m \varepsilon_{frpu} + \varepsilon_{bi}}{h - c} \right) c = 0.000638$$

Verify the strains in steel and FRP.

$$\varepsilon_s = \left(\frac{\varepsilon_c}{c} \right)(d - c) = 0.00833 > 0.005 \Rightarrow \textbf{OK}$$

$$\varepsilon_{fe} = \varepsilon_{frp} = \left(\frac{\varepsilon_c}{c} \right)(h - c) - \varepsilon_{bi} = 0.00918 = \kappa_m \varepsilon_{frpu} = 0.00918 \Rightarrow \textbf{OK}$$

The nominal strength is

$$M_n = A_s f_y \left(d - \frac{a}{2} \right) + A_{frp}(E_{frp} \kappa_m \varepsilon_{frpu}) \left(h - \frac{a}{2} \right) = 18{,}572{,}735.6 \text{ lb-in}$$

The strength reduction factor for tension-controlled failure with steel yield and FRP rupture is $\phi = 0.9$. In addition to the use of the strength reduction factor required by ACI 318, an additional strength reduction factor ($\psi_f = 0.85$) is applied to the flexural strength provided by the FRP only. The design strength of the FRP strengthened beam is

$$\phi M_n = \phi\left[A_s f_y\left(d - \frac{a}{2}\right) + \psi_f A_{frp}\left(E_{frp}\kappa_m \varepsilon_{frpu}\right)\left(h - \frac{a}{2}\right)\right] = \boxed{\mathbf{1{,}366.6}}\ \textbf{k-ft}$$

which is larger than the ultimate strength $M_u = 1{,}270.7$ k-ft.

Step8: Check Service Stresses in the Reinforcing Steel, the FRP, and the Concrete

Calculate the depth of the cracked neutral axis by summing the first moment of the area of the elastic transformed section without accounting for the compression reinforcement.

First try rectangular beam analysis:

$$k = \sqrt{\left(\rho_s n_s + \rho_f n_f\right)^2 + 2\left(\rho_s n_s + \rho_f n_f\left(\frac{h}{d}\right)\right)} - \left(\rho_s n_s + \rho_f n_f\right) = 0.253$$

$kd = 9.01$ in, which is larger than the flange thickness, h_f. Therefore, T-beam analysis is needed (see Figure B.3)

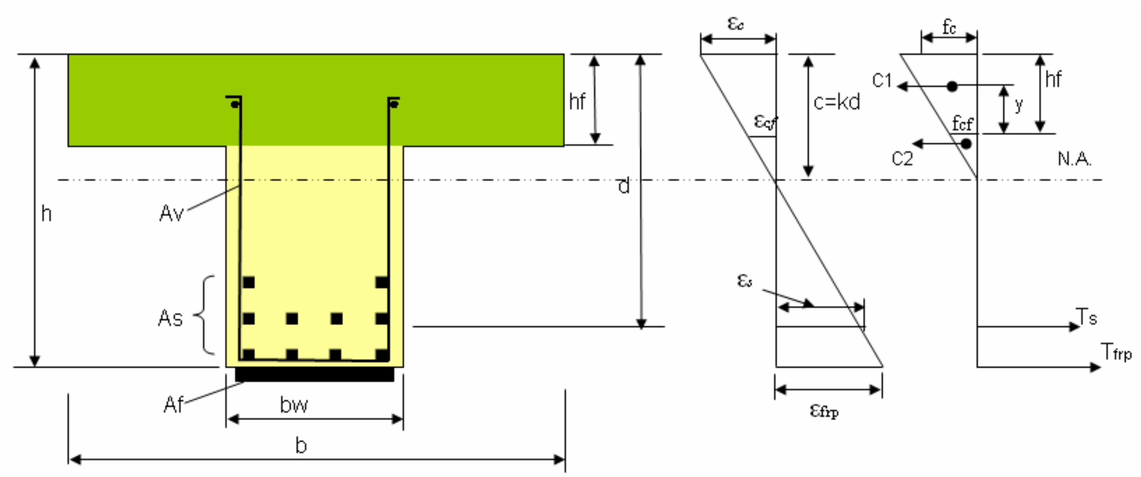

Figure B.3: Stress and Strain Distribution in FRP Reinforced concrete T-beam (Interior) under Service Load

Considering the force equilibrium in a cracked T-beam, referring to similar triangles, and using Hooke's Law, we obtain the depth of neutral axis under dead load,

$$c = \frac{-\left(h_f b - h_f b_w + A_s n_s + A_f n_f\right) + \sqrt{\left(h_f b - h_f b_w + A_s n_s + A_f n_f\right)^2 + b_w (h_f^2 b + 2A_s n_s d + 2A_f n_f h - b_w h_f^2)}}{b_w}$$

$= \boxed{9.02}$ in

Taking moments about the centroid of compression force resultant C_1, we obtain

$$M_s = A_s (E_s \varepsilon_s)(d - h_f + y) + A_f (E_f \varepsilon_f)(h - h_f + y) - \frac{1}{2} b_w f_{cf} (c - h_f)(y + \frac{c - h_f}{3})$$

where $y = \dfrac{h_f (3c - h_f)}{3(2c - h_f)}$, and $f_{cf} = f_c \dfrac{c - h_f}{c} = E_c \varepsilon_c \dfrac{c - h_f}{c}$.

Substituting $f_{cf} = E_c \varepsilon_c \dfrac{c - h_f}{c}$, $f_{s,s} = E_s \varepsilon_s$, $\varepsilon_b = \varepsilon_s \dfrac{h - c}{d - c}, \varepsilon_c = \varepsilon_s \dfrac{c}{d - c}$, and $\varepsilon_f = \varepsilon_b - \varepsilon_{bi}$ into the above equation and multiply both sides by E_s and simplifying, we obtain the stress level in the reinforcing steel:

$$f_{s,s} = \frac{6\left[M_s + A_f E_f \varepsilon_{bi}\left(h - h_f + y\right)\right]\left(d - c\right)E_s}{6A_s E_s \left(d - h_f + y\right)\left(d - c\right) + 6A_f E_f \left(h - c\right)\left(h - h_f + y\right) - b_w E_c \left(c - h_f\right)^2 \left(3y + c - h_f\right)}$$

$= \boxed{18{,}711.9}$ psi $< 0.8 f_y = 29{,}600 \Rightarrow$ **OK**

The stress level in the FRP system:

$$f_{f,s} = \left(\varepsilon_b - \varepsilon_{bi}\right)E_f = \varepsilon_s \frac{h - c}{d - c} E_f - \varepsilon_{bi} E_f = f_{s,s}\left(\frac{E_f}{E_s}\right)\left(\frac{h - c}{d - c}\right) - \varepsilon_{bi} E_f = \boxed{1{,}754.6} \text{ psi}$$

The creep-rupture stress limit for a carbon FRP system:

$F_{f,s} = 0.55 f_{fu} = 59{,}372.5$ psi

Check if $f_{f,s} < F_{f,s}$

$1{,}754.6 < 59{,}372.5 \Rightarrow$ **OK**

The stress level in the concrete under the service load:

$$f_{c,s} = \varepsilon_c E_c = \varepsilon_s \frac{c}{d-c} E_c = f_{s,s}\left(\frac{E_c}{E_s}\right)\left(\frac{c}{d-c}\right) = \boxed{880.7} \text{ psi}$$

$$F_{c,s} = 0.45 f_c^{'} = 2{,}252.3 \text{ psi}$$

$f_{c,s} < F_{c,s}$, i.e., $880.7 < 2{,}252.3 \Rightarrow$ **OK**

Therefore, the stress levels in the reinforcing steel, the FRP, and the concrete are within the recommended limit.

Step9: Compute the Cracking Moment M_{cr}

The tensile concrete cover splitting failure mode is controlled, in part, by the level of stress at the termination point of FRP laminate. To avoid this type of failure, for simply supported beams, the plies should extend a distance 6" past the point along the span corresponding to the cracking moment M_{cr} under factored loads. In addition, if the factored shear force at the termination point is greater than 2/3 the concrete shear strength ($V_u > 0.67V_c$), the FRP laminates should be anchored with transverse reinforcement to prevent the concrete cover layer from splitting (ACI 440.2R-02).

$$M_{cr} = f_r I_g / y_t = \boxed{290.9} \text{ k-ft}$$

where $f_r = 7.5\sqrt{f_c^{'}} = 530.6$ psi

$$\bar{y} = \frac{b_w\left(h-h_f\right)\left(\frac{h+h_f}{2}\right) + bh_f \frac{h_f}{2}}{b_w\left(h-h_f\right) + bh_f} = 15.2 \text{ in}$$

$$y_t = h - \bar{y} = 26.3 \text{ in}$$

$$I_g = \frac{bh_f^3}{12} + bh_f\left(\bar{y} - \frac{h_f}{2}\right)^2 + \frac{b_w\left(h-h_f\right)^3}{12} + b_w\left(h-h_f\right)\left(\frac{h+h}{2} - \bar{y}\right)^2$$

$$=173{,}162 \text{ in}^4$$

The position of M_{cr} is about 2.7 ft away from the support. Therefore, the length of the FRP laminate should be at least 40’7” (total length of the girder is 45’). In addition, since $V_u > 0.67V_c$ at the termination point, the FRP laminate should be anchored.

Summary: Use one layer carbon FRP wet-layup laminate with 15” wide bottom face of T-beam covered with composite layer. The length of FRP laminate should be at least 40’7” and anchors are needed at the termination point.

2. Exterior Girder 1

The T-beam shown in Figure B.4 is required resist a dead load, live load, and factored moments of $M_{DL} = 424.9$, $M_{LL} = 216.2$, and $M_u = 1021.8$ kips-ft, respectively.

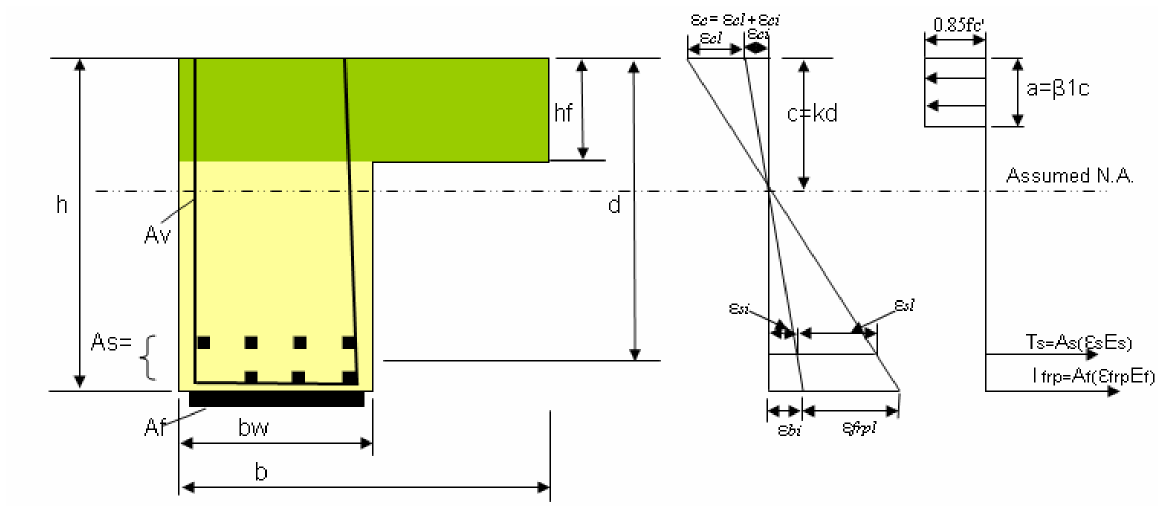

(a) (b) (c)

Figure B.4: Stress and Strain Distribution in FRP Reinforced concrete T-beam (Exterior Girder 1) under Ultimate Load.

- **Beam and Rebar Properties**

  Concrete compressive strength: fc' = 2,212 psi (linear reduction with measured pulse velocity)

  Effective depth of T-beam, d = 36.6 in (centroid of the rebar group)

Steel yield stress, fy = 37,000 psi

Elastic modulus of steel, Es = 29,000,000 psi

Effective width of T-beam, b = 39.4 in

Rebar area, As = 8.86 in2

Web width of T-beam, bw = 17.8 in

T-beam depth, h = 41.5 in

Elastic modulus of concrete, Ec = 2,680,819 psi

Flange thickness, hf = 8.5 in

- **Calculate Existing Flexural Capacity of T-Beam without Composites**

Step1: Determining the depth of the equivalent rectangular stress block *a*

$0.85 f_c^{'} ab = A_s f_y$ (C = T) (Assume *a* is within the flange)

$a = \dfrac{A_s f_y}{0.85 f_c^{'} b} =$ 4.42 in

$\beta_1 = 0.85$ for $f_c^{'} \leq 4{,}000$ psi

$c = a / \beta_1 = \boxed{5.20}$ in N.A. depth from the top surface of beam

$k = c / d =$ 0.142

Is *a* in the flange? Yes, assumption is correct.

Step2: Calculating the existing moment capacity

$M_n = A_s f_y (d - a/2) =$ 11267902 lb-in = 939 k-ft

$\Rightarrow \phi M_n = \boxed{845.1}$ k-ft < $M_u = 1{,}021.8$ k-ft

$(\phi M_n)_{w/oFRP} =$ 845.1 k-ft > $(1.2 M_{DL} + 0.85 M_{LL})_{new} =$ 693.7 k-ft

The existing moment capacity without FRP wrap is greater than the unstrengthened moment limit. The level of strengthening is acceptable because the criterion of the strength limit is satisfied.

The properties of the existing reinforcing steel:

$$\rho_s = \frac{A_s}{bd} = 0.00614$$

$$n_s = \frac{E_s}{E_c} = 10.8$$

$$\rho_s n_s = 0.0664$$

$$\rho_{\min} = 3\frac{\sqrt{f_c^{'}}}{f_y} = 0.00381$$

$$\rho_{provided} > \rho_{\min} \ (0.00614 > 0.00381)$$

The strain in steel:

$$\varepsilon_s = 0.003\left(\frac{d-c}{c}\right) = 0.0181 > 0.005$$

$$\varepsilon_y = \varepsilon_{sy} = \frac{f_y}{E_s} = 0.00128$$

The beam is ductile with a steel strain exceeding the yield value of 0.00128 and the minimum limit of tension-controlled failure mode strain value of 0.005. A nominal strength reduction factor $\phi = 0.9$ will be used.

- **Flexural Strengthening with Composites**

<u>Step3</u>: Material Properties of FRP and Preliminary Calculations

Use carbon FRP wet-layup laminate.

Environmental Durability Factor, $C_E = 0.85$

Ultimate tensile strength, $f_{fu} = C_E f_{fu}^* = 0.85(127000) = 107{,}950$ psi

Elastic modulus, $E_f = 10{,}500{,}000$ psi

Ultimate strain, $\varepsilon_{fu} = C_E \varepsilon_{fu}^* = 0.85(0.012) = 0.0102$

Nominal thickness of lamiante, $t_f = 0.04$ in

Number of FRP laminate layer, n = 2

Width of FRP strip, $w_f = 15$ in

Area of FRP strip, $A_f = n*t_f*w_f = 1.2$ in^2

$$\rho_f = \frac{A_f}{bd} = 0.00083$$

$$n_f = \frac{E_f}{E_c} = 3.92$$

$$\rho_f n_f = 0.00326$$

Step4: Determine the Existing State of Strain on the Soffit

The existing state of strain is calculated assuming the beam is cracked and the only loads acting on the beam at the time of the FRP installation are dead loads.

First try rectangular beam analysis:

$$k = \sqrt{(\rho_s n_s)^2 + 2(\rho_s n_s)} - (\rho_s n_s) = 0.304$$

$c = kd = 11.1$ in, which is larger than the flange thickness, h_f. Therefore *T-beam analysis is needed* (see Figure B.5)

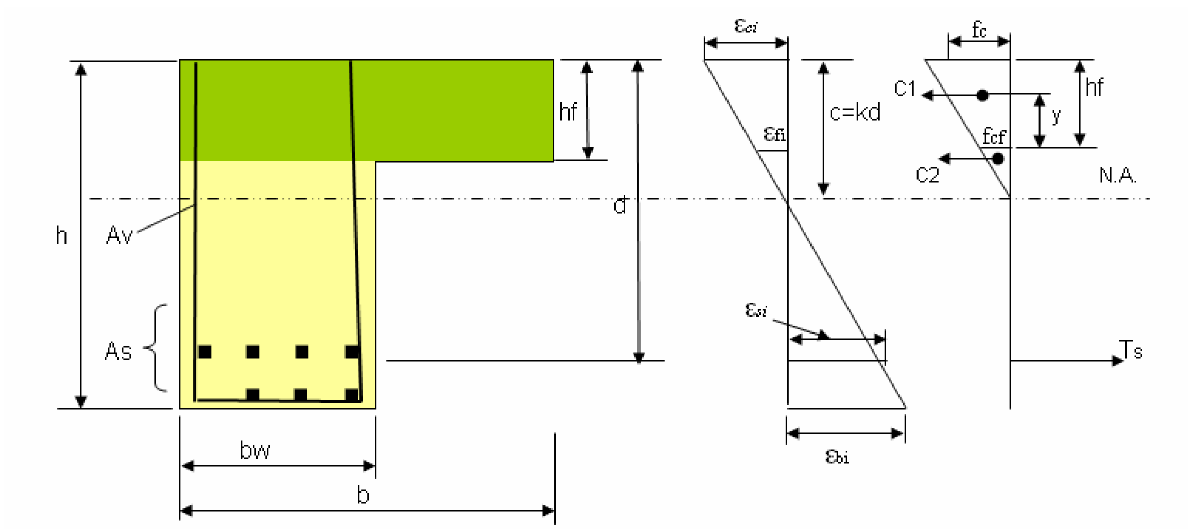

Figure B.5: Stress and Strain Distribution in Steel Reinforced concrete T-beam (Exterior Girder 1) under Dead Load

Considering the force equilibrium in a cracked T-beam, referring to similar triangles, and using Hooke's Law, we obtain

$$c = \frac{-(h_f b - h_f b_w + A_s n_s) + \sqrt{(h_f b - h_f b_w + A_s n_s)^2 + b_w (h_f^2 b + 2A_s n_s d - b_w h_f^2)}}{b_w} = \boxed{11.3} \text{ in}$$

The moment of inertia of cracked cross-section is

$$I_{cr} = \frac{1}{12} b h_f^3 + b h_f \left(c - h_f / 2\right)^2 + \frac{1}{3} b_w \left(c - h_f\right)^3 + n_s A_s \left(d - c\right)^2 = 80{,}080.8 \text{ in}^4$$

Therefore, the initial strain level is

$$\varepsilon_{bi} = \frac{M_{DL}(h-c)}{I_{cr} E_c} = \boxed{0.000718}$$

Step5: Determine the Bond-dependent Coefficient of the FRP System

The dimensionless bond-dependent coefficient for flexure, κ_m, is calculated using the following equation:

$$\kappa_m = \begin{cases} \dfrac{1}{60\varepsilon_{fu}} \left(1 - \dfrac{nE_f t_f}{2{,}000{,}000}\right) \le 0.90 & (nE_f t_f \le 1{,}000{,}000) \\ \dfrac{1}{60\varepsilon_{fu}} \left(\dfrac{500{,}000}{nE_f t_f}\right) \le 0.90 & (nE_f t_f > 1{,}000{,}000) \end{cases}$$

$nE_f t_f = 840{,}000 < 1{,}000{,}000$

Therefore,

$\kappa_m = 0.948 > 0.9 \Rightarrow$ Thus, choose $\kappa_m = \boxed{0.9}$

Step6: Determine the Depth of the Neutral Axis for a Balanced Failure and the Amount of FRP Reinforcement Needed for a Balanced Failure

Compare the calculated amount of FRP reinforcement for a balanced failure and compare it with the amount of FRP provided to determine the possible failure mode for the FRP strengthened beam.

Hypothetical balanced failure mode is assumed to occur when strain in extreme tension and compression fibers have reached their limit values simultaneously.

Strain in concrete: $\varepsilon_c = \varepsilon_{cu} = 0.003$

Strain in steel: $\varepsilon_s = \varepsilon_y$ (this is a consequence of strain in extreme FRP tension fiber reaching its ultimate value)

Strain in FRP: $\varepsilon_{frp} = \varepsilon_{frpu}$

These strain conditions at balanced failure can be expressed as follows from similar triangles principle:

$$\frac{c_b}{h} = \frac{\varepsilon_{cu}}{\varepsilon_{cu} + \varepsilon_{bi} + \varepsilon_{frpu}} \text{ or } a_b = \beta_1 h\left(\frac{\varepsilon_{cu}}{\varepsilon_{cu} + \varepsilon_{bi} + \varepsilon_{frpu}}\right)$$

where $\varepsilon_b =_{bi} + \varepsilon_{frpu}$ and $\varepsilon_{bi} = \left(\frac{\varepsilon_{ci} + \varepsilon_{si}}{d}\right)h - \varepsilon_{ci} = \frac{M_{DL}(h-kd)}{I_{cr}E_c}$

$\varepsilon_{bi} =$ 0.000718 (from Step 4)

$a_b =$ 7.60 in

Force equilibrium:

$$0.85 f_c^{'} a_b b = A_s f_y + A_{frp} E_{frp} \varepsilon_{frpu}$$

Therefore,

$$A_{frp,b} = \frac{0.85 f_c^{'} b a_b - A_s f_y}{E_{frp}\varepsilon_{frpu}} = 2.20 > 1.2 \text{ (provided)}$$

The area of FRP needed for a balanced failure is 2.20 in^2, which is larger than the provided area of 1.26 in^2. Hence, the failure mode is tension-controlled failure with FRP rupture*.

* The maximum strain level that can be achieved in the FRP reinforcement will be governed by the strain level developed in the FRP at the point at which the FRP debonds from the substrate.

Step7: Determine the Depth of the Neutral Axis and Design Strength

Assuming the failure mode to be tension-controlled with FRP rupture, and verify if the conditions for tension-controlled failure mode with FRP rupture are satisfied, i.e., $\varepsilon_s \geq 0.005$ and the FRP is at the point of incipient rupture,

$\varepsilon_{frp} = \kappa_m \varepsilon_{frpu}$.

$$a = \frac{A_s f_y + A_{frp}(E_{frp}\kappa_m\varepsilon_{frpu})}{0.85 f_c^{'} b} = \boxed{5.98} \text{ in}$$

$c = a/\beta_1 =$ 7.04 in

$$\varepsilon_c = \left(\frac{\kappa_m \varepsilon_{frpu} + \varepsilon_{bi}}{h - c} \right) c = \ 0.00202$$

Verify the strains in steel and FRP.

$$\varepsilon_s = \left(\frac{\varepsilon_c}{c} \right) (d - c) = \ 0.008849 > 0.005 \qquad \Rightarrow \textbf{OK}$$

$$\varepsilon_{fe} = \varepsilon_{frp} = \left(\frac{\varepsilon_c}{c} \right) (h - c) - \varepsilon_{bi} = \ 0.00918 = \ \kappa_m \varepsilon_{frpu} = 0.00918 \Rightarrow \textbf{OK}$$

The nominal strength is

$$M_n = A_s f_y \left(d - \frac{a}{2} \right) + A_{frp} (E_{frp} \kappa_m \varepsilon_{frpu}) \left(h - \frac{a}{2} \right) = \ 15{,}466{,}574.5 \text{ lb-in}$$

The strength reduction factor for tension-controlled failure with steel yield and FRP rupture is $\phi = 0.9$. In addition to the use of the strength reduction factor required by ACI 318, an additional strength reduction factor ($\psi_f = 0.85$) is applied to the flexural strength provided by the FRP only. The design strength of the FRP strengthened beam is

$$\phi M_n = \phi \left[A_s f_y \left(d - \frac{a}{2} \right) + \psi_f A_{frp} \left(E_{frp} \kappa_m \varepsilon_{frpu} \right) \left(h - \frac{a}{2} \right) \right] = \boxed{\mathbf{1{,}109.9}} \textbf{ k-ft}$$

which is larger than the ultimate strength $M_u = 1{,}021.8$ k-ft.

Step8: Check Service Stresses in the Reinforcing Steel, the FRP, and the Concrete

Calculate the depth of the cracked neutral axis by summing the first moment of the area of the elastic transformed section without accounting for the compression reinforcement.

First try rectangular beam analysis:

$$k = \sqrt{(\rho_s n_s + \rho_f n_f)^2 + 2 \left(\rho_s n_s + \rho_f n_f \left(\frac{h}{d} \right) \right)} - (\rho_s n_s + \rho_f n_f) = \ 0.311$$

$kd = $ 11.4 in, which is larger than the flange thickness, h_f. Therefore, T-beam analysis is needed (see Figure B.6)

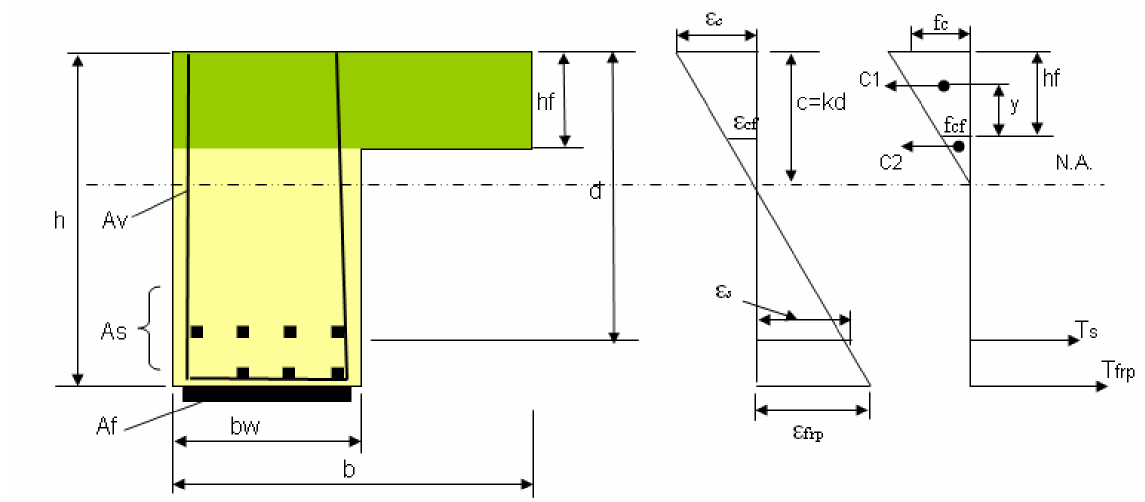

Figure B.6: Stress and Strain Distribution in FRP Reinforced concrete T-beam (Exterior Girder 1) under Service Load

Considering the force equilibrium in a cracked T-beam, referring to similar triangles, and using Hooke's Law, we obtain

$$c = \frac{-\left(h_f b - h_f b_w + A_s n_s + A_f n_f\right) + \sqrt{\left(h_f b - h_f b_w + A_s n_s + A_f n_f\right)^2 + b_w (h_f^2 b + 2A_s n_s d + 2A_f n_f h - b_w h_f^2)}}{b_w}$$

$= \boxed{11.6}$ in

Taking moments about the centroid of compression force resultant C_1, we obtain

$$M_s = A_s(E_s\varepsilon_s)(d - h_f + y) + A_f(E_f\varepsilon_f)(h - h_f + y) - \frac{1}{2} b_w f_{cf}(c - h_f)(y + \frac{c - h_f}{3})$$

where $y = \dfrac{h_f(3c - h_f)}{3(2c - h_f)}$, and $f_{cf} = f_c \dfrac{c - h_f}{c} = E_c \varepsilon_c \dfrac{c - h_f}{c}$.

Substituting $f_{cf} = E_c \varepsilon_c \dfrac{c - h_f}{c}$, $f_{s,s} = E_s \varepsilon_s$, $\varepsilon_b = \varepsilon_s \dfrac{h - c}{d - c}$, $\varepsilon_c = \varepsilon_s \dfrac{c}{d - c}$, and

$\varepsilon_f = \varepsilon_b - \varepsilon_{bi}$ into the above equation and multiply both sides by E_s and simplifying, we obtain the stress level in the reinforcing steel:

$$f_{s,s} = \frac{6\left[M_s + A_f E_f \varepsilon_{bi}\left(h - h_f + y\right)\right]\left(d - c\right)E_s}{6A_s E_s\left(d - h_f + y\right)\left(d - c\right) + 6A_f E_f\left(h - c\right)\left(h - h_f + y\right) - b_w E_c\left(c - h_f\right)^2\left(3y + c - h_f\right)}$$

$= \boxed{21{,}759.8}$ psi $< 0.8 f_y = 29{,}600 \Rightarrow$ **OK**

The stress level in the FRP system:

$$f_{f,s} = (\varepsilon_b - \varepsilon_{bi})E_f = \varepsilon_s \frac{h-c}{d-c} E_f - \varepsilon_{bi} E_f = f_{s,s}\left(\frac{E_f}{E_s}\right)\left(\frac{h-c}{d-c}\right) - \varepsilon_{bi} E_f = \boxed{1{,}890.3} \text{ psi}$$

The creep-rupture stress limit for a carbon FRP system:

$F_{f,s} = 0.55 f_{fu} =$ 59,372.5 psi

Check if $f_{f,s} < F_{f,s}$

1,890.3 < 59,372.5 $\Rightarrow$ **OK**

The stress level in the concrete under the service load:

$$f_{c,s} = \varepsilon_c E_c = \varepsilon_s \frac{c}{d-c} E_c = f_{s,s}\left(\frac{E_c}{E_s}\right)\left(\frac{c}{d-c}\right) = \boxed{930.5} \text{ psi}$$

$F_{c,s} = 0.45 f_c^{'} =$ 995.4 psi

$f_{c,s} < F_{c,s}$, i.e., 930.5 < 995.4 $\Rightarrow$ **OK**

Therefore, the stress levels in the reinforcing steel, the FRP, and the concrete are within the recommended limit.

Step9: Compute the Cracking Moment M_{cr}

The tensile concrete cover splitting failure mode is controlled, in part, by the level of stress at the termination point of FRP laminate. To avoid this type of failure, for simply supported beams, the plies should extend a distance 6" past the point along the span corresponding to the cracking moment M_{cr} under factored loads. In addition, if the factored shear force at the termination point is greater than 2/3 the concrete shear strength ($V_u > 0.67V_c$), the FRP laminates should be anchored with transverse reinforcement to prevent the concrete cover layer from splitting (ACI 440.2R-02).

$M_{cr} = f_r I_g / y_t = \boxed{179.6}$ k-ft where $f_r = 7.5\sqrt{f_c^{'}} =$ 352.7 psi

$$\bar{y} = \frac{b_w\left(h - h_f\right)\left(\frac{h + h_f}{2}\right) + bh_f\,\frac{h_f}{2}}{b_w\left(h - h_f\right) + bh_f} = 17.4 \text{ in}$$

$$y_t = h - \bar{y} = 24.1 \text{ in}$$

$$I_g = \frac{bh_f^3}{12} + bh_f\left(\bar{y} - \frac{h_f}{2}\right)^2 + \frac{b_w\left(h - h_f\right)^3}{12} + b_w\left(h - h_f\right)\left(\frac{h + h}{2} - \bar{y}\right)^2$$

$$= 146{,}973 \text{ in}^4$$

The position of M_{cr} is about 1.6 ft away from the support. Therefore, the length of the FRP laminate should be at least 42'7" (total length of the girder is 45'). In addition, since $V_u > 0.67V_c$ at the termination point, the FRP laminate should be anchored.

<u>**Summary**</u>: Use two layers carbon FRP wet-layup laminate with 15" wide bottom face of T-beam covered with composite layer. The length of FRP laminate should be at least 42'7" and anchors are needed at the termination point.

3. Exterior Girder 6

The T-beam shown in Figure B.7 is required resist a dead load, live load, and factored moments of M_{DL} =424.9, M_{LL} =216.2, and M_u = 1021.8 kips-ft, respectively.

- **Beam and Rebar Properties**

  Concrete compressive strength: fc' = 2,212 psi (linear reduction with measured pulse velocity)

  Effective depth of T-beam, d = 36.9 in (centroid of the rebar group)

  Steel yield stress, fy = 37,000 psi

  Elastic modulus of steel, Es = 29,000,000 psi

  Effective width of T-beam, b = 39.4 in

Rebar area, As = 10.1 in2

Web width of T-beam, bw = 17.8 in

T-beam depth, h = 41.5 in

Elastic modulus of concrete, Ec = 2,680,819 psi

Flange thickness, hf = 8.5 in

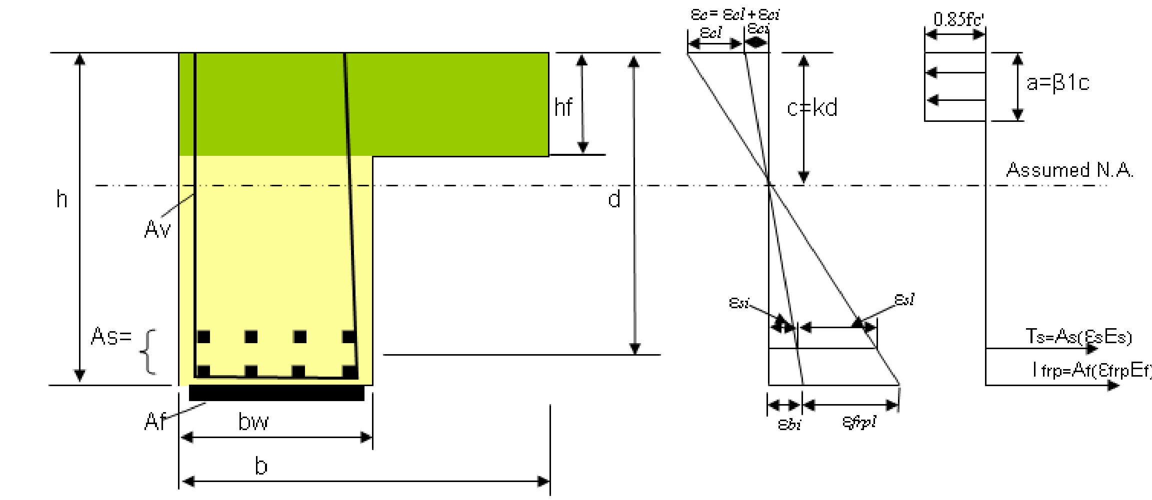

(a) (b) (c)

Figure B.7: Stress and Strain Distribution in FRP Reinforced concrete T-beam (Exterior Girder 6) under Ultimate Load.

- **Calculate Existing Flexural Capacity of T-Beam without Composites**

Step1: Determining the depth of the equivalent rectangular stress block *a*

$$0.85 f_c^{'} ab = A_s f_y \text{ (C = T) (Assume } a \text{ is within the flange)}$$

$$a = \frac{A_s f_y}{0.85 f_c^{'} b} = 5.05 \text{ in}$$

$$\beta_1 = 0.85 \text{ for } f_c^{'} \leq 4{,}000 \text{ psi}$$

$$c = a / \beta_1 = \boxed{5.94} \text{ in} \qquad \text{N.A. depth from the top surface of beam}$$

$$k = c / d = 0.161$$

Is *a* in the flange? Yes, assumption is correct.

Step2: Calculating the existing moment capacity

$$M_n = A_s f_y (d - a/2) = 12867951 \text{ lb-in} = 1{,}072.3 \text{ k-ft}$$

$$\Rightarrow \phi M_n = \boxed{965.1} \text{ k-ft} < M_u = 1{,}021.8 \text{ k-ft}$$

$(\phi M_n)_{w/oFRP}$ = 965.1 k-ft > $(1.2M_{DL} + 0.85M_{LL})_{new}$ = 693.7 k-ft

The existing moment capacity without FRP wrap is greater than the unstrengthened moment limit. The level of strengthening is acceptable because the criterion of the strength limit is satisfied.

The properties of the existing reinforcing steel:

$$\rho_s = \frac{A_s}{bd} = 0.00696$$

$$n_s = \frac{E_s}{E_c} = 10.8$$

$$\rho_s n_s = 0.0753$$

$$\rho_{\min} = 3\frac{\sqrt{f_c^{'}}}{f_y} = 0.00381$$

$$\rho_{provided} > \rho_{\min} \ (0.00696 > 0.00381)$$

The strain in steel:

$$\varepsilon_s = 0.003\left(\frac{d-c}{c}\right) = 0.0156 > 0.005$$

$$\varepsilon_y = \varepsilon_{sy} = \frac{f_y}{E_s} = 0.00128$$

The beam is ductile with a steel strain exceeding the yield value of 0.00128 and the minimum limit of tension-controlled failure mode strain value of 0.005. A nominal strength reduction factor $\phi = 0.9$ will be used.

- **Flexural Strengthening with Composites**

Step3: Material Properties of FRP and Preliminary Calculations

Use carbon FRP wet-layup laminate.

Environmental Durability Factor, C_E = 0.85

Ultimate tensile strength, $f_{fu} = C_E f_{fu}^{*} = 0.85(127000) = 107{,}950$ psi

Elastic modulus, E_f = 10,500,000 psi

Ultimate strain, $\varepsilon_{fu} = C_E \varepsilon^*_{fu} = 0.85(0.012) = 0.0102$

Nominal thickness of laminate, t_f = 0.04 in

Number of FRP laminate layer, n = 1

Width of FRP strip, w_f = 15 in

Area of FRP strip, $A_f = n*t_f*w_f = 0.6$ in^2

$$\rho_f = \frac{A_f}{bd} = 0.00041$$

$$n_f = \frac{E_f}{E_c} = 3.92$$

$$\rho_f n_f = 0.00162$$

Step4: Determine the Existing State of Strain on the Soffit

The existing state of strain is calculated assuming the beam is cracked and the only loads acting on the beam at the time of the FRP installation are dead loads.

First try rectangular beam analysis:

$$k = \sqrt{(\rho_s n_s)^2 + 2(\rho_s n_s)} - (\rho_s n_s) = 0.320$$

$c = kd = 11.8$ in, which is larger than the flange thickness, h_f. Therefore *T-beam analysis is needed* (see Figure B.8)

Considering the force equilibrium in a cracked T-beam, referring to similar triangles, and using Hooke's Law, we obtain

$$c = \frac{-\left(h_f b - h_f b_w + A_s n_s\right) + \sqrt{\left(h_f b - h_f b_w + A_s n_s\right)^2 + b_w(h_f^2 b + 2A_s n_s d - b_w h_f^2)}}{b_w} = \boxed{12.04} \text{ in}$$

The moment of inertia of cracked cross-section is

$$I_{cr} = \frac{1}{12} b h_f^3 + b h_f \left(c - h_f / 2\right)^2 + \frac{1}{3} b_w \left(c - h_f\right)^3 + n_s A_s \left(d - c\right)^2 = 90{,}177.7 \text{ in}^4$$

Therefore, the initial strain level is

$$\varepsilon_{bi} = \frac{M_{DL}(h-c)}{I_{cr}E_c} = \boxed{0.000621}$$

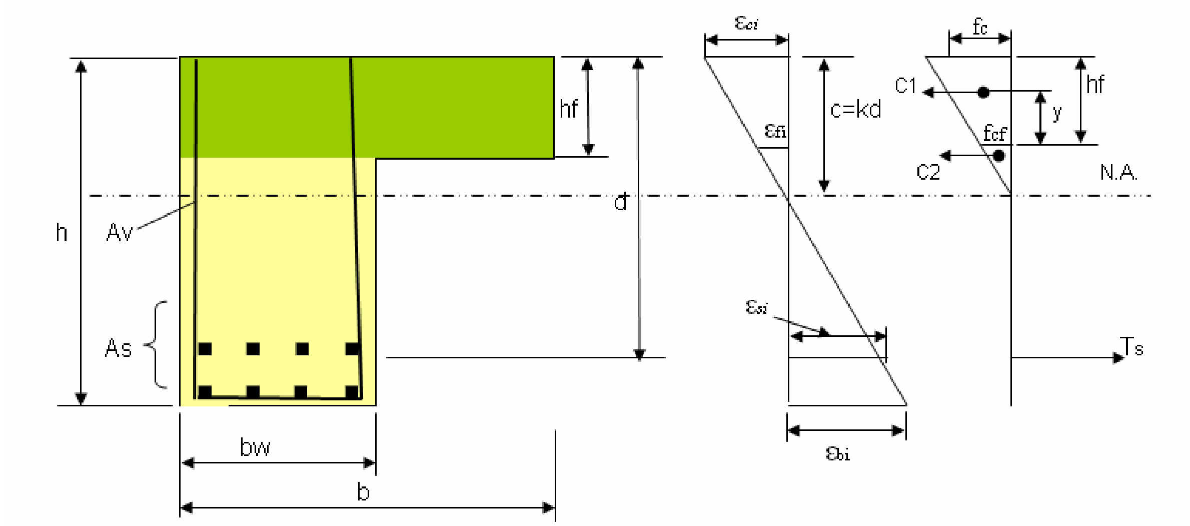

Figure B.8: Stress and Strain Distribution in Steel Reinforced concrete T-beam (Exterior Girder 1) under Dead Load

Step5: Determine the Bond-dependent Coefficient of the FRP System

The dimensionless bond-dependent coefficient for flexure, κ_m, is calculated using the following equation:

$$\kappa_m = \begin{cases} \dfrac{1}{60\varepsilon_{fu}}\left(1 - \dfrac{nE_f t_f}{2{,}000{,}000}\right) \leq 0.90 & (nE_f t_f \leq 1{,}000{,}000) \\ \dfrac{1}{60\varepsilon_{fu}}\left(\dfrac{500{,}000}{nE_f t_f}\right) \leq 0.90 & (nE_f t_f > 1{,}000{,}000) \end{cases}$$

$$nE_f t_f = 420{,}000 < 1{,}000{,}000$$

Therefore,

$\kappa_m = 0.129 > 0.9 \;\; \Rightarrow$ Thus, choose $\kappa_m = \boxed{0.9}$

Step6: Determine the Depth of the Neutral Axis for a Balanced Failure and the Amount of FRP Reinforcement Needed for a Balanced Failure

Compare the calculated amount of FRP reinforcement for a balanced failure and compare it with the amount of FRP provided to determine the possible failure mode for the FRP strengthened beam.

Hypothetical balanced failure mode is assumed to occur when strain in extreme tension and compression fibers have reached their limit values simultaneously.

Strain in concrete: $\varepsilon_c = \varepsilon_{cu} = 0.003$

Strain in steel: $\varepsilon_s = \varepsilon_y$ (this is a consequence of strain in extreme FRP tension fiber reaching its ultimate value)

Strain in FRP: $\varepsilon_{frp} = \varepsilon_{frpu}$

These strain conditions at balanced failure can be expressed as follows from similar triangles principle:

$$\frac{c_b}{h} = \frac{\varepsilon_{cu}}{\varepsilon_{cu} + \varepsilon_{bi} + \varepsilon_{frpu}} \text{ or } a_b = \beta_1 h\left(\frac{\varepsilon_{cu}}{\varepsilon_{cu} + \varepsilon_{bi} + \varepsilon_{frpu}}\right)$$

where $\varepsilon_b =_{bi} + \varepsilon_{frpu}$ and $\varepsilon_{bi} = \left(\frac{\varepsilon_{ci} + \varepsilon_{si}}{d}\right)h - \varepsilon_{ci} = \frac{M_{DL}(h-kd)}{I_{cr}E_c}$

$\varepsilon_{bi} =$ 0.000621 (from Step 4)

$a_b =$ 7.66 in

Force equilibrium:

$$0.85 f_c^{'} a_b b = A_s f_y + A_{frp} E_{frp} \varepsilon_{frpu}$$

Therefore,

$$A_{frp,b} = \frac{0.85 f_c^{'} b a_b - A_s f_y}{E_{frp} \varepsilon_{frpu}} = 1.8 > 0.6 \text{ (provided)}$$

The area of FRP needed for a balanced failure is 1.8 in^2, which is larger than the provided area of 0.6 in^2. Hence, the failure mode is tension-controlled failure with FRP rupture*.

* The maximum strain level that can be achieved in the FRP reinforcement will be governed by the strain level developed in the FRP at the point at which the FRP debonds from the substrate.

Step7: Determine the Depth of the Neutral Axis and Design Strength

Assuming the failure mode to be tension-controlled with FRP rupture, and verify if the conditions for tension-controlled failure mode with FRP rupture are satisfied, i.e., $\varepsilon_s \geq 0.005$ and the FRP is at the point of incipient rupture,

$\varepsilon_{frp} = \kappa_m \varepsilon_{frpu}$.

$$a = \frac{A_s f_y + A_{frp}(E_{frp}\kappa_m \varepsilon_{frpu})}{0.85 f_c' b} = \boxed{5.83} \text{ in}$$

$$c = a/\beta_1 = 6.86 \text{ in}$$

$$\varepsilon_c = \left(\frac{\kappa_m \varepsilon_{frpu} + \varepsilon_{bi}}{h-c}\right)c = 0.00194$$

Verify the strains in steel and FRP.

$$\varepsilon_s = \left(\frac{\varepsilon_c}{c}\right)(d-c) = 0.00849 > 0.005 \Rightarrow \textbf{OK}$$

$$\varepsilon_{fe} = \varepsilon_{frp} = \left(\frac{\varepsilon_c}{c}\right)(h-c) - \varepsilon_{bi} = 0.00918 = \kappa_m \varepsilon_{frpu} = 0.00918 \Rightarrow \textbf{OK}$$

The nominal strength is

$$M_n = A_s f_y\left(d - \frac{a}{2}\right) + A_{frp}(E_{frp}\kappa_m \varepsilon_{frpu})\left(h - \frac{a}{2}\right) = 14{,}953{,}316.8 \text{ lb-in}$$

The strength reduction factor for tension-controlled failure with steel yield and FRP rupture is $\phi = 0.9$. In addition to the use of the strength reduction factor required by ACI 318, an additional strength reduction factor ($\psi_f = 0.85$) is applied to the flexural strength provided by the FRP only. The design strength of the FRP strengthened beam is

$$\phi M_n = \phi\left[A_s f_y\left(d - \frac{a}{2}\right) + \psi_f A_{frp}\left(E_{frp}\kappa_m \varepsilon_{frpu}\right)\left(h - \frac{a}{2}\right)\right] = \boxed{\textbf{1,096.4}} \textbf{ k-ft}$$

which is larger than the ultimate strength $M_u = 1{,}021.8$ k-ft.

Step8: Check Service Stresses in the Reinforcing Steel, the FRP, and the Concrete

Calculate the depth of the cracked neutral axis by summing the first moment of the area of the elastic transformed section without accounting for the compression reinforcement.

First try rectangular beam analysis:

$$k=\sqrt{\left(\rho_s n_s+\rho_f n_f\right)^2+2\left(\rho_s n_s+\rho_f n_f\left(\frac{h}{d}\right)\right)}-\left(\rho_s n_s+\rho_f n_f\right)=\ 0.323$$

$kd=$ 11.4 in, which is larger than the flange thickness, h_f. Therefore, T-beam analysis is needed (see Figure B.9)

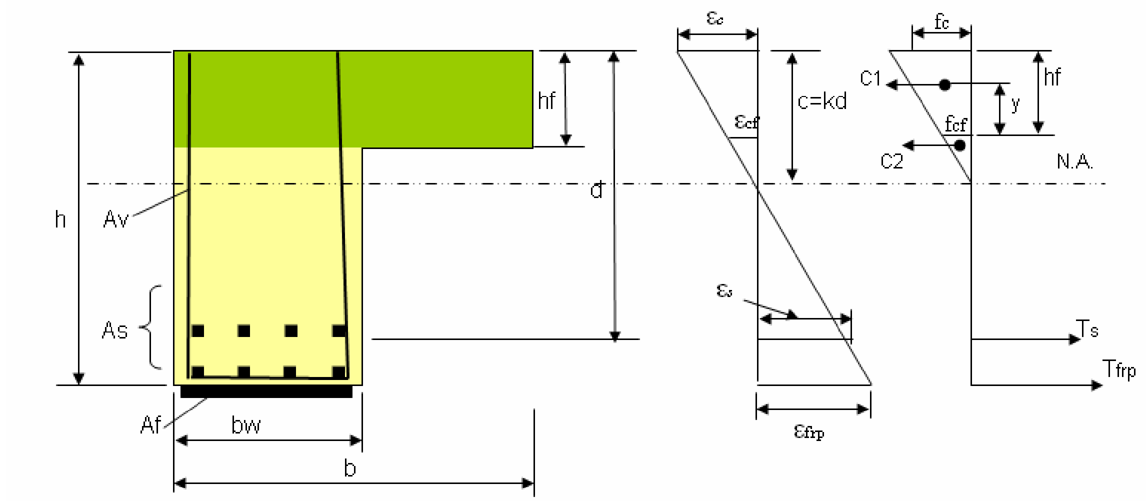

Figure B.9: Stress and Strain Distribution in FRP Reinforced concrete T-beam (Exterior Girder 6) under Service Load

Considering the force equilibrium in a cracked T-beam, referring to similar triangles and using Hooke's Law, we obtain

$$c=\frac{-\left(h_f b-h_f b_w+A_s n_s+A_f n_f\right)+\sqrt{\left(h_f b-h_f b_w+A_s n_s+A_f n_f\right)^2+b_w(h_f^2 b+2A_s n_s d+2A_f n_f h-b_w h_f^2)}}{b_w}$$

$=\boxed{12.2}$ in

Taking moments about the centroid of compression force resultant C_1, we obtain

$$M_s=A_s(E_s\varepsilon_s)(d-h_f+y)+A_f(E_f\varepsilon_f)(h-h_f+y)-\frac{1}{2}b_w f_{cf}(c-h_f)(y+\frac{c-h_f}{3})$$

where $y=\dfrac{h_f(3c-h_f)}{3(2c-h_f)}$, and $f_{cf}=f_c\dfrac{c-h_f}{c}=E_c\varepsilon_c\dfrac{c-h_f}{c}$.

Substituting $f_{cf}=E_c\varepsilon_c\dfrac{c-h_f}{c}$, $f_{s,s}=E_s\varepsilon_s$, $\varepsilon_b=\varepsilon_s\dfrac{h-c}{d-c}$, $\varepsilon_c=\varepsilon_s\dfrac{c}{d-c}$, and

$\varepsilon_f = \varepsilon_b - \varepsilon_{bi}$ into the above equation and multiply both sides by E_s and simplifying, we obtain the stress level in the reinforcing steel:

$$f_{s,s} = \frac{6\left[M_s + A_f E_f \varepsilon_{bi}\left(h - h_f + y\right)\right]\left(d-c\right)E_s}{6A_s E_s\left(d - h_f + y\right)\left(d-c\right) + 6A_f E_f\left(h-c\right)\left(h - h_f + y\right) - b_w E_c\left(c - h_f\right)^2\left(3y + c - h_f\right)}$$

$= \boxed{19{,}205.8}$ psi $< 0.8 f_y = 29{,}600 \Rightarrow$ **OK**

The stress level in the FRP system:

$$f_{f,s} = \left(\varepsilon_b - \varepsilon_{bi}\right)E_f = \varepsilon_s \frac{h-c}{d-c} E_f - \varepsilon_{bi} E_f = f_{s,s}\left(\frac{E_f}{E_s}\right)\left(\frac{h-c}{d-c}\right) - \varepsilon_{bi} E_f = \boxed{1{,}730.5} \text{ psi}$$

The creep-rupture stress limit for a carbon FRP system:

$F_{f,s} = 0.55 f_{fu} = 59{,}372.5$ psi

Check if $f_{f,s} < F_{f,s}$

$1{,}730.5 < 59{,}372.5 \Rightarrow$ **OK**

The stress level in the concrete under the service load:

$$f_{c,s} = \varepsilon_c E_c = \varepsilon_s \frac{c}{d-c} E_c = f_{s,s}\left(\frac{E_c}{E_s}\right)\left(\frac{c}{d-c}\right) = \boxed{874.7} \text{ psi}$$

$F_{c,s} = 0.45 f_c' = 995.4$ psi

$f_{c,s} < F_{c,s}$, i.e., $874.7 < 995.4 \Rightarrow$ **OK**

Therefore, the stress levels in the reinforcing steel, the FRP, and the concrete are within the recommended limit.

Step9: Compute the Cracking Moment M_{cr}

The tensile concrete cover splitting failure mode is controlled, in part, by the level of stress at the termination point of FRP laminate. To avoid this type of failure, for simply supported beams, the plies should extend a distance 6” past the point along the span corresponding to the cracking moment M_{cr} under factored loads. In addition, if the factored shear force at the termination point is greater than 2/3 the concrete shear strength ($V_u > 0.67V_c$), the FRP laminates should be anchored with transverse reinforcement to prevent the concrete cover layer from splitting (ACI 440.2R-02).

$$M_{cr} = f_r I_g / y_t = \boxed{179.6} \text{ k-ft}$$

where $f_r = 7.5\sqrt{f_c^{'}} = 352.7$ psi

$$\bar{y} = \frac{b_w\left(h-h_f\right)\left(\dfrac{h+h_f}{2}\right)+bh_f\dfrac{h_f}{2}}{b_w\left(h-h_f\right)+bh_f} = 17.4 \text{ in}$$

$$y_t = h - \bar{y} = 24.1 \text{ in}$$

$$I_g = \frac{bh_f^3}{12} + bh_f\left(\bar{y}-\frac{h_f}{2}\right)^2 + \frac{b_w\left(h-h_f\right)^3}{12} + b_w\left(h-h_f\right)\left(\frac{h+h}{2}-\bar{y}\right)^2$$

$$= 146{,}973 \text{ in}^4$$

The position of M_{cr} is about 1.6 ft away from the support. Therefore, the length of the FRP laminate should be at least 42'7" (total length of the girder is 45'). In addition, since $V_u > 0.67V_c$ at the termination point, the FRP laminate should be anchored.

Summary: Use one layer carbon FRP wet-layup laminate with 15" wide bottom face of T-beam covered with composite layer. The length of FRP laminate should be at least 42'7" and anchors are needed at the termination point.

Appendix C – Design of FRP Shear Strengthening for Girders

FRP strengthening is needed for Region 3 of the interior girders. The T-beam shown in Figure C.1 is required to resist a factored load shear of $V_u = 152.6$, 129.1, 106.8, and 69.0 kips at Section 1, 2, 3 and 4, respectively.

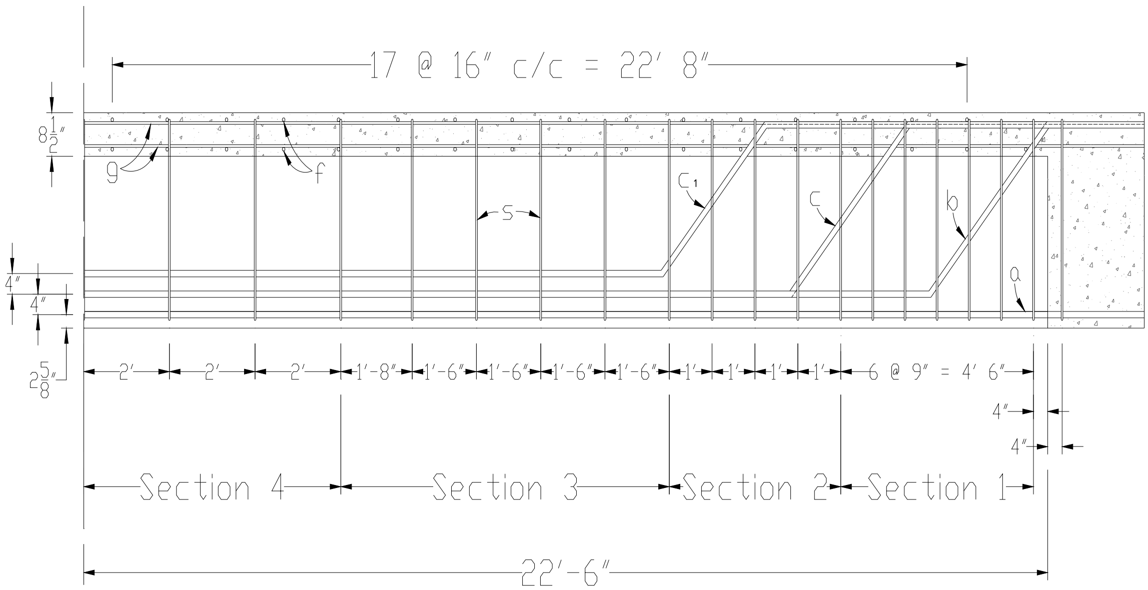

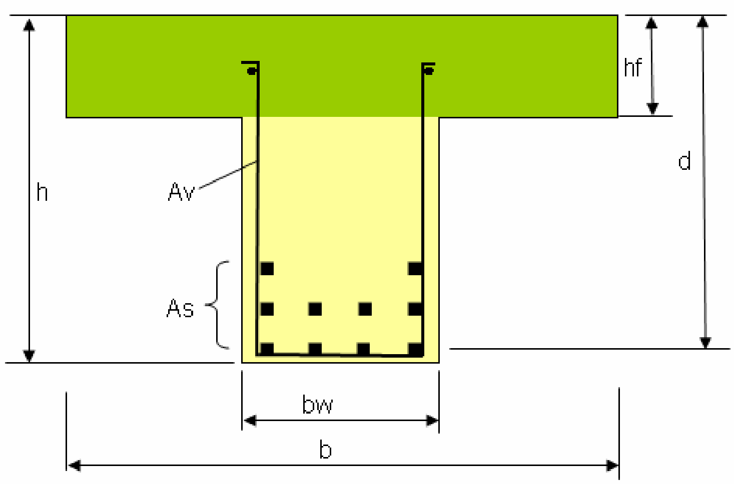

Figure C.1: Interior T-beam Cross-section.

Beam and Stirrup Properties:

Concrete compressive strength, fc' = 5,005 psi (lower value from deck core samples)

Effective depth of beam, d = 38.9 in (remove bottom cover)

Steel yield stress of stirrups, fy = 37 ksi

Elastic modulus of steel, Es = 29,000 ksi

Stirrup spacing, S = 9 in, 12 in, 18 in, and 24 in for Region 1, 2, 3, and 4 respectively

Steel area in shear for each stirrup, Avs = (2 legs) = 0.353 in^2 (80% of original value)

Steel area in bent, Avb = 2.53 in^2 (measured dimension)

Web width, bw = 12.5 in (remove side cover)

Calculate Existing Shear Capacity of Beam without Composites

Calculate shear capacity of beam using following equation:

$$V_n = V_c + V_s = 2\sqrt{f_c^{'}} b_w d + \frac{A_{vs} f_y d}{s_s} + A_{vb} f_y \sin\alpha$$

where $\alpha = 45^o$.

V_n = 205.3 kips, 192 kips, 105.3 kips, and 101.3 kips for Region 1, 2, 3, and 4 respectively.

Design strength,

$\phi V_n = \boxed{154.0}$ kips, $\boxed{144.0}$ kips, $\boxed{\mathbf{79.0}}$ kips, and $\boxed{76.0}$ kips for Region 1, 2, 3, and 4 respectively. Where $\phi = 0.75$ (ACI 318-02).

<u>The existing beams do not have adequate capacity to resist the anticipated shear in Region 3.</u>

FRP Shear Strengthening Design for Region C

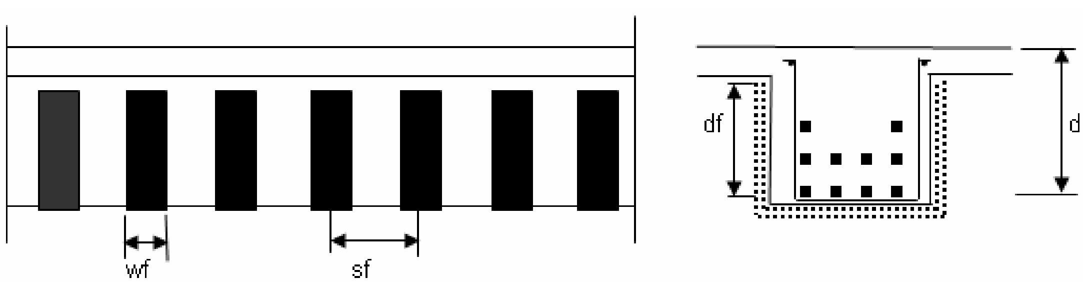

Figure C.2: FRP Shear Strengthening Design

Each FRP strip consists of one layer laminate (n = 1)

d = 41.4 in

df = 28.4 in

wf = 10 in, width of each strip

sf = 12 in, span between each strip

Use carbon FRP wet-layup laminate:

Ultimate tensile strength, $f_{fu} = C_E f_{fu}^* = 0.85(127{,}000) = 107.95$ ksi

Elastic modulus, $E_f = 10{,}500$ ksi

Rupture strain, $\varepsilon_{fu} = C_E \varepsilon_{fu}^* = 0.85(0.012) = 0.0102$

Thickness of laminate, $t_f = 0.04$ in

Angle of primary fiber orientation, $\alpha = 90^o$

Calculate the Effective Strain Level in the FRP Shear Reinforcement:

$$L_e = \frac{2500}{(nt_f E_f)^{0.58}} = 1.37 \text{ in}$$

$$k_1 = \left(\frac{f_c^{'}}{4000}\right)^{2/3} = 1.16$$

$$k_2 = \left(\frac{d_f - L_e}{d_f}\right) = 0.952$$

$$k_v = \frac{k_1 k_2 L_e}{468\varepsilon_{fu}} \leq 0.75 \Rightarrow 0.317 < 0.75 \Rightarrow \textbf{OK}$$

$$\varepsilon_{fe} = k_v \varepsilon_{fu} \leq 0.004 \Rightarrow 0.00323 < 0.004 \Rightarrow \textbf{OK}$$

Calculate the Contribution of the FRP Reinforcement to the Shear Capacity:

The area of FRP shear reinforcement can be computed as follows:

$$A_{fv} = 2nt_f w_f = 0.8 \text{ in}^2$$

The effective stress in the FRP is:

$$f_{fe} = \varepsilon_{fe} E_f = 33.9 \text{ ksi}$$

The shear contribution of the FRP is calculated as:

$$V_f = \frac{A_{fv} f_{fe} (\sin\alpha + \cos\alpha) d_f}{s_f} = \boxed{64.2} \text{ kips}$$

Calculate the Shear Capacity of the Section:

$\phi V_n = \phi(V_C + V_s + \psi_f V_f) = \boxed{\mathbf{113.7}}$ kips > $V_u = 106.8$ kips (required for Region 3)

$\psi_f = 0.85$ for three-sided U-wraps (bond critical applications)

Therefore, the strengthened section (Region 3) is capable of supporting the required shear load.

Check Reinforcement Limits

$V_s + \psi_f V_f \leq 8\sqrt{f_c'} b_w d$?

Region 1: 177.3 < 275.0 $\Rightarrow$ OK

Region 2: 163.1 < 275.0 $\Rightarrow$ OK

Region 3: 82.8 < 275.0 $\Rightarrow$ OK

Region 4: 75.8 < 275.0 $\Rightarrow$ OK

$V_u > 0.67 V_c$?

Region 1: 152.6 > 46.1 $\Rightarrow$ OK

Region 2: 129.1 > 46.1 $\Rightarrow$ OK

Region 3: 106.8 > 46.1 $\Rightarrow$ OK

Region 4: 69.0 > 46.1 $\Rightarrow$ OK